



## AN ABSTRACT OF THE DISSERTATION OF

Andrew M. Hau for the degree of Doctor of Philosophy in Pharmacy presented on December 3, 2012.

Title: Biological Characterization of Coibamide A, a Marine Natural Product from a Panamanian Cyanobacterium

Abstract approved:

---

Jane E. Ishmael

Coibamide A is a methyl-stabilized cyclic depsipeptide with a lariat side chain that was isolated from a marine cyanobacterium as part of an International Cooperative Biodiversity Groups program based in Panama. Previous testing of this potent and selective growth-inhibitory agent in the National Cancer Institute (NCI) in vitro 60 human cell line panel revealed a "COMPARE-negative" profile indicative of a unique mechanism of action. Presented herein is a collection of studies characterizing the mechanism of action of coibamide A and cataloguing the cytotoxicities of putative coibamide A and related structures from efforts at its total synthesis. We report that coibamide A induces apoptotic and non-apoptotic cell death in human U87-MG and NCI-SF-295 glioblastoma cells, respectively, which can occur independently of a rapid and sustained mTOR-independent autophagic response. Loss of cell viability from coibamide A exposure was concentration-dependent and time-sensitive, characterized by extensive cytoplasmic vacuolization and an absence of apoptotic morphology and DNA fragmentation prior to cell rounding and detachment from the substratum. Coibamide A also induces a cytostatic effect mediated by a G1 phase specific cell cycle arrest and inhibits glioma cell invasion but not migration. Lastly, structure activity relationships suggest that linearization, loss of *N*-methylation and disjoining of the cyclic and side chain structures of coibamide A are not well-tolerated modifications to retain activity.



© Copyright by Andrew M. Hau

December 3, 2012

All Rights Reserved

Biological Characterization of Coibamide A, a Marine Natural Product from a  
Panamanian Cyanobacterium

by

Andrew M. Hau

A DISSERTATION

submitted to

Oregon State University

in partial fulfillment of

the requirements for the

degree of

Doctor of Philosophy

Presented December 3, 2012

Commencement June 2013

Doctor of Philosophy dissertation of Andrew M. Hau presented on December 3, 2012.

APPROVED:

---

Major Professor, representing Pharmacy

---

Dean of the College of Pharmacy

---

Dean of the Graduate School

I understand that my dissertation will become part of the permanent collection of Oregon State University libraries. My signature below authorizes release of my dissertation to any reader upon request.

---

Andrew M. Hau, Author

## ACKNOWLEDGEMENTS

I would like to thank my friends and family for their support over the course of my graduate studies at OSU. I thank my adviser, Dr. Jane E. Ishmael, for her support and guidance in becoming a better scientist and allowing me the freedom to conduct research independently. I also wish to extend an acknowledgement to the OSU College of Pharmacy for financial support.

## CONTRIBUTION OF AUTHORS

Dr. Jane E. Ishmael contributed to research design, data analysis, writing and editing. Dr. Ian Ganley contributed to research design and data analysis of autophagic flux and EGFR degradation assays. Training and technical assistance on the transmission electron microscope (TEM) was provided by Teresa Sawyer at the OSU Electron Microscopy Facility. Expert cytological analysis of images captured on the TEM was provided by Dr. Christiane V. Löhr. Operation of the Beckman Coulter FC500 flow cytometer for cell cycle analysis was performed by Daniel J. Coleman and Samuel Bradford. Technical assistance with transwell migration and invasion assays and fluorescent microscopy on the Zeiss Axiovert S100TV was provided by Drs. Hyo Sang Jang and Jeffrey A. Greenwood. Syntheses and preparation of putative coibamide A and related structures were performed by Dong Li and Dr. Takashi L. Suyama under the guidance's of Drs. Philip J. Proteau and Kerry L. McPhail.

## TABLE OF CONTENTS

	<u>Page</u>
CHAPTER ONE: GENERAL INTRODUCTION.....	1
Preface .....	2
Cancer and Regulation of the Cell Cycle .....	5
Programmed Cell Death and Apoptosis .....	7
Autophagy: Regulation and Relevance to Cancer .....	10
Programmed Necrosis.....	14
Other PCD Mechanisms with Relevance to Human Disease.....	15
Bibliography.....	17
Figures .....	21
CHAPTER TWO: COIBAMIDE A INDUCES mTOR-INDEPENDENT AUTOPHAGY AND CELL DEATH IN HUMAN GLIOBLASTOMA CELLS .....	26
Abstract .....	27
Introduction.....	28
Materials and Methods .....	30
Results .....	36
Discussion .....	44
Acknowledgments .....	49
Bibliography.....	50
Figures .....	53
Supplementary Figures .....	64
CHAPTER THREE: THE MARINE NATURAL PRODUCT COIBAMIDE A INDUCES A G1 PHASE SPECIFIC CELL CYCLE ARREST AND INHIBITS U87-MG GLIOBLASTOMA CELL INVASION .....	66
Abstract .....	67
Introduction.....	68
Materials and Methods .....	70
Results .....	73
Discussion .....	76
Bibliography.....	79
Figures .....	81

## TABLE OF CONTENTS (Continued)

	<u>Page</u>
CHAPTER FOUR: CYTOTOXICITIES AND STRUCTURE ACTIVITY RELATIONSHIPS OF PUTATIVE COIBAMIDE A AND RELATED STRUCTURES..	85
Abstract .....	86
Introduction.....	87
Materials and Methods .....	89
Results .....	91
Discussion .....	95
Bibliography.....	98
Figures .....	99
Supplementary Figures .....	104
CHAPTER FIVE: GENERAL CONCLUSIONS.....	109
Bibliography.....	115

## LIST OF FIGURES

<u>Figure</u>	<u>Page</u>
Figure 1.1 The eukaryotic cell cycle and its regulation.....	21
Figure 1.2 The extrinsic apoptotic programmed cell death pathway .....	22
Figure 1.3 The intrinsic apoptotic programmed cell death pathway .....	23
Figure 1.4 Autophagy and its regulation.....	24
Figure 1.5 The mTOR signaling pathway .....	25
Figure 2.1 Cytotoxic effect of coibamide A on human glioblastoma cells .....	53
Figure 2.2 Coibamide A induces a time- and concentration-dependent decrease in plasma membrane integrity .....	54
Figure 2.3 Coibamide A induces activation of caspase-3,7 and apoptosis in a cell type-specific manner .....	55
Figure 2.4 The broad-spectrum caspase inhibitor Z-VAD-FMK inhibits LDH release but does not prevent coibamide A-induced cell death.....	56
Figure 2.5 Linearized analogs of coibamide A are not cytotoxic .....	57
Figure 2.6 Coibamide A induces biochemical and morphological features of autophagy.....	58
Figure 2.7 Coibamide A induces autophagosome accumulation in U87-MG cells.....	59
Figure 2.8 Coibamide A does not block ligand-induced degradation of EGFR .....	60
Figure 2.9 Coibamide A induces autophagy in an ATG5-dependent manner.....	61
Figure 2.10 Coibamide A induces mTOR-independent autophagy.....	62
Figure 2.11 Coibamide A induces cell death in the absence of ATG5 and intrinsic apoptotic activating factor 1 (Apaf-1).....	63



## LIST OF FIGURES (Continued)

<u>Figure</u>	<u>Page</u>
Supplementary Figure S2.1 Coibamide A is cytotoxic to wild-type MEFs.....	64
Supplementary Figure S2.2 Expression of apoptotic markers in wild-type MEFs and human U87-MG glioblastoma cells in response to coibamide A treatment.....	65
Figure 3.1 Reduced proliferation of U87-MG cells in response to coibamide A treatment is not due to a change in migratory capacity.....	81
Figure 3.2 The anti-proliferative action of coibamide A is induced by a block in G1 cell cycle progression .....	82
Figure 3.3 Expression of the nuclear proliferation marker Ki-67 is decreased in coibamide A-treated cells .....	83
Figure 3.4 The invasive capacity of U87-MG cells is reduced upon coibamide A exposure.....	84
Figure 4.1 Structures of desmethyl tetrameric side chains and corresponding EC <sub>50</sub> values in U87-MG and MDA-MB-231 cells.....	99
Figure 4.2 Structures of hepta- and nanopeptide macrocycles and corresponding EC <sub>50</sub> values in U87-MG and MDA-MB-231 cells .....	100
Figure 4.3 Structures of putative coibamide A compounds and corresponding EC <sub>50</sub> values in U87-MG and MDA-MB-231 cells.....	101
Figure 4.4 Structures of desmethylcoibamide analogs and corresponding EC <sub>50</sub> values in U87-MG and MDA-MB-231 cells .....	103
Supplementary Figure S4.1 Dose-response plots for desmethyl tetrameric side chains ( <b>1a</b> and <b>1b</b> ).....	104
Supplementary Figure S4.2 Dose-response plots for hepta- and nanopeptide macrocycles ( <b>2</b> and <b>3</b> ).....	105
Supplementary Figure S4.3 Dose-response plots for putative coibamide A structures ( <b>4a-c</b> ).....	106

## LIST OF FIGURES (Continued)

<u>Figure</u>	<u>Page</u>
Supplementary Figure S4.4 Dose-response plots for D- <i>N</i> -MeAla coibamide ( <b>5</b> ) and coibamide A.....	107
Supplementary Figure S4.5 Dose-response plots for desmethylcoibamide analogs ( <b>6a-d</b> ).....	108

## GENERAL INTRODUCTION

### CHAPTER ONE

Andrew M. Hau

## Preface

Cancer is a group of heterogeneous diseases caused by a number of environmental and genetic factors. The American Cancer Society estimates that nearly 580,000 Americans will die of cancer in 2012, making it the second most common cause of death behind heart disease (Source: Cancer Facts & Figures 2012, American Cancer Society, [www.cancer.org](http://www.cancer.org)). In a seminal review in 2000, Hanahan and Weinberg proposed that the complexity of cancer can be summarized with six underlying principles: (1) self-sufficiency in growth signals, (2) insensitivity to anti-growth signals, (3) tissue evasion and metastasis, (4) limitless replicative potential, (5) sustained angiogenesis, and (6) evading apoptosis [1]. These so-called 'hallmarks of cancer' have therefore driven intense research efforts that focus on exploiting these traits with the development, improvement and discovery of novel anti-cancer treatments and agents.

Over the last 40 years, marine organisms have been an attractive source for the discovery of new anti-cancer compounds, largely owing to the vastly unexplored and rich biodiversity of life in the Earth's seas in contrast to terrestrial areas. The success in identifying drug leads has been accelerated by screening services generated by collaborative efforts between academia and agency-funded programs such as the National Cooperative Drug Discovery Program and Developmental Therapeutics Program of the National Cancer Institute (NCI). The isolation and purification of natural products from crude samples can often be tedious and time-consuming. However, the nature of the compound(s) of interest (neutral, basic, acidic, lipophilic, amphiphilic) can facilitate sample isolation using one of several common extraction strategies and regardless of the procedure chosen, fractionation of a crude sample is almost always guided by suitable bioassay(s) to track activity. In cases where the discovery of anti-tumor compounds is anticipated, basic 3-(4,5-dimethylthiazol-2-yl)-2,5-diphenyltetrazolium bromide (MTT) assays in transformed cells are usually performed to determine the cytotoxicities of crude to pure fractions. Upon the arrival at a purified sample, identification and structure elucidation of the compound is achieved using nuclear magnetic resonance (NMR) and mass spectrometry-based techniques. Examples along these lines are the reports of two

new grassypeptolides, grassypeptolides D and E, and a lyngbyastatin analog, Ibu-epidemethoxy-lyngbyastatin 3, as well as four cytotoxic macrolides, mandelalides A-D, by the McPhail laboratory [2,3]. Finally, more extensive biological characterization to determine the mechanism of action and potentially the *in vivo* efficacy of the newly discovered compound is carried out as part of early-stage drug development.

To date, ~22,000 marine compounds have been discovered and a relatively significant subset of these compounds have been developed clinically or pre-clinically as anti-cancer agents [4,5]. Among these are trabectedin (also, ecteinascidin-743; Yondelis®), dolastatin-10 and analogs (Soblidotin, Cemadotin® and Synthadotin), and dehydrodidemnin B (Aplidin®), which have mechanisms of action in line with targeting one or multiple hallmarks of cancer [6-11]. In light of marine natural products drug discovery, the following chapters present a collection of studies undertaken to characterize the biological action of coibamide A, a natural product cyclic depsipeptide isolated from a marine cyanobacterium collected from the Coiba National Park, Panama [12]. Coibamide A showed high selectivity and exhibited potent cytotoxicity at sub- to low-nanomolar concentrations to CNS, breast, colon and ovarian cancer cells based on the NCI 60 cancer cell line panel. Chapter 2 represents an investigation of the mechanism of action of coibamide A in apoptosis-resistant human malignant U87-MG glioblastoma cells. The work therein considers the inherent resistance of cancer cells to apoptotic programmed cell death and the role of autophagy in cancer, which are topics elaborated in more detail in the remainder of this chapter.

Chapter 3 investigates the cytostatic potential of coibamide A in highly invasive U87-MG glioma cells. Interestingly, coibamide A is found to affect cell motility by inhibiting cell invasion but not cell migration. This result is consistent with a G1 phase rather than G2/M specific cell cycle arrest observed upon coibamide A treatment as previous investigation has ruled out coibamide A as an inhibitor of actin and tubulin, which are cytoskeletal components required during mitosis. The chapter concludes by considering the signaling pathways of matrix metalloproteinases as possible targets of coibamide A inhibition.

Chapter 4 catalogs a collaborative effort between medicinal chemistry and pharmacology in the synthesis of coibamide A. The activities of putative coibamide A

and related structures were determined by MTT bioassay in U87-MG glioma and human MDA-MB-231 breast cancer cell lines. Evaluation of the synthetic products against natural coibamide A has revealed several structure activity relationships that are important considerations in generating biologically active coibamide A analogs in future studies.

Finally, the concluding chapter, Chapter 5, summarizes the outcomes of the studies performed in Chapters 2-4 and provides general remarks on future work with coibamide A as well as comments on studying programmed cell death and autophagy.

### Cancer and Regulation of the Cell Cycle

Superficially, the connection between cancer and the cell cycle is obvious as one of the hallmarks of cancer is limitless replicative potential and a function of the cell cycle is to control cell proliferation. The eukaryotic cell cycle is divided into two periods: interphase, the period in which cells grow and accumulate nutrients for DNA replication in preparation for cell division, and mitosis (M), the phase during which a cell splits itself into two daughter cells (Figure 1.1) [13]. Interphase is further divided into three stages, G1, synthesis (S) and G2, which are tightly regulated through checkpoint (G1/S, or restriction, and G2/M) mechanisms by pairs of cyclins and cyclin-dependent kinases (CDKs). An additional resting phase, G0, is often viewed as an extension of G1 where cells are quiescent and terminally differentiated. Following interphase, cells quickly proceed through four additional nuclear division stages (prophase, metaphase, anaphase, and telophase) of mitosis before re-entry into G1/G0.

Under normal conditions, the cyclin-CDK checkpoint mechanisms between each stage in interphase function to assess DNA damage and prevent premature transition into the subsequent phase [13]. However, in cancer cells, progression through cell cycle checkpoints occurs without regulation due to the (self)-activation of growth stimulating pathways [e.g., mitogen-activated protein kinase (MAPK) and phosphoinositide 3-kinase (PI3K)/protein kinase B (PKB/Akt)] and/or downregulation of cell cycle inhibitors (e.g., cyclins, CDKs and p53) [14]. Both factors consequently contribute to the limitless proliferative potential of tumor cells. Restoration of cell cycle regulation to inhibit cancer cell proliferation is therefore an attractive therapeutic approach to combat malignancy. Indeed, many compounds, notably of marine origin, have been reported to induce cell cycle arrest in various human tumor cell lines. These include: nidurufin, a G2/M inhibitor in K562 leukemia cells, from the fungus *Penicillium flavidorsum* SHK1-27, pectenotoxin-2, also a G2/M inhibitor in MDA-MB-231 and MCF-7 breast cancer cells, from the microalgae *Dinophysis* sp., and sansalvamide, a G1/S inhibitor in AsPC-1 and CD18 pancreatic cells, from the fungus of the genus *Fusarium* [15-17]. Also, as reported in Chapter 3, coibamide A has been

characterized as a potent inducer of a G1 phase cell cycle arrest in U87-MG and SF-295 glioblastoma tumor cells.



## Programmed Cell Death and Apoptosis

Programmed cell death (PCD), which has traditionally included apoptosis, autophagy and necrosis, plays an integral role in normal human function and development but these mechanisms are commonly dysregulated in disease states such as cancer and neurodegeneration [18]. While the aforementioned cell death modalities are among the most extensively studied and will therefore be a primary focus of this chapter, several more recently characterized and atypical PCD mechanisms with relevance to human disease such as anoikis, methuosis and paraptosis will also be briefly described [19-21].

Apoptosis as a mode of PCD was first introduced in the 1960s and was subsequently classified as 'type I cell death' by Schweichel and Merker in 1973 [22]. This classification was based purely on numerous morphological characteristics of apoptotic cells that include membrane blebbing, cell shrinkage, nuclear fragmentation and DNA condensation. It is now clear that several of these events are mediated through the activity of caspases which are a family of cysteine proteases that are synthesized as inactive proforms and are sequentially activated along a catalytic cascade. Along these lines, the development of biochemical assays to scrutinize the fine molecular details of cells undergoing PCD has therefore prompted the disfavor of a morphological classification of apoptosis. This has in part also occurred because of the discovery of other apoptosis-like cell death pathways that share similar morphotypes. Consequently, biochemical analysis of apoptotic PCD has led to the definitions of 'extrinsic' and 'intrinsic' apoptosis with the initiating factor(s) being extracellular stimuli or intracellular stress signals, respectively. Regardless of the pathway, however, transmission of death signal is caspase dependent and both signaling cascades converge following caspase-3 activation (discussed further below).

The extrinsic pathway begins outside the cell through the activation of pro-apoptotic death receptors upon binding of ligand (Figure 1.2). A prototypic signaling cascade involves the ligation of FAS ligand (FASL) to the FAS receptor (FASR), which triggers the trimerization of FASR subunits and assembly of a multi-protein death inducing signaling complex (DISC) onto the cytosolic death-domain (DD)

containing C-terminal tail of the receptor [23]. Also recruited to the DISC of FASR include apoptosis-promoting effectors—FAS-associated protein with a DD (FADD) and receptor-interacting protein kinase 1 (RIPK1)—as well as anti-apoptotic proteins—cellular FADD-like IL- $\beta$ -converting enzyme inhibitory protein (c-FLIP) and inhibitor of apoptosis proteins (IAPs)—that regulate the activity of the initiator caspase-8 (or -10). Caspase-8 then mediates the activation of the executioner caspase-3 that is responsible for proteolytic cleavage of downstream structural (e.g., Actin, Fodrin and Gas2) and regulatory [e.g., poly-ADP ribose polymerase (PARP), inhibitor of caspase-activated DNase (ICAD) and caspase-activated DNase (CAD)] proteins resulting in apoptosis [24].

Similar cascades of events of FASL-induced death receptor signaling have also been described for the binding of lethal ligands, tumor necrosis factor  $\alpha$  (TNF $\alpha$ ) and TNF-related apoptosis-inducing ligand (TRAIL), to their respective death receptors, TNFR1 and TRAIL-R1/2 [23]. Fundamentally, however, TNF $\alpha$  differs from FASL or TRAIL-induced apoptosis in that it also results in the recruitment of TNFR-associated DD (TRADD), and notably TNFR-associated factor 2 (TRAF2) and TRAF5 in addition to FADD, RIPK1 and c-FLIP to the DISC. Following receptor activation and the assembly of the DISC, the activity and regulation of RIPK1 has been demonstrated to have one of three possible downstream effects depending on cell type, cell activation status, and microenvironment [25]. In one scenario, polyubiquitylation of RIPK1 by IAPs in the DISC creates a docking platform for transforming growth factor- $\beta$ -activated kinase 1 (TAK1), TAK1-binding protein 2 (TAB2) and TAB3 [26]. Together, this complex activates the pro-survival canonical NF- $\kappa$ B signaling pathway [27], which suggests that death receptor activation does not always entail apoptosis. On the contrary, in situations where IAP levels are depleted the activities of RIPK1 and its cognate kinase, RIPK3, are regulated and inactivated by caspase-8 proteolytic cleavage. This allows cells to enter an ‘apoptotic mode’ with caspase-8 initiating the extrinsic apoptotic caspase cascade. The third pathway, necroptosis, resulting from death receptor signaling has more recently been characterized and is discussed in further detail below [28].

In contrast to apoptosis mediated by extrinsic pathways, a number of intracellular stress signals including DNA damage, oxidative stress, and excitotoxicity

can lead to cellular demise (Figure 1.3) [29]. Regardless of the stimulus, intrinsic pro-apoptotic signaling is intricately tied to a central mitochondrial control mechanism that is regulated by the B-cell lymphoma 2 (Bcl-2) family of apoptosis regulatory proteins. During this process, Bcl-2 proteins such as Bcl-2-associated X protein (Bax) and Bcl-2 homologous antagonist killer (Bak) co-localize to mitochondria and induce mitochondrial outer membrane permeabilization (MOMP) resulting in the release of several apoptogenic effectors into the cytosol. These effectors include cytochrome c, apoptosis-inducing factor (AIF), endonuclease G (ENDOG), direct IAP-binding protein with low PI (DIABLO, also known as second mitochondria-derived activator of caspase, SMAC), and high temperature requirement protein A2 (HTRA2). Among these proteins only cytochrome c directly leads to the caspase-9 → caspase-3 proteolytic cascade through association with the apoptosome, a dynamic protein complex centered around the adapter protein apoptotic protease activating factor 1 (Apaf-1). The downstream cellular and biochemical events that ensue following caspase-3 activation essentially resemble those that occur via the extrinsic pathway [24].

The releases of AIF, ENDOG, DIABLO/SMAC, and HTRA2 following MOMP have pro-apoptotic effects that are mediated both dependently and independently of caspases [30]. Once in the cytosol, AIF and ENDOG translocate into the nucleus and directly induce large-scale DNA fragmentation and chromatin condensation. In contrast, the execution of cell death through DIABLO/SMAC and HTRA2 are mediated by the repression of IAPs, a family of endogenous caspase inhibitors. Interestingly, an investigation of IAP expression in the National Cancer Institute panel of 60 human cancer cell lines showed that the best-characterized IAP, XIAP, is frequently upregulated and presumably imbues tumor cells with an inherent resistance to caspase-dependent PCD [31]. Later studies confirmed this discovery in a variety of tumor cell lines and cancer tissues while also demonstrating high basal levels of activated caspases with an absence of apoptosis in the model systems [32]. In light of these findings, considerable interest has developed over the past decade to strategically target IAPs with novel inhibitors as a cancer-specific therapeutic approach [33,34].

### Autophagy: Regulation and Relevance to Cancer

The term 'autophagic cell death' (originally catalogued as type II PCD by Schweichel and Merker) has mainly been used as a morphological definition in instances of cell demise that are accompanied by extensive cytoplasmic vacuolation [22]. In most known cases, however, it is now apparent that autophagy functions as a quality control mechanism to help maintain cellular homeostasis through the degradation of long-lived or damaged proteins, organelles, lipids and other macromolecules. Autophagy also constitutes a cytoprotective response activated by cells to deal with stress induced by low nutrient levels or genotoxic agents. However, a question of intense debate is the role of autophagy in cancer. Many studies in mouse models with impaired autophagy machinery support the notion that autophagy deficiency can be a predisposition to tumor formation [35-37]. Interestingly, upon establishment of a tumor, autophagy mechanisms then act to promote cell survival as a result of the lack of blood supply to the core of the tumor. In this respect, pharmacological inhibition of autophagy has become an attractive strategy for cancer therapy.

The molecular basis of autophagy was elucidated upon the breakthrough in yeast genetics with the discovery of the so-called autophagy-related genes (ATGs) [38]. The process of autophagy can be described through five stages: initiation, elongation, closure, maturation, and degradation (Figure 1.4) [39]. In the initiation phase, an isolation membrane known as a phagophore is formed and begins expanding to encapsulate cargo macromolecules through the elongation phase. The closure of the phagophore results in the formation of a double-membrane autophagosome, a morphological feature of autophagic cells commonly identified by electron microscopy [40]. Facilitated by lipidated LC3 (also known as ATG8/microtubule-associated protein 1 light chain 3) recruitment to the autophagosome, the loaded vesicle matures through fusion with the lysosome forming the autophagolysosome (or autolysosome) thereby promoting the degradation of its contents by lysosomal hydrolases. Using model systems in

mammalian cells, the regulation of this evolutionarily conserved process is attributed to four groups of core machinery [41].

The initiation phase of autophagy is regulated by the ATG1/unc-51-like kinase (ULK1/2) complex, including ATG13 and focal adhesion kinase family interacting protein of 200 kD (FIP200), and a second complex containing vesicular protein sorting 34 (Vps34), ATG6/Beclin1, and p150. As will be discussed in further detail below, both complexes are activated by upstream signals mediated by the energy-sensing PI3K/Akt/mammalian target of rapamycin (mTOR) cascade. Interestingly, deletion of Beclin1 is commonly seen in 40-75% of sporadic human breast and ovarian cancer cases suggesting that the loss of autophagic regulation is correlated with tumorigenicity [42,43]. In the elongation and closure stages of autophagy, a complex containing ATG5, ATG12 and ATG16L regulates the insertion of the autophagy marker, LC3, into the inner and outer membranes of the autophagosome. Prior to LC3 processing into autophagosomes, however, the protein is first cleaved by ATG4 to generate LC3-I and then lipidated to LC3-II through its conjugation with phosphatidylethanolamine (PE) by ATG3 and ATG7. A fourth core group composed of ATG9 and vacuole membrane protein 1 (VMP1) has also been identified as being indispensable for autophagy but its exact function is not well understood.

The mTOR protein is a serine/threonine kinase that belongs to the PI3K-related kinase family and plays an important role in regulating autophagy in response to a number of biological cues including growth factor receptor signaling, hypoxia, and ATP levels. In cancer, mTOR is frequently hyperactivated and its inhibition has been clinically validated [44,45]. Mammalian TOR nucleates two distinct complexes: mTOR complex 1 (mTORC1) and mTOR complex 2 (mTORC2), the former being more important in the regulation of mTOR-dependent autophagy (Figure 1.5) [46].

The rapamycin-sensitive mTORC1 is composed of mTOR, regulatory associated protein of mTOR (Raptor), mammalian lethal with Sec13 protein 8 (mLST8, also known as GβL), proline-rich Akt/PKB substrate of 40 kDa (PRAS40), and DEP-domain-containing mTOR-interacting protein (Deptor). Under nutrient-rich conditions, PI3K/Akt signaling regulates mTOR by phosphorylation and inactivation of mTOR's negative regulator TSC1/2, a GTPase containing protein that regulates

Rheb GTPase. Released from repression, mTOR then activates downstream targets, S6 kinase (S6K) and eukaryotic translation initiation factor 4E-binding protein 1 (4EBP1), which promote protein synthesis and cell growth. mTOR activity also regulates the ULK complex by phosphorylation, thereby inhibiting autophagy initiation. In contrast to these conditions, low nutrient and/or energy levels stimulate the AMP-activated protein kinase (AMPK) signaling axis, which negatively regulates mTOR activity and induces autophagy [47].

Studies on the pharmacological inhibition of mTOR have revealed that autophagy can be activated through mTORC1-independent pathways [48]. One of the first examples of this observation came from the use of rapamycin, a lipophilic macrolide antibiotic that potently induces autophagy in mammalian cells. Biochemically, rapamycin functions as an inhibitor of mTOR through its association with the 12 kD FK506-binding protein (FKBP12) and allosteric binding to mTORC1 [49]. The inhibited kinase activity of mTOR thereby relieves the repression on the ULK complex and autophagy initiation ensues. However, an interesting observation from these studies was that S6K and 4EBP1 activity downstream of mTORC1 was not completely abolished upon rapamycin treatment even at high concentrations [50]. It was therefore postulated that either the rapamycin-insensitive mTORC2 plays a role in autophagy regulation or autophagy activation can occur independently of mTOR. However, in contrast to these hypotheses, subsequent studies later revealed that rapamycin is an incomplete inhibitor of mTORC1 thus explaining how some mTOR functions are rapamycin-resistant [51]. This finding may also account for why current clinically used mTOR inhibitors such as rapamycin are not fully efficacious in the treatment of cancer. Accordingly, the phosphorylation levels of S6K and 4EBP1 are now being used as markers of mTORC1 activity that result from its inhibition by pharmacological agents. Along these lines, several mTOR inhibitors such as Torin1, perhexiline, niclosamide, amiodaron and rottlerin have been identified from chemical screens and are now being investigated for their potential to inhibit mTORC1 and/or mTORC2 and induce autophagy through alternative pathways [51,52].

Recent efforts to identify mTOR-independent autophagy pathways revealed some level of negative regulation by inositol 1,4,5-triphosphate (IP<sub>3</sub>) mediated through the cyclical Ca<sup>2+</sup>/calpain/Gα<sub>s</sub> and cyclic AMP/exchange protein directly

activated by cAMP/phospholipase C $\epsilon$ /inositol triphosphate (cAMP/Epac/PLC $\epsilon$ /IP<sub>3</sub>) signaling axes in several neuropathies [53,54]. Although the precise mechanisms by which these pathways modulate autophagy are still under investigation, the fact that autophagy can be regulated independently of mTORC1 raises intense interest in developing or discovering novel modulators of these pathways for potential use with mTOR inhibitors in cancer chemotherapy.

### Programmed Necrosis

Dying cells that fail to exhibit the morphological features of apoptosis or autophagy were originally catalogued as necrotic [18]. Cells undergoing necrosis are characterized by an increasingly translucent cytoplasm, swelling of organelles and increased cell volume, and culminates in the disruption of the plasma membrane. Most importantly, necrotic cells do not fragment and their nuclei remain intact in contrast to their apoptotic counterparts. Consequently, this 'type III cell death' was generally viewed as a non-physiological, passive and accidental form of cell death that resulted from physical or chemical insult and is in part still perceived as such today. However, it is now clear that necrosis may be regulated through a mechanism referred to as necroptosis, or programmed necrosis [28]. This discovery was partially revealed by studies showing that some cell lines and primary cells failed to be rescued when co-treated with an apoptosis-inducer and the broad-spectrum caspase inhibitor, Z-VAD-FMK, thus suggesting a caspase-independent cell death pathway. Like cell death mediated by the extrinsic apoptosis signaling, programmed necrosis is initiated through the ligation of FAS, TNF $\alpha$ , or TRAIL to its respective death receptor. Among these lethal ligand-receptor interactions, necroptosis is most well understood along the TNF $\alpha$   $\rightarrow$  TNFR1 axis.

As discussed above, regulation of RIPK1 activity dictates the biological response to TNF $\alpha$  stimulation [25]. However, through a mechanism not fully understood under physiological conditions, the activity of the deubiquitinase, CYLD, and absence of caspase-8 activation drives cells down a RIPK1 and RIPK3-dependent pathway favoring necroptosis [55,56]. The execution of this program appears to involve a number of downstream events including reactive oxygen species generation and oxidative stress, MOMP, and autophagy, all of which are pathologically implicated in neuronal excitotoxicity resulting from stroke or in association with neurodegenerative disorders [57]. Therefore, understanding of the physiological switch between cytoprotection and cytotoxicity that occurs through death receptor signaling is an important consideration in developing therapeutic agents for neuroprotection in stroke and Alzheimer's and Parkinson's diseases.



### Other PCD Mechanisms with Relevance to Human Disease

Owing to the development and/or improvement of new technologies and methodologies [e.g., transmission electron microscopy (TEM) and genetic manipulation of cell or animal models] to study PCD, numerous other cell death modalities that are biochemically distinct from apoptosis have been detailed. In some cases, these alternative cell death pathways are fundamentally different from apoptosis in that they are caspase-independent or cell death does not appear to be mediated through the activity of caspases. As will also be briefly discussed in Chapter 2, the description of a novel form of non-apoptotic cell death discovered by Overmeyer et al. called methuosis, for instance, was revealed by TEM studies showing large cytoplasmic vacuoles in glioblastoma cells with an activated Ras oncogene [58]. Interestingly, although cells undergoing methuosis are accompanied by caspase activation, pharmacological inhibition of caspase proteolysis with Z-VAD-FMK does not prevent cell death.

Another atypical PCD mechanism that has garnered attention is paraptosis, a process that involves mitochondrial and endoplasmic reticular swelling and extensive cytoplasmic vacuolation similar to methuosis [21]. Paraptosis appears to be mediated by MAPK and/or c-Jun *N*-terminal kinase (JNK) signaling, a member of the TNF receptor family, and caspase-9 activity independent of Apaf-1 and the apoptosome [59]. More recently, the marine algal cytotoxin yessotoxin has served as a tool to study paraptosis in a number of cancer cell model systems [60,61]. Like in methuosis, administration of Z-VAD-FMK to cells co-treated with yessotoxin did not protect against paraptotic cell death signaling. This observation points to the possibility that caspase-9 may have dual functions in inducing apoptotic and non-apoptotic cell death in cell-specific contexts. Further understanding of the mechanism(s) underlying paraptosis may therefore help reveal non-apoptotic cell death pathways that can be targeted complementarily to current apoptosis-based approaches in cancer therapy.

The capacity of tumors to become malignant owes to their ability to metastasize while avoiding an apoptotic response known as anoikis. Anoikis was first coined by Frisch and Francis in 1994 and describes a form of caspase-dependent

apoptosis that normally occurs following cell detachment from the extracellular matrix (ECM) [62]. Studies since the discovery of anoikis have now revealed that cellular ECM detachment results in significant changes in metabolic control that would normally overwhelm protective responses that prevent cell death [19]. The oncogene human epidermal growth factor receptor 2 (HER2/ErbB2) is one protein that appears to help compensate for detachment-induced deficiencies in ATP as its overexpression has been shown to rescue metabolic defects including decreased uptake of glucose, glutamine and pyruvate [63]. Interestingly, the activation of autophagy until nutrient rescue mechanisms are restored upon angiogenesis has also been hypothesized to explain how metastatic cancers cells can overcome anoikis.

### Bibliography

1. Hanahan D, Weinberg RA (2000) The hallmarks of cancer. *Cell* 100: 57-70.
2. Thornburg CC, Thimmaiah M, Shaala LA, Hau AM, Malmo JM, et al. (2011) Cyclic depsipeptides, grassypeptolides D and E and Ibu-epidemethoxylyngbyastatin 3, from a Red Sea *Leptolyngbya* cyanobacterium. *J Nat Prod* 74: 1677-1685.
3. Sikorska J, Hau AM, Anklin C, Parker-Nance S, Davies-Coleman MT, et al. (2012) Mandelalides A-D, cytotoxic macrolides from a new *Lissoclinum* species of South African tunicate. *J Org Chem* 77: 6066-6075.
4. Blunt JW, Copp BR, Keyzers RA, Munro MH, Prinsep MR (2012) Marine natural products. *Nat Prod Rep* 29: 144-222.
5. Blunt JW, Copp BR, Munro MH, Northcote PT, Prinsep MR (2011) Marine natural products. *Nat Prod Rep* 28: 196-268.
6. Garcia-Rocha M, Garcia-Gravalos MD, Avila J (1996) Characterisation of antimitotic products from marine organisms that disorganise the microtubule network: ecteinascidin 743, isohomohalichondrin-B and LL-15. *Br J Cancer* 73: 875-883.
7. D'Incalci M, Galmarini CM (2010) A review of trabectedin (ET-743): a unique mechanism of action. *Mol Cancer Ther* 9: 2157-2163.
8. Bai R, Pettit GR, Hamel E (1990) Dolastatin 10, a powerful cytostatic peptide derived from a marine animal. Inhibition of tubulin polymerization mediated through the vinca alkaloid binding domain. *Biochem Pharmacol* 39: 1941-1949.
9. Poncet J (1999) The dolastatins, a family of promising antineoplastic agents. *Curr Pharm Des* 5: 139-162.
10. Urdiales JL, Morata P, Nunez De Castro I, Sanchez-Jimenez F (1996) Antiproliferative effect of dehydroadidemin B (DDB), a depsipeptide isolated from Mediterranean tunicates. *Cancer Lett* 102: 31-37.
11. Erba E, Bassano L, Di Liberti G, Muradore I, Chiorino G, et al. (2002) Cell cycle phase perturbations and apoptosis in tumour cells induced by aplidine. *Br J Cancer* 86: 1510-1517.
12. Medina RA, Goeger DE, Hills P, Mooberry SL, Huang N, et al. (2008) Coibamide A, a potent antiproliferative cyclic depsipeptide from the Panamanian marine cyanobacterium *Leptolyngbya* sp. *J Am Chem Soc* 130: 6324-6325.
13. Schafer KA (1998) The cell cycle: a review. *Vet Pathol* 35: 461-478.
14. Williams GH, Stoeber K (2012) The cell cycle and cancer. *J Pathol* 226: 352-364.
15. Ren H, Liu WW (2011) Nidurufin as a new cell cycle inhibitor from marine-derived fungus *Penicillium flavidorsum* SHK1-27. *Arch Pharm Res* 34: 901-905.
16. Moon DO, Kim MO, Nam TJ, Kim SK, Choi YH, et al. (2010) Pectenotoxin-2 induces G2/M phase cell cycle arrest in human breast cancer cells via ATM and Chk1/2-mediated phosphorylation of cdc25C. *Oncol Rep* 24: 271-276.
17. Heiferman MJ, Salabat MR, Ujiki MB, Strouch MJ, Cheon EC, et al. (2010) Sansalvamide induces pancreatic cancer growth arrest through changes in the cell cycle. *Anticancer Res* 30: 73-78.
18. Galluzzi L, Vitale I, Abrams JM, Alnemri ES, Baehrecke EH, et al. (2012) Molecular definitions of cell death subroutines: recommendations of the Nomenclature Committee on Cell Death 2012. *Cell Death Differ* 19: 107-120.

19. Buchheit CL, Rayavarapu RR, Schafer ZT (2012) The regulation of cancer cell death and metabolism by extracellular matrix attachment. *Semin Cell Dev Biol* 23: 402-411.
20. Overmeyer JH, Young AM, Bhanot H, Maltese WA (2011) A chalcone-related small molecule that induces methuosis, a novel form of non-apoptotic cell death, in glioblastoma cells. *Mol Cancer* 10: 69.
21. Sperandio S, de Belle I, Bredesen DE (2000) An alternative, nonapoptotic form of programmed cell death. *Proc Natl Acad Sci U S A* 97: 14376-14381.
22. Schweichel JU, Merker HJ (1973) The morphology of various types of cell death in prenatal tissues. *Teratology* 7: 253-266.
23. Schulze-Osthoff K, Ferrari D, Los M, Wesselborg S, Peter ME (1998) Apoptosis signaling by death receptors. *Eur J Biochem* 254: 439-459.
24. Fan TJ, Han LH, Cong RS, Liang J (2005) Caspase family proteases and apoptosis. *Acta Biochim Biophys Sin (Shanghai)* 37: 719-727.
25. Green DR, Oberst A, Dillon CP, Weinlich R, Salvesen GS (2011) RIPK-dependent necrosis and its regulation by caspases: a mystery in five acts. *Mol Cell* 44: 9-16.
26. Ea CK, Deng L, Xia ZP, Pineda G, Chen ZJ (2006) Activation of IKK by TNF $\alpha$  requires site-specific ubiquitination of RIP1 and polyubiquitin binding by NEMO. *Mol Cell* 22: 245-257.
27. Scheidereit C (2006) IkappaB kinase complexes: gateways to NF-kappaB activation and transcription. *Oncogene* 25: 6685-6705.
28. Vandenabeele P, Galluzzi L, Vanden Berghe T, Kroemer G (2010) Molecular mechanisms of necroptosis: an ordered cellular explosion. *Nat Rev Mol Cell Biol* 11: 700-714.
29. Fulda S, Debatin KM (2006) Extrinsic versus intrinsic apoptosis pathways in anticancer chemotherapy. *Oncogene* 25: 4798-4811.
30. Kroemer G, Galluzzi L, Brenner C (2007) Mitochondrial membrane permeabilization in cell death. *Physiol Rev* 87: 99-163.
31. Tamm I, Kornblau SM, Segall H, Krajewski S, Welsh K, et al. (2000) Expression and prognostic significance of IAP-family genes in human cancers and myeloid leukemias. *Clin Cancer Res* 6: 1796-1803.
32. Yang L, Cao Z, Yan H, Wood WC (2003) Coexistence of high levels of apoptotic signaling and inhibitor of apoptosis proteins in human tumor cells: implication for cancer specific therapy. *Cancer Res* 63: 6815-6824.
33. Wang S, Bai L, Lu J, Liu L, Yang CY, et al. (2012) Targeting Inhibitors of Apoptosis Proteins (IAPs) For New Breast Cancer Therapeutics. *J Mammary Gland Biol Neoplasia*.
34. Fulda S, Vucic D (2012) Targeting IAP proteins for therapeutic intervention in cancer. *Nat Rev Drug Discov* 11: 109-124.
35. Marino G, Salvador-Montoliu N, Fueyo A, Knecht E, Mizushima N, et al. (2007) Tissue-specific autophagy alterations and increased tumorigenesis in mice deficient in Atg4C/autophagin-3. *J Biol Chem* 282: 18573-18583.
36. Qu X, Yu J, Bhagat G, Furuya N, Hibshoosh H, et al. (2003) Promotion of tumorigenesis by heterozygous disruption of the beclin 1 autophagy gene. *J Clin Invest* 112: 1809-1820.

37. Takahashi Y, Coppola D, Matsushita N, Cualing HD, Sun M, et al. (2007) Bif-1 interacts with Beclin 1 through UVRAG and regulates autophagy and tumorigenesis. *Nat Cell Biol* 9: 1142-1151.
38. Tsukada M, Ohsumi Y (1993) Isolation and characterization of autophagy-defective mutants of *Saccharomyces cerevisiae*. *FEBS Lett* 333: 169-174.
39. Glick D, Barth S, Macleod KF (2010) Autophagy: cellular and molecular mechanisms. *J Pathol* 221: 3-12.
40. Eskelinen EL (2008) Fine structure of the autophagosome. *Methods Mol Biol* 445: 11-28.
41. Yang Z, Klionsky DJ (2010) Mammalian autophagy: core molecular machinery and signaling regulation. *Current Opinion in Cell Biology* 22: 124-131.
42. Aita VM, Liang XH, Murty VV, Pincus DL, Yu W, et al. (1999) Cloning and genomic organization of beclin 1, a candidate tumor suppressor gene on chromosome 17q21. *Genomics* 59: 59-65.
43. Liang XH, Jackson S, Seaman M, Brown K, Kempkes B, et al. (1999) Induction of autophagy and inhibition of tumorigenesis by beclin 1. *Nature* 402: 672-676.
44. Shor B, Gibbons JJ, Abraham RT, Yu K (2009) Targeting mTOR globally in cancer: thinking beyond rapamycin. *Cell Cycle* 8: 3831-3837.
45. Meric-Bernstam F, Gonzalez-Angulo AM (2009) Targeting the mTOR signaling network for cancer therapy. *J Clin Oncol* 27: 2278-2287.
46. Laplante M, Sabatini DM (2012) mTOR signaling in growth control and disease. *Cell* 149: 274-293.
47. Gwinn DM, Shackelford DB, Egan DF, Mihaylova MM, Mery A, et al. (2008) AMPK phosphorylation of raptor mediates a metabolic checkpoint. *Mol Cell* 30: 214-226.
48. Fleming A, Noda T, Yoshimori T, Rubinsztein DC (2011) Chemical modulators of autophagy as biological probes and potential therapeutics. *Nat Chem Biol* 7: 9-17.
49. Vilella-Bach M, Nuzzi P, Fang Y, Chen J (1999) The FKBP12-rapamycin-binding domain is required for FKBP12-rapamycin-associated protein kinase activity and G1 progression. *J Biol Chem* 274: 4266-4272.
50. Thoreen CC, Sabatini DM (2009) Rapamycin inhibits mTORC1, but not completely. *Autophagy* 5: 725-726.
51. Thoreen CC, Kang SA, Chang JW, Liu Q, Zhang J, et al. (2009) An ATP-competitive mammalian target of rapamycin inhibitor reveals rapamycin-resistant functions of mTORC1. *J Biol Chem* 284: 8023-8032.
52. Balgi AD, Fonseca BD, Donohue E, Tsang TC, Lajoie P, et al. (2009) Screen for chemical modulators of autophagy reveals novel therapeutic inhibitors of mTORC1 signaling. *PLoS One* 4: e7124.
53. Sarkar S, Floto RA, Berger Z, Imarisio S, Cordenier A, et al. (2005) Lithium induces autophagy by inhibiting inositol monophosphatase. *J Cell Biol* 170: 1101-1111.
54. Garcia-Arencibia M, Hochfeld WE, Toh PP, Rubinsztein DC (2010) Autophagy, a guardian against neurodegeneration. *Semin Cell Dev Biol* 21: 691-698.
55. Cho YS, Challa S, Moquin D, Genga R, Ray TD, et al. (2009) Phosphorylation-driven assembly of the RIP1-RIP3 complex regulates programmed necrosis and virus-induced inflammation. *Cell* 137: 1112-1123.

56. He S, Wang L, Miao L, Wang T, Du F, et al. (2009) Receptor interacting protein kinase-3 determines cellular necrotic response to TNF- $\alpha$ . *Cell* 137: 1100-1111.
57. Artal-Sanz M, Tavernarakis N (2005) Proteolytic mechanisms in necrotic cell death and neurodegeneration. *FEBS Lett* 579: 3287-3296.
58. Overmeyer JH, Kaul A, Johnson EE, Maltese WA (2008) Active ras triggers death in glioblastoma cells through hyperstimulation of macropinocytosis. *Mol Cancer Res* 6: 965-977.
59. Sperandio S, Poksay K, de Belle I, Lafuente MJ, Liu B, et al. (2004) Paraptosis: mediation by MAP kinases and inhibition by AIP-1/Alix. *Cell Death Differ* 11: 1066-1075.
60. Korsnes MS (2012) Yessotoxin as a tool to study induction of multiple cell death pathways. *Toxins (Basel)* 4: 568-579.
61. Korsnes MS, Espenes A, Hetland DL, Hermansen LC (2011) Paraptosis-like cell death induced by yessotoxin. *Toxicol In Vitro* 25: 1764-1770.
62. Frisch SM, Francis H (1994) Disruption of epithelial cell-matrix interactions induces apoptosis. *J Cell Biol* 124: 619-626.
63. Schafer ZT, Grassian AR, Song L, Jiang Z, Gerhart-Hines Z, et al. (2009) Antioxidant and oncogene rescue of metabolic defects caused by loss of matrix attachment. *Nature* 461: 109-113.

## Figures

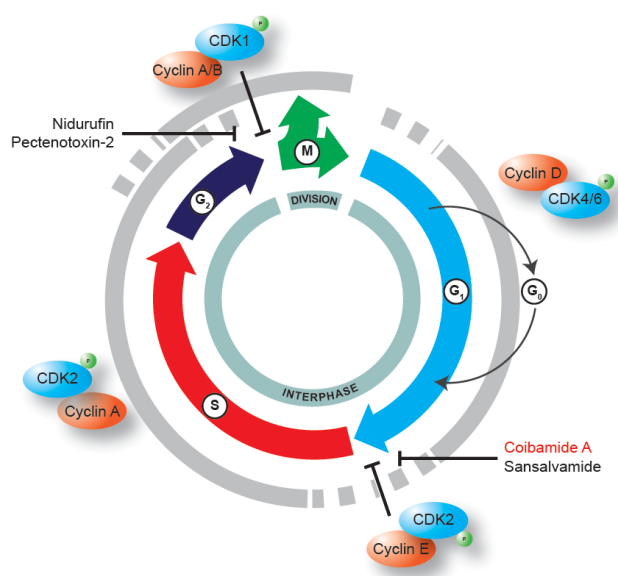


**Figure 1.1** The eukaryotic cell cycle and its regulation.

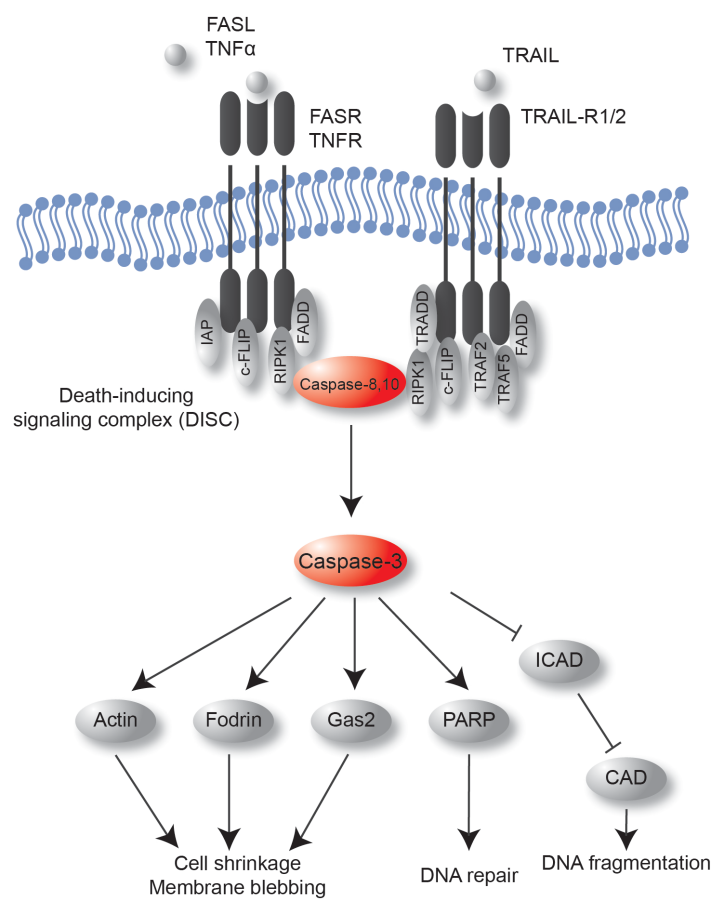


**Figure 1.2** The extrinsic apoptotic programmed cell death pathway.



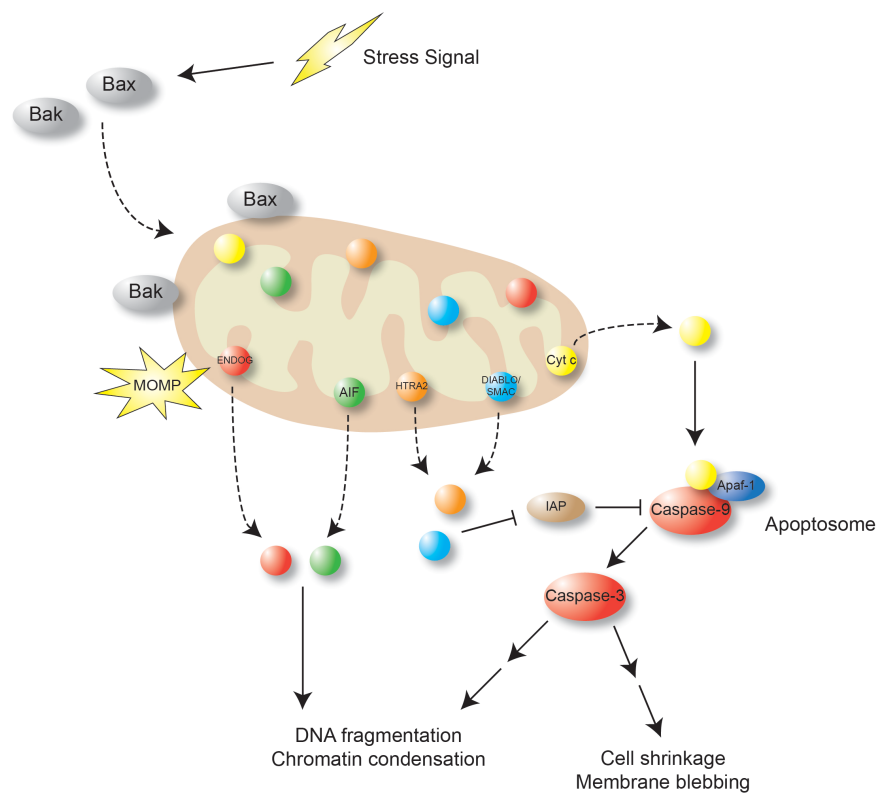


**Figure 1.3** The intrinsic apoptotic programmed cell death pathway.

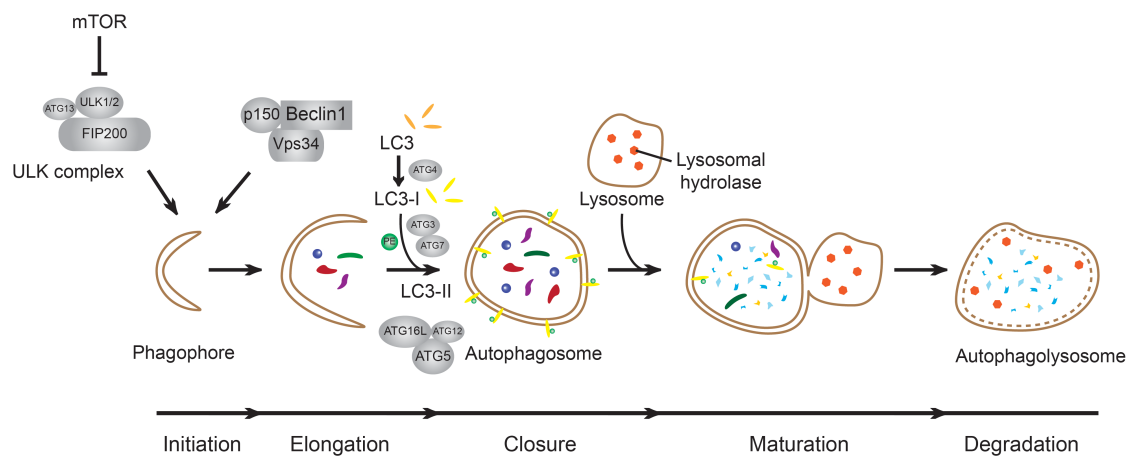


**Figure 1.4** Autophagy and its regulation.

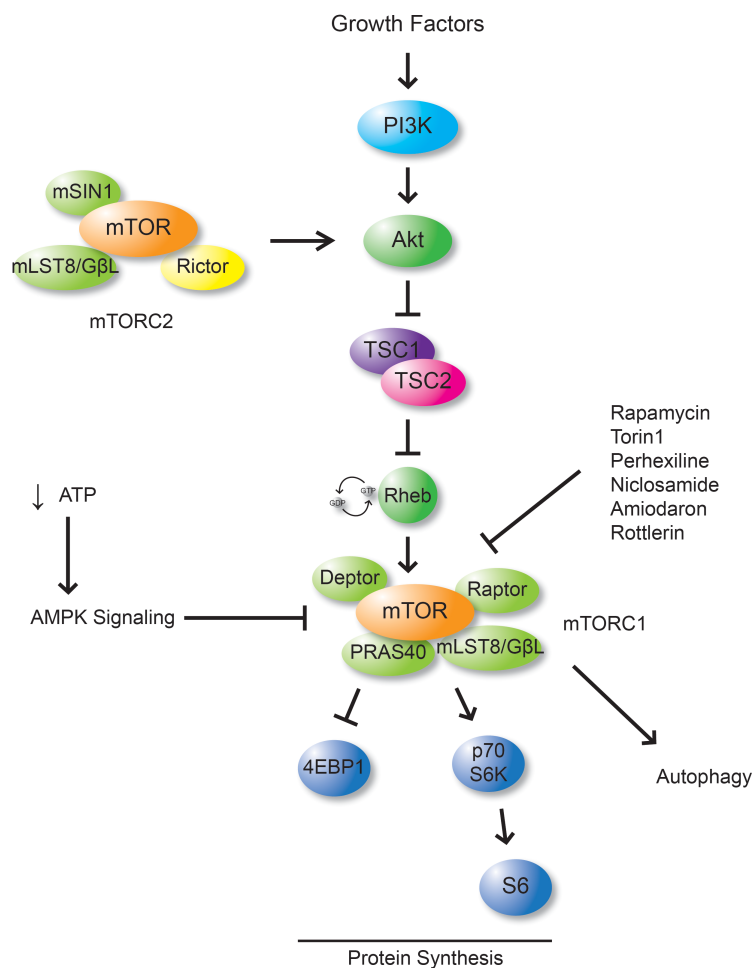


**Figure 1.5** The mTOR signaling pathway.

COIBAMIDE A INDUCES mTOR-INDEPENDENT AUTOPHAGY AND CELL DEATH  
IN HUMAN GLIOBLASTOMA CELLS

CHAPTER TWO

Andrew M. Hau, Jeffrey A. Greenwood, Christiane V. Löhr, Jeffrey D. Serrill, Philip J.  
Proteau, Ian G. Ganley, Kerry L. McPhail, Jane E. Ishmael

### Abstract

Coibamide A is an *N*-methyl-stabilized lariat macrocycle that was isolated from a marine cyanobacterium as part of an International Cooperative Biodiversity Groups (ICBG) program based in Panama. Previous testing of coibamide A in the NCI *in vitro* 60 cell line panel revealed a potent anti-proliferative response and “COMPARE-negative” profile indicative of a unique mechanism of action. We report that coibamide A is a more potent and efficacious cytotoxin than was previously appreciated, inducing concentration- and time-dependent cytotoxicity ( $EC_{50} < 100$  nM) in human U87-MG and SF-295 glioblastoma cells and mouse embryonic fibroblasts (MEFs). This activity was lost upon linearization of the molecule highlighting the importance of the cyclized structure for both anti-proliferative and cytotoxic responses. We show that coibamide A induces autophagosome accumulation in U87-MG glioma and MEFs via an mTOR-independent mechanism; no change was observed in the phosphorylation state of ULK1 (Ser-757), p70 S6K1 (Thr389), S6 ribosomal protein (Ser-235/236) and 4EBP-1 (Thr-37/46). Coibamide A also induces morphologically distinct forms of cell death according to cell type. SF-295 glioblastoma cells showed caspase-3 activation and evidence of apoptotic cell death in a pattern that was also seen in wild-type and autophagy-deficient (ATG5 null) MEFs. In contrast, U87-MG glioblastoma cells underwent caspase-independent cell death characterized by extensive cytoplasmic vacuolization and a lack of apoptotic features. Cell death was attenuated, but still triggered, in Apaf-1 null MEFs lacking a functional mitochondria-mediated apoptotic pathway. From the study of ATG5 null MEFs we conclude that a conventional autophagy response is not required for coibamide A-induced cell death, but likely occurs in dying cells in response to treatment. Coibamide A represents a natural product scaffold with potential for the study of mTOR-independent signaling and cell death mechanisms in apoptotic-resistant cancer cells.

## Introduction

There is high demand for new small molecules that can strategically target the dysregulated signaling pathways that underlie aggressive solid cancers such as glioblastoma. Glioblastoma multiforme (GBM), classed by the World Health Organization (WHO) as a high-grade IV astrocytoma-like tumor, is the most common malignant primary tumor of the central nervous system and is associated with a particularly poor prognosis. The present therapeutic strategies have had little impact on the overall survival rate, with the median patient survival times remaining between 14 and 19 months depending on the treatment regimen [1,2,3]. Collective efforts to classify the pathogenesis of gliomas have shown that GBM frequently harbors a signature of mutations that tend to attenuate the function of tumor suppressor genes, such as p53 and PTEN, or enhance activation of receptor tyrosine kinases such as epidermal growth factor receptor (EGFR) and platelet-derived growth factor receptor (PDGFR) (reviewed in [3,4]). In turn, cell signaling driven by growth factors, such as the mitogen-activated protein kinase (MAPK) and phosphatidylinositol 3-kinase (PI3K) pathways, is dramatically enhanced. Together these aberrant signaling networks tend to promote cell survival and lend GBM a natural resistance to apoptosis, rendering conventional chemotherapeutic drugs that typically induce apoptosis ineffective for the treatment of this condition [3]. Consequently, there is a great need for new pharmacologic tools that cause cell death in glioblastoma and other apoptosis-resistant cancer cells.

As part of the ICBG program based in Panama, we previously reported the discovery of an *N*-methyl-stabilized cyclopeptide natural product, coibamide A [5]. Coibamide A, named for its isolation from a marine cyanobacterium collected from the Coiba National Park, displayed an unprecedented profile in the National Cancer Institute 60 (NCI-60) human cancer cell line panel, showing sub-nanomolar potency as a growth inhibitory agent in many of the cell lines tested. Coibamide A was deemed “COMPARE-negative”, in that the pattern of cellular responses to coibamide A showed no significant correlation with any known agents in the NCI database. Initial characterization of the biological effects of coibamide A indicated that it did not interfere with tubulin or actin in cytoskeletal assays, or inhibit histone deacetylase

activity. However, coibamide A was found to arrest cell cycle progression of MDA-MB-435 cancer cells at the G<sub>1</sub> phase indicative of the antiproliferative action of this cyanobacterial depsipeptide [5].

Coibamide A previously showed histological selectivity for several cancer cell types, with all six human glioma lines in the NCI's *in vitro* cell panel showing high sensitivity [5]. When considered together, coibamide A produced mean cytostatic (GI<sub>50</sub> and TGI) and cytotoxic (LC<sub>50</sub>) values in the CNS cell lines as follows: GI<sub>50</sub> = 4.93 ± 6.31 nM [log GI<sub>50</sub>, -8.60 (0.80)]; TGI = 3.86 ± 1.32 μM [log TGI, -6.25 (3.12)] and LC<sub>50</sub> values estimated as greater than 10 μM [log LC<sub>50</sub>, -5.00 (0)]. Given the potential of coibamide A as an experimental anticancer agent, the objective of the present study was to investigate the cytotoxic potential of coibamide A against glioma cells. We focused on two human glioblastoma cell lines: U87-MG, a well characterized, grade IV astrocytoma and, SF-295, representing one of the CNS tumor lines in the NCI-60 panel, and also utilized mouse embryonic fibroblasts (MEFs) derived from wild-type and genetically-modified animals. We report that coibamide A induces a rapid and sustained autophagic response via an mTOR-independent pathway, and is also a more potent and efficacious cytotoxic agent against human glioma cells than was previously appreciated. We show that autophagy is not required for coibamide A-induced cell death that, depending on the cellular context, can proceed via apoptotic or non-apoptotic pathways.

## Materials and Methods

**Reagents.** The isolation of coibamide A and preparation of linearized coibamide A products has been described previously [5]. Purified coibamide A was reconstituted in 100% DMSO (2.0-2.3 mM), aliquoted and stored in amber borosilicate glass vials at -20°C for up to 6 months for use in biological studies. AZD 8055 was a kind gift from Professor Dario Alessi. Rapamycin, bafilomycin A1 and 3-(4,5-dimethylthiazol-2-yl)-2,5-diphenyltetrazolium bromide (MTT) were purchased from Sigma-Aldrich Corp. (St. Louis, MO). The caspase inhibitor Z-VAD-FMK was from EMD Millipore (Billerica, MA). Cell culture-grade DMSO was used as the vehicle for all treatments and never exceeded a final concentration of 0.1%. General reagents were purchased from Sigma-Aldrich Corp.

**Antibodies and vital stains.** Primary and secondary antibodies were from commercial sources and used according to the recommendations of the supplier. For immunoblot analysis, antibodies to LC3-A/B (#4108), GAPDH (#2118), phospho-ULK1 Thr-757 (#6888), phospho-p70 S6 Kinase Thr-389 (#9205), p70 S6 Kinase (#2408), phospho-S6 ribosomal protein Ser-235/236 (#4348), total S6 ribosomal protein (#2217), phospho-4E-BP1 Thr-37/46 (#2855), 4E-BP1 (#9452), both full length and the 89 kDa fragment of PARP1 (#9532), the cleaved 89 kDa fragment of PARP1 (#9544), and caspase-3 (#9662) were from Cell Signaling Technology, Inc. (Davers, MA). The antibody to EGF receptor (#sc-03) was from Santa Cruz Biotechnology, Inc., (Santa Cruz, CA), alpha-tubulin (#cp-06) was from EMD Millipore and antibodies to ULK1 (#A7481) and actin (#A5060) were from Sigma-Aldrich. Secondary antibodies coupled to horseradish peroxidase (HRP) were from EMD Millipore or Thermo Fischer Scientific Inc. (Waltham, MA). For immunocytochemistry of endogenous LC3 we used a mouse monoclonal antibody (#M152-3B) from MBL International (Woburn, MA), with an Alexa Fluor 594-coupled goat anti-mouse secondary antibody (#A-11005) from Molecular Probes-Invitrogen (Life Technologies, Grand Island, NY). ProLong Gold mounting medium with DAPI counterstain and monodansylcadaverine (MDC) were also from Invitrogen.



**Cell culture.** Human U87-MG glioblastoma cells and mouse neuroblastoma Neuro-2A cells were purchased from the American Type Culture Collection (ATCC, Manassas, VA). Human SF-295 glioblastoma cells were obtained from the National Cancer Institute (NCI) cell line repository (Frederick, MD). ATG5 null MEF cells were a kind gift from Dr. Noboru Mizushima, Tokyo Medical and Dental University, and Apaf-1-null MEFs a kind gift from Dr. Tak Mak at the University of Toronto. U87-MG cells and MEFs were routinely maintained in Dulbecco's Modified Eagle's Medium (DMEM; MediaTech Inc., Manassas, VA) supplemented with 10% fetal bovine serum (FBS; HyClone, Logan, UT), L-glutamine (2 mM) and 1% penicillin/streptomycin (MediaTech Inc.). Neuro-2A and SF-295 cells were cultured in RPMI-1640 medium supplemented with L-glutamine (2 mM), sodium pyruvate (1 mM), sodium bicarbonate (1.5 g/L), and penicillin/streptomycin and 10% FBS. All cell lines were routinely maintained in a humidified chamber at 37°C with 5% CO<sub>2</sub>.

**Cell viability assays.** For MTT, Trypan Blue exclusion and LDH assays, cells were seeded into 96-well flat-bottom microtiter plates (BD Biosciences, Franklin Lakes, NJ) and maintained overnight before treatment as indicated. MTT assays were based on a method described by Mosmann [6]. MTT was dissolved in phosphate-buffered saline (PBS) and added to each well at a final concentration of 0.5 mg/mL. Plates were allowed to incubate for 2 h at 37°C, after which time the medium was removed and the purple formazan product solubilized with DMSO (100 µL). The optical density of each well was determined at 550 nm using a Synergy HT microplate reader with Gen5 software (Bio-Tek Instruments, Inc, Winooski, VT). Cytotoxicity was determined in at least three independent experiments. The viabilities of vehicle-treated cells ranged from 97.6 to 104.6 % relative to untreated cells, thus the viability of untreated control cells was defined as 100%. For Trypan Blue exclusion assays, the medium was aspirated from each well at the time points indicated and the cells detached with 0.25% trypsin-EDTA (20 µL). Cells were then collected by the addition of serum-free DMEM (40 µL) mixed with Trypan Blue and the viable cells counted. LDH activity was measured as previously described [7] using a CytoTox 96® Non-Radioactive Cytotoxicity Assay (Promega) according to the manufacturer's instructions.

**Caspase activity assay.** Cells were seeded in 96-well white-walled, clear-bottom plates (Greiner Bio-One, Monroe, NC) and treated with or without coibamide A (10 nM to 300 nM) for the times indicated. Caspase-3,7 activity was measured using a luminescence-based Caspase-Glo® 3/7 assay (Promega). The Caspase-Glo® reagent, which also serves to lyse the cells, was added directly to each well (50 µL) and the resulting luminescence was measured every 10 min for 2 h using a Synergy HT microplate reader.

**Autophagy Assays.** To assess autophagic flux, cells were incubated with coibamide A (30 nM) or vehicle (DMSO) for 4 h, in the presence (+) or absence (-) of bafilomycin A (10 nM) added for the final hour of treatment. For starvation-induced autophagy, cell monolayers were washed twice and then incubated in Earle's Balanced Salt Solution (GIBCO-EBSS, Life Technologies) for 4 h.

**Epidermal Growth Factor (EGF) receptor degradation assay.** EGF receptor degradation assays were based on a method described previously [8]. On the day of the experiment, U87-MG cell monolayers were rinsed twice and then incubated in serum-free medium for 2.5 h. Coibamide A (30 nM) or DMSO (control) was then added to the plates for a further 1 h incubation. At time zero, the medium was replaced with serum-free medium plus EGF (100 ng/mL), and cyclohexamide (25 µg/mL), with either vehicle (DMSO), coibamide A (30 nM), or bafilomycin A1 (100 nM). Cells were returned to the incubator until the indicated times when they were lysed and processed for immunoblot analysis.

**Cell lysis and immunoblot analysis.** At the end of treatment cells were placed on ice, washed with PBS and lysed in ice-cold buffer containing 50 mM Tris-HCl, pH 7.5, 1 mM EDTA, 1 mM EDTA, 1% Triton X-100, 0.27 M sucrose, 50 mM sodium fluoride, 1 mM sodium orthovanadate, 5 mM sodium pyrophosphate, 1 mM PMSF and 1 mM benzamidine. For preparation of lysates from detached cells, the culture medium was removed and cells collected by gentle centrifugation at 800×g for 5 min. The cell

pellet was rinsed in PBS and then resuspended in the same lysis buffer; adherent cells from these plates were processed as above. All cell lysates were cleared by centrifugation at 16,000×g for 20 min at 4°C and the protein concentration determined using the bicinchoninic acid (BCA) method according to the manufacturer's recommendations (Thermo Fisher Scientific Inc.). For immunoblot analysis, cell lysates were adjusted for protein content and equal amounts (20 µg) separated by SDS-PAGE. Proteins were immobilized onto either Hybond-ECL (Amersham, Piscataway, NJ) or PVDF (Thermo Fisher Scientific) membranes. Membranes were blocked in 5% (w/v) non-fat dry milk in 50 mM Tris-HCl, pH 7.4, 150 mM NaCl (TBS) plus 0.1% Tween-20 (TBS-Tween), and then incubated for 16 h at 4°C with the appropriate primary antibody in 5% (w/v) or 5% (w/v) bovine serum albumin (BSA). The following day, membranes were washed in TBS-Tween (3 x 10 min) then incubated with the appropriate HRP-conjugated secondary antibody for 1 h at room temperature. Membranes were washed again in TBS-Tween (4 x 5 min), and proteins revealed using an enhanced chemiluminescence (ECL) reagent.

**Fluorescence microscopy.** For live imaging cells were grown on MatTek 35 mm glass-bottom culture dishes (MatTek Corp., Ashland, MA) in complete medium (in the presence of absence of coibamide A (20 nM), rapamycin (100 nM) or vehicle (DMSO) as indicated. The procedure for vital staining with MDC was adapted from procedures described by others [9,10]. Briefly, cells were rinsed in Hank's Buffered Salt Solution (HBSS), before incubation with MDC (50 nM) in HBSS for 10 min at 37°C. The MDC solution was then removed, the cells rinsed in HBSS and maintained in HBSS for immediate observation using a Zeiss Axiovert S100TV fluorescent microscope with a Hoechst filter set and MetaMorph imaging software. Images were captured using a Photometrics CoolSNAP HQ CCD camera.

For immunocytochemistry of LC3, cells were grown and treated on glass coverslips as indicated. At the end of the treatment cells were washed twice in PBS and fixed in 3.7% formaldehyde in PBS for 20 min at room temperature. Cells were then washed twice and incubated in DMEM/10 mM HEPES (pH 7.4) for 10 min to quench the formaldehyde. After two washes in PBS, cells were permeabilized with 0.2% NP-40 in PBS for 3 min at room temperature. Cells were washed twice, to

remove the NP-40, and then blocked for 15 min with 1% BSA in PBS (BSA/PBS). Cells were incubated with anti-LC3, diluted 1:500 in BSA/PBS, for 1 h. The coverslips were washed in BSA/PBS (3 x 10 min) and then incubated with an Alexa Fluor-conjugated secondary antibody, diluted 1:500 BSA/PBS, for 30 min at room temperature. Coverslips were again washed in BSA/PBS (3 x 10 min), mounted onto glass microscope slides and cells observed using a Nikon Eclipse Ti-S microscope equipped with a Nikon DS-digital CCD camera. Images were analyzed using NIS-Elements imaging software (Nikon Instruments).

**Transmission Electron Microscopy (TEM).** The preparation of cells for ultrastructural analysis was adapted from the method of Shingu et al [11]. Briefly, U87-MG cells were treated with or without coibamide A (20 nM) or vehicle (DMSO) as indicated. Cells were washed three times with PBS, collected by trypsinization and fixed in a solution containing 2.5% glutaraldehyde/1% paraformaldehyde in cacodylate buffer, then post-fixed with 1% buffered osmium tetroxide for 30 min. After dehydration in acetone, infiltration and embedding in Spurr's medium, the cell samples were polymerized for 24 h at 65°C. Samples were cut into ultrathin sections with a Sorvall MT-2 microtome (Thermo Fisher Scientific), and then stained with uranyl acetate and lead citrate in a Leica EM Stainer (Leica, Deerfield, IL). Sections were examined with a Phillips CM12 scanning transmission electron microscope (Phillips, Andover, MA) at an accelerating voltage of 80 kV.

**Data Analysis.** Concentration-response relationships were analyzed using GraphPad Prism Software (GraphPad Software Inc., San Diego, CA), and EC<sub>50</sub> values derived using nonlinear regression analysis fit to a logistic equation. For Trypan Blue exclusion studies, time-response relationships were analyzed with the same software and fit to a standard exponential growth curve. For analysis of EGFR degradation and LC3 flux by immunoblot, the intensity of EGFR or LC3 signals was normalized to the intensity of tubulin and quantified relative to control using Image J software ([rsbweb.nih.gov/ij](http://rsbweb.nih.gov/ij)). For quantitation of mean LC3 puncta per cell by immunocytochemistry, images were captured from two random fields of view per coverslip and LC3 puncta (Alexa Fluor 594) counted with NIS-Elements software and

compared to the total number of cells (DAPI). Statistical significance of data derived from MTT viability assays, LDH efflux and caspase activity was performed using a one-way analysis of variance (ANOVA) followed by a Student's *t*-test comparing untreated controls and treatment groups. *P*-values of 0.05 or less were considered statistically significant.

## Results

### **Cytotoxic effect of coibamide A on human glioblastoma cells**

Coibamide A produced concentration- and time-dependent cell death in human U87-MG and SF-295 glioblastoma cells. Overt cytotoxicity was not evident within the first 24 to 36 h of coibamide A exposure. When treatment times were extended however, coibamide A caused progressive rounding and detachment of both glioma cell lines from the culture plates. As illustrated in Figure 2.1A, both U87-MG and SF-295 cells showed reduced proliferation and significant changes in morphology by 72 h of exposure to coibamide A (20 nM) relative to vehicle-treated cultures. Coibamide A-induced cytotoxicity was concentration dependent with  $EC_{50}$  values of  $28.8 \pm 8.4$  nM and  $96.2 \pm 23$  nM for U87-MG and SF-295 cells, respectively (Figure 2.1B).

To examine the temporal nature of coibamide A-induced toxicity, we used Trypan Blue exclusion to monitor cell viability for up to 96 h after treatment with a fixed concentration of coibamide A (20 nM). U87-MG cells showed no change in their ability to exclude Trypan Blue until between 24 and 36 h after exposure to coibamide A, but thereafter the number of viable cells began to decrease in a time-dependent manner (Figure 2.2A). Few coibamide A-treated U87-MG cells remained viable after 96 h relative to untreated or vehicle-treated cultures. The observed loss of membrane integrity over time prompted us to also investigate the potential of coibamide A to induce release of LDH, a biomarker of membrane damage. For these studies the culture medium was collected from coibamide A-treated cells and the LDH content of the medium determined relative to total LDH in the remaining adherent cells. We found no significant increase in LDH leakage in cultures treated with 20 nM coibamide A, however LDH was significantly elevated in cultures exposed to 100 nM coibamide A (Figure 2.2B). SF-295 glioblastoma cells showed the same pattern of cytotoxicity in that the number of viable cells decreased in a time-dependent manner after 24 h (Figure 2.2C) and LDH was elevated significantly in exposed cultures (Figure 2.2D). Together these results indicate that coibamide A induces both time- and concentration-dependent cytotoxicity in human glioma cells.

### **Coibamide A induces activation of caspase-3/7 and apoptosis in a cell type-specific manner**

To provide some insight into the potential mechanism of coibamide A-induced cell death we tested the ability of coibamide A to activate the downstream effector caspases of the major apoptotic signaling pathways: caspase-3 and caspase-7. Coibamide A induced activation of caspase-3/7 in U87-MG and SF-295 glioma cells over a time frame consistent with loss of viability, however the activation profile for each cell line was distinct. Although U87-MG cells were more sensitive than SF-295 cells to coibamide A-induced cell death, as determined by MTT cell viability assays (Figure 2.1B), relatively high concentrations of coibamide A were required to induce late activation of caspase-3/7 in these cells (Figure 2.3A C). In contrast, coibamide A was a much more potent and effective activator of caspase-3/7 in the SF-295 glioma cell line (Figure 2.3B D). We therefore collected attached and detaching coibamide A-treated cells over the course of a 96 h exposure period and analyzed cell lysates for expression of PARP1, a major downstream target of caspase-dependent apoptosis and several alternative cell death pathways [12]. An 89 kDa band corresponding to the caspase 3-cleaved form of PARP1 was readily detected by 48 h indicative of apoptotic cell death in SF-295 cells, whereas only trace levels of this fragment were observed in late, detaching U87-MG cell lysates (Figure 2.3E).

Given the potential for coibamide A to induce cell type-specific caspase-3/7 activation, we investigated the influence of pharmacologic inhibition of caspase activity with the broad-spectrum caspase inhibitor Z-VAD-FMK. Co-treatment of cells with coibamide A and Z-VAD-FMK (100  $\mu$ M) produced significant inhibition of coibamide A-induced LDH efflux from U87-MG cells (Figure 2.4A). However this caspase activity appeared to be non-essential as the inhibitor failed to protect against cell death and instead tended to exacerbate coibamide A-induced cytotoxicity in U87-MG cells (Figure 2.4B). Z-VAD-FMK was also effective at suppressing coibamide A-induced LDH release from SF-295 cells (Figure 2.4C), but in this case afforded some protection from coibamide A-induced cell death (Figure 2.4D). The addition of Z-VAD-FMK attenuated the cytotoxic efficacy of coibamide A with 40% of the SF-295

population remaining viable after 72 h in response to relatively high concentrations of coibamide A (1 $\mu$ M). Taken together, these findings indicate that coibamide A can induce apoptosis via activation of a caspase-3 dependent pathway in SF-295 cells, but can also trigger caspase-independent cell death via an alternate pathway in U87-MG glioma cells.

### **Linearized forms of coibamide A lack cytotoxic potential**

Coibamide A is a lariat depsipeptide that features a highly methylated 22-membered macrocycle and tetrameric side chain (**1**; Figure 2.5A). In order to confirm the cyclization point of coibamide A, the natural product was originally subjected to base hydrolysis, producing four linear derivatives [5]. The two full-length linearized analogs were designated coibamide dehydrated seco acid (**2**; Figure 2.5A) and coibamide seco acid (**3**; Figure 2.5A). Towards the goal of determining the coibamide A pharmacophore, we studied the biological activity of **2** and **3** in U87-MG and SF-295 glioblastoma, and mouse Neuro-2A neuroblastoma cells (Figure 2.5B D). Both MTT and Trypan Blue exclusion viability assays were used to monitor the extent and pattern of toxicity in the three tumor lines for up to 96 h after treatment with coibamide A (20 nM), or 0.3  $\mu$ g/mL of linear derivatives **2** or **3** (~230-260 nM). In the native form, coibamide A produced a significant, time-sensitive reduction in the viability of U87-MG, SF-295 and Neuro-2A cells relative to vehicle or untreated control cultures (Figure 2.5B to D). However, no significant change in the viability of these three cell types was observed in response to treatment with the linearized derivatives **2** or **3** (Figure 5B to 5D). U87-MG cells remained 87% and 98% viable relative to vehicle-treated cells after 96 h exposure to **2** and **3**, respectively (Figure 2.5B). Similarly, the viability of Neuro-2A neuroblastoma cells was 98% and 107% following exposure to **2** and **3**, respectively (Figure 2.5C). When examined by Trypan Blue exclusion (shown for SF-295 cells in Figure 2.5D), those cultures treated with **2** or **3** were found to be indistinguishable from either untreated or vehicle-treated control cultures.



### **Coibamide A induces autophagosome accumulation in apoptotic-resistant U87-MG cells**

To investigate coibamide A-induced signaling further, we studied the potential of coibamide A to induce autophagy using biochemical and morphological criteria. Microtubule-associated protein light chain 3 (LC3), also termed autophagy-related (ATG) protein 8, is commonly used as a biochemical marker of autophagy because it is directly recruited to autophagosomes [13,14]. LC3 can be detected as two distinct bands by immunoblot analysis: LC3-I is the cytosolic form that migrates more slowly than LC3-II, which is recruited to the membrane of autophagosomes. We analyzed the expression of endogenous LC3 in lysates derived from adherent U87-MG cells that had been treated with coibamide A for up to 48 h. By 1 h we observed a clear increase in LC3-II expression in coibamide A-treated cells relative to control (Figure 2.6A). This increase in LC3-II expression was generally sustained through 48 h and comparable to that observed with rapamycin (Figure 2.6A), a known inducer of autophagy in glioblastoma cells [10]. We next stained treated cells with MDC, a fluorescent marker used as a probe for mature autophagosomes [15]. Vital staining of coibamide A-treated U87-MG cells with MDC, revealed increased accumulation of the dye relative to control cells (Figure 2.6B, panels a and b). Furthermore, we found this effect to be qualitatively indistinguishable from cytosolic MDC accumulation observed for cells treated with the macrolide natural product rapamycin (Figure 2.6B, panels b and c). We also utilized TEM to visualize the ultrastructure of adherent U87-MG cells following exposure to coibamide A at 16 and 48 h (Figure 2.6C). These studies revealed no evidence of nuclear condensation and segregation, or cytoplasmic shrinking expected of cells undergoing apoptosis. The nuclear membrane frequently had an undulating character to it, but was discernable as an intact double-membrane. Cells exposed to coibamide A for 16 h showed small electron lucent vacuoles that were absent in control cells (Figure 2.6C, panels a and b). Empty vacuoles were also observed at 48 h by TEM, with 20% of cells containing one or more large ( $> 2 \mu\text{m}$ ) cytoplasmic vacuole (Figure 2.6C, panel c). At higher magnification (Figure 2.6C, panels d and e) empty vacuoles lacking an organized double-membrane could be clearly distinguished from autophagosomes (A), that were delineated by a smooth

double-membrane containing cellular material, intact mitochondria (M) and more electron-dense lysosomal (L) structures.

As an apparent increase in autophagosome number could be the result of increased formation, or decreased degradation of autophagosomes, we employed a standard technique to assess autophagic flux in U87-MG cells in response to coibamide A exposure. For these studies cells were treated with or without coibamide A for 4 h, in the presence or absence of the macrolide natural product bafilomycin A1 for the last hour of treatment. Bafilomycin A1 is a potent inhibitor of the vacuolar-type  $H^+$ -ATPase that is required for fusion of autophagosomes with lysosomes and thus blocks lysosomal degradation of LC3 [16,17]. Under these conditions, immunoblot analysis revealed an increase in endogenous LC3-II in response to coibamide A that was enhanced further by the addition of bafilomycin A1 (Figure 2.7A B). In control cultures, bafilomycin A1 alone also produced a clear increase in LC3-II reflecting the basal level of autophagic flux in U87-MG cells (Figure 2.7A and B). The magnitude of this increase was essentially equivalent to that seen in coibamide A treated cells, when comparing the intensity of the LC3-II signal in the absence and presence of bafilomycin A1 (Figure 2.7A and B). Thus, coibamide A did not appear to change the overall rate of autophagic flux through the pathway. We used this same experimental design to study the staining pattern of endogenous LC3 in U87-MG cells using fluorescence microscopy. We found that coibamide A treatment induced a punctate distribution of LC3, particularly in the peri-nuclear region of the cytoplasm, and this was consistently enhanced by the addition of bafilomycin A1 (Figure 2.7C and D). The magnitude of the increase in the number of LC3 puncta per cell, seen in the presence of bafilomycin A1, was the same in control and coibamide A treated cells (Figure 2.7C and D). Thus, in accordance with our Western blot analyses, these data suggest that although coibamide A induces an autophagic response in U87-MG cells, the rate of autophagosome formation and degradation in coibamide A-treated cells remains equivalent.

### **Coibamide A does not change the rate of EGF receptor degradation**

Autophagy requires a coordinated series of specific endomembrane fusion events to traffic the contents of autophagosomes to the lysosomes for degradation.

We therefore assessed the potential of coibamide A to interfere with a major endocytic-lysosomal pathway by studying turnover of endogenous EGFR. For these studies, U87-MG cells were serum-starved to promote localization of EGFR to the plasma membrane and were then chased with EGF (100 ng/mL), to induce internalization of EGFR, plus cycloheximide (25  $\mu$ g/mL) to inhibit protein synthesis. In the presence of coibamide A, ligand-induced EGFR degradation progressed at a rate that could not be distinguished from vehicle-treated control cells (Figure 2.8A and B). This finding was in contrast to U87-MG cells cultured in the presence of bafilomycin A1. Bafilomycin A1 dramatically inhibited endocytosis-mediated degradation of EGFR over the time course of these experiments (Figure 2.8A and B), in a manner consistent with its ability to block lysosomal degradation of EGFR. Taken together our findings indicate that the autophagic-lysosomal pathway remains functional in U87-MG cells in the presence of coibamide A and that coibamide A does not produce a global block in endocytosis.

### **Coibamide A induces a conventional form of autophagy in Mouse Embryonic Fibroblasts**

The best-characterized form of macroautophagy in mammalian cells is that which is dependent on ATG5, an essential component of the protein complex that regulates formation of the autophagosome [18] [19]. As an initial evaluation of coibamide A-induced responses in MEFs revealed that this cell type was also vulnerable to coibamide A-induced cell death (Figure S2.1), we evaluated the potential of coibamide A to induce autophagosome accumulation in both immortalized wild-type and ATG5 null MEFs. For these studies, cells were treated with or without coibamide A for 4 h in the presence or absence of bafilomycin A1 for the last hour of treatment. Under these conditions, wild-type MEFs showed a clear increase in endogenous LC3-II in response to coibamide A and this signal was enhanced further by the addition of bafilomycin A1. In contrast, endogenous LC3-II was not detected in ATG5 null MEFs in response to any of the treatment conditions (Figure 2.9A and B). When visualized using fluorescence microscopy, control wild-type MEFs showed relatively few LC3 puncta, whereas coibamide A-treated cells showed numerous LC3 puncta per cell (Figure 2.9C and D). Furthermore, the number of LC3 puncta per cell

was enhanced when wild-type MEFs were exposed to coibamide A in the presence of bafilomycin A1 (Figure 2.9C and D). These data indicate that coibamide A induces autophagosome formation in an ATG5-dependent manner but, consistent with the findings in U87-MG cells, does not dramatically alter the rate of autophagic flux in MEFs inasmuch as the rate of autophagosome formation is generally equivalent to the rate of degradation in coibamide A-treated cells.

### **Coibamide A-induced autophagy is mTOR-independent**

To explore the molecular mechanisms underlying coibamide A-induced signaling, we compared coibamide A responses to both starvation- and pharmacologically-induced autophagy in MEF and U87-MG cells. For these studies we incubated cells in EBSS starvation medium for 4 h, or treated cells with either coibamide A (30 nM) or the dual mTOR complex inhibitor, AZD 8055 [20,21] (300 nM), in standard nutrient-rich medium for 4 h. Cell lysates were then analyzed to determine the impact of coibamide A on the mTORC1 protein kinase complex. We evaluated the phosphorylation state of the major mTORC1 target site on ULK1, Ser-757, and found no decrease in phosphorylation of this residue in coibamide A-treated cells (Figure 2.10). In contrast, starved and AZD 8055-treated control MEFs and U87-MG glioma cell lysates showed dephosphorylation of Ser-757 or a corresponding shift in the mobility of total ULK1, consistent with an mTOR-mediated response (Figure 2.10). We also examined the downstream effectors of mTORC1 in MEFs and U87-MG cell lysates and found no decrease in the phosphorylation state of p70 S6K1 (Thr389), S6 ribosomal protein (Ser-235/236) and 4EBP-1 (Thr-37/46) in these cells in response to coibamide A treatment (Figure 2.10). These results indicate that coibamide A is not an inhibitor of the mTORC1 protein complex and likely regulates autophagy via an mTOR-independent signaling pathway.

### **Coibamide A induces cell death in the absence of ATG5 and intrinsic apoptotic activating factor 1 (Apaf-1)**

To investigate the relationship between autophagy and coibamide A-induced cell death we compared coibamide A-induced cytotoxicity in wild-type and ATG5 null MEFs, to coibamide A-induced responses in MEFs lacking the adapter protein Apaf-

1. Apaf-1 null MEFs have previously been shown to be resistant to a variety of apoptotic stimuli, as Apaf-1 is a critical component of the apoptosome complex driving the intrinsic apoptotic pathway [22]. Consistent with our findings in CNS cancer cell types and wild-type MEFs, we found coibamide A to induce time- and concentration-dependent cytotoxicity in both knockout MEF lines. Coibamide A was equally efficacious in its ability to induce cell death in wild-type and ATG5 null MEFs, with essentially no viable cells remaining after a 48 h exposure to coibamide A concentrations of 100 nM or greater (Figure 2.11A). Under the same conditions, coibamide A had more limited efficacy against Apaf-1 null MEFs yet still induced significant cell death; approximately 50% of Apaf-1 null MEFs remained viable by 48 h in the presence of coibamide A (100 nM or greater) (Figure 2.11A). When the attached and detached coibamide A-treated MEF populations were collected and subjected to immunoblot analysis we observed distinct patterns of coibamide A-induced cell death. An 89 kDa fragment of PARP1, corresponding to the caspase 3-cleaved form of this protein, was expressed in both wild-type and ATG5 null MEFs, with concomitant detection of cleaved caspase 3 (Figure 2.11B). In addition, coibamide A-treated wild-type MEFs showed enhanced levels of endogenous LC3-II in both attached and detached cells, whereas LC3-II immunoreactivity was absent in the equivalent populations of treated ATG5 null MEFs (Figure 2.11B). Coibamide A-treated Apaf-1 null MEFs, however, did show an autophagy response with enhanced levels of endogenous LC3-II in both attached and detached cell populations (Figure 2.11B). We found no evidence of caspase-3 activation in these cells in response to coibamide A treatment (Figure 2.11B), consistent with the pattern of caspase-independent cell death observed in U87-MG glioma cells (Figure 2.4B and Figure S2.2). Together these results indicate that coibamide A can induce caspase-mediated apoptotic cell death in the presence or absence of an autophagy response, and can also trigger cell death in the absence of Apaf-1.

## Discussion

Coibamide A is a marine natural product that represents a lead structure in anti-cancer drug discovery [5]. In the present study we investigated the cytotoxic potential of coibamide A against human glioblastoma cells and immortalized MEFs from genetically manipulated animals. Using several independent measures of general cytotoxicity we found that coibamide A dramatically reduced the viability of U87-MG and SF-295 glioma cells in both a concentration- and time-dependent manner. Exposure to coibamide A (100 nM or less) resulted in: a progressive decrease in the ability of cells to reduce MTT, a loss of plasma membrane integrity and detachment of cells from culture dishes. This potent nanomolar activity was lost upon linearization of the molecule, indicating the importance of the intact lariat macrocycle for inducing growth inhibitory and cytotoxic responses. Our more detailed analysis of the mechanisms by which coibamide A induces cell death showed that distinct signaling pathways can be initiated according to cell type. SF-295 glioblastoma cells underwent caspase-3 activation and apoptosis in response to coibamide A, in a pattern that was also seen in wild-type and autophagy-deficient MEFs. In contrast, U87-MG glioblastoma cells, which were approximately three-fold more sensitive to coibamide A, underwent a form of caspase-independent cell death that was exacerbated by the caspase inhibitor Z-VAD-FMK and characterized by extensive cytoplasmic vacuolization and a lack of apoptotic features. Further analysis of Apaf-1 null MEFs revealed that coibamide A can indeed trigger significant cell death in the absence of the cytochrome *c*-mediated apoptotic pathway. Taken together, our studies provide the first insight into the potential of coibamide A to induce two morphologically distinct forms of cell death in a cancer cell type that is typically treatment resistant.

A notable feature of the cellular response to coibamide A was the finding that coibamide A induces early autophagosome accumulation without inhibition of the mTOR pathway. We used a variety of approaches including analysis of the phosphorylation state of mTOR target proteins, analysis of LC3 flux in U87-MG and wild-type and mutant MEFs, plus analysis of endocytosis-mediated EGFR

degradation to conclude that this is likely a specific mTOR-independent cellular response. Autophagy is a highly regulated process that is tightly linked to the nutrient-sensing pathway of the cell [23]. During cellular stress or starvation, cells undergo a form of self-eating whereby cytoplasmic components are engulfed by double-membrane bound vesicles known as autophagosomes. Autophagosomes subsequently fuse with lysosomes forming the autolysosome and thereby promoting the degradation of its contents by lysosomal hydrolases. This process provides both a source of energy for the cell and an alternative to the ubiquitin-proteasome system that function in removal of organelles and aggregated proteins [23]. Multiple signal transduction mechanisms are known to regulate autophagy and these can be broadly classified as those that signal via the mammalian target of rapamycin (mTOR) pathway (mTOR-dependent), and those that do not (mTOR-independent). mTOR is a serine/threonine kinase that functions in the context of two distinct protein complexes: mTOR complex 1 (mTORC1) and mTOR complex 2 (mTORC2). We compared the action of coibamide A to that of two pharmacologic inducers of autophagy: rapamycin which is an effective, but incomplete, inhibitor of mTORC1 [24,25], and AZD 8055 which inhibits both mTOR complexes [20,21]. Although initial comparisons of rapamycin- and coibamide A-induced effects in U87-MG cells revealed increases in LC3-II and a pattern of MDC staining that were qualitatively similar, we found no evidence for inhibition of the mTOR pathway after analysis of the phosphorylation state of key residues on ULK1, p70 S6K1, S6 ribosomal protein and 4EBP-1, relative to starvation- and AZD 8055-induced autophagy. This lack of mTOR inhibition, together with the observation that the overall rate of autophagic flux was not changed dramatically by coibamide A, supports our observation that cytotoxicity was somewhat delayed in response to coibamide A. Had the energy status of the cell been compromised within hours of coibamide A exposure, indirect inhibition of the mTOR pathway could have been anticipated through activation of AMP-activated protein kinase (AMPK), the cellular sensor of energy stress [26]. Taken together, our results place coibamide A with a growing list of autophagy modulators that signal independently of mTOR. Further work will be required to determine if coibamide A acts via a known mTOR-independent pathway or via a new target.

Based on our study of ATG5 null MEFs, our results indicate that autophagy is not required for coibamide A-induced cell death even though autophagy persisted in cells dying via apoptotic or non-apoptotic mechanisms in response to treatment. This finding is consistent with the current consensus that autophagy is usually a survival response by the cell that may change the rate of cell death but rarely initiates cell death [27]. Defective autophagy has now been implicated in many chronic human diseases including cancer and neurodegenerative conditions [28,29]. Furthermore, different cancers have varying susceptibility to the signaling pathways that are currently known to regulate mammalian autophagy. This raises the issue of whether autophagy is a positive or negative regulator of cancer cell survival [30,31]. As the molecular target of coibamide A is not yet known, the potential separation of autophagic and cytotoxic responses following coibamide A exposure represents a significant step as many small molecules induce autophagy in normal and cancer cell types, but do not necessarily cause cell death. For example, rapamycin has long been considered to be a potent cytostatic natural product, rather than a cytotoxic, agent [32]. Similarly, a recent comparison of rapamycin, rottlerin and three drugs approved for human use (amiodarone, niclosamide and perhexiline), highlights the fact that transient induction of autophagy under conditions of nutrient sufficiency is not harmful to the cell [33]. All five compounds were capable of stimulating mTOR-dependent autophagy but only amiodarone induced cell death, leading the authors to conclude that, in the case of amiodarone, cytotoxicity is likely a consequence of activity at cellular targets other than mTORC1 [33].

Our results demonstrate that coibamide A is a more potent cytotoxin against human glioblastoma cells than was previously appreciated [5]. As coibamide A was found to be cell cycle active [5], we exposed cells beyond the 48 h that is routinely used in the NCI in vitro drug discovery screen to reveal a clear concentration-dependent cytotoxic response. Cell death in response to coibamide A was apoptotic in SF-295 glioma cells, yet proceeds via a caspase-independent, non-apoptotic pathway in U87-MG glioma cells. The genetic background of U87-MG cells is classified as PTEN-deficient with normal p53 function, whereas SF-295 cells are deficient in both p53 and PTEN signaling pathways. Mutations in these two genes occur very frequently in GBM; analysis of 601 genes from 91 GBM patient samples,



recently completed as part of The Cancer Genome Atlas project, showed the incidence of *TP53* and *PTEN* mutations to be 42% and 33%, respectively [4]. Of the six glioma cell lines represented in the NCI60 panel against which coibamide A was tested, four (SF-295, SF-539, U251, SNB-19) are characterized as being variant in both PTEN and p53 pathways, whereas two (SNB-75, SF-268) have variations in the p53 pathway, but normally functioning PTEN. Taken together these data suggest that coibamide A may be an effective cancer cell toxin regardless of p53 and PTEN status.

With increasing recognition of alternate cell death pathways, the inherent ability of a small molecule to induce more than one mode of cell death may be a particularly useful pharmacological property in cancer therapeutics [34]. The histone deacetylase inhibitor, suberoylanilide hydroxamic acid (SAHA), for instance, is a strong inducer of autophagy and caspase-dependent apoptotic cell death in several cell types [35,36]. However, non-apoptotic cell death still occurs when caspase activation is blocked via pharmacologic or genetic manipulation of these cells [35,36]. Furthermore, inhibition of autophagy can enhance both apoptotic and non-apoptotic forms of SAHA-induced cell death defining a general protective role of autophagy in response to SAHA treatment [36]. Sanguilutine is another small molecule that has been reported to induce autophagy in human A-375 melanoma cells with cell death mediated by a non-apoptotic caspase-independent pathway [37]. In addition, the marine algal toxin, yessotoxin, has been shown to induce autophagy and cell death through both apoptotic and non-apoptotic pathways in numerous model cell systems [38]. Together with coibamide A, these small molecule cytotoxins may be useful pharmacological tools for studying non-apoptotic cell death particularly in cancer cells.

Natural products from terrestrial and marine organisms have a track record of potent cancer cell toxicity that has led to the development of several as clinical candidates [39]. Notable historical examples are anti-tubulin agents, the cryptophycins, dolastatins 10 and 15 and curacin A [39,40]. Marine cyanobacteria in particular have continued to be a prolific source of cytotoxic depsipeptides applicable to cancer research and pharmaceutical development [41,42]. The peptidic molecular structure of coibamide A is stabilized by a high degree of methylation that favors cell

membrane permeability and proteolytic stability. Our data also indicate that cyclization of the peptide is a critical determinant of the cellular response to coibamide A, with two linear forms showing no cytotoxicity to glio- and neuroblastoma cells. This phenomenon has guided ongoing efforts to chemically synthesize biologically active analogs of coibamide A. Our findings are also in contrast to the example of desmethoxy-majusculamide C (DMMC), a cyclic depsipeptide isolated from a Fijian *Lyngba majuscula* marine cyanobacterium [43]. DMMC is a potent disrupter of the actin cytoskeleton, which exhibits nanomolar cytotoxicity in linear form that is equivalent to the activity of the intact cyclic natural product.

In summary, coibamide A is an unusual cyclopeptide that potently inhibits cell growth and induces cell death in human glioblastoma cells. Although the molecular target of coibamide A has still to be established, our findings provide insight into a new marine natural product structure that may be an invaluable tool for the study of both mTOR-independent autophagy and cell death signaling in apoptotic-resistant cancer cells. Our clarification of the cytotoxic potential of coibamide A, together with the identification of MEFs as a sensitive cell type, will facilitate further evaluation of coibamide A as an anti-cancer structure.

### Acknowledgments

We thank the Autoridad Nacional del Ambiente (ANAM), Panama for permission to make recollections of the coibamide A-producing cyanobacterium, Chris Thornburg, Marcy Balunas and Roger Linington for recollection of the cyanobacterium, and the Smithsonian Tropical Research Institute for facilitating this research. We also thank Dario Alessi for helpful discussions, and Teresa Sawyer of the OSU Electron Microscopy Facility for expert technical assistance. Financial support was provided by: the NIH Fogarty International Center ICBG grant TW006634-06, the Medical Research Foundation of Oregon, the American Foundation for Pharmaceutical Education and the OSU College of Pharmacy and Division of Health Sciences. We are also grateful for services provided by the Cell Imaging and Analysis Facilities and Services Core of the OSU Environmental Health Sciences Center (NIEHS grant P30-ES000210).

### Bibliography

1. Brown PD, Krishnan S, Sarkaria JN, Wu W, Jaeckle KA, et al. (2008) Phase I/II trial of erlotinib and temozolomide with radiation therapy in the treatment of newly diagnosed glioblastoma multiforme: North Central Cancer Treatment Group Study N0177. *Journal of clinical oncology* 26: 5603-5609.
2. Prados MD, Chang SM, Butowski N, DeBoer R, Parvataneni R, et al. (2009) Phase II study of erlotinib plus temozolomide during and after radiation therapy in patients with newly diagnosed glioblastoma multiforme or gliosarcoma. *Journal of clinical oncology* 27: 579-584.
3. Krakstad C, Chekenya M (2010) Survival signalling and apoptosis resistance in glioblastomas: opportunities for targeted therapeutics. *Molecular cancer* 9: 135.
4. Brennan C (2011) Genomic profiles of glioma. *Current neurology and neuroscience reports* 11: 291-297.
5. Medina RA, Goeger DE, Hills P, Mooberry SL, Huang N, et al. (2008) Coibamide A, a potent antiproliferative cyclic depsipeptide from the Panamanian marine cyanobacterium *Leptolyngbya* sp. *J Am Chem Soc* 130: 6324-6325.
6. Mosmann T (1983) Rapid colorimetric assay for cellular growth and survival: application to proliferation and cytotoxicity assays. *Journal of immunological methods* 65: 55-63.
7. Collins A, Larson MK, Pfaff JE, Ishmael JE (2007) Survival of Swiss-Webster mouse cerebellar granule neurons is promoted by a combination of potassium channel blockers. *Toxicol Lett* 171: 60-68.
8. Ganley IG, Wong PM, Gammoh N, Jiang X (2011) Distinct autophagosomal-lysosomal fusion mechanism revealed by thapsigargin-induced autophagy arrest. *Molecular cell* 42: 731-743.
9. Munafo DB, Colombo MI (2001) A novel assay to study autophagy: regulation of autophagosome vacuole size by amino acid deprivation. *J Cell Sci* 114: 3619-3629.
10. Takeuchi H, Kondo Y, Fujiwara K, Kanzawa T, Aoki H, et al. (2005) Synergistic augmentation of rapamycin-induced autophagy in malignant glioma cells by phosphatidylinositol 3-kinase/protein kinase B inhibitors. *Cancer Res* 65: 3336-3346.
11. Shingu T, Fujiwara K, Bogler O, Akiyama Y, Moritake K, et al. (2009) Inhibition of autophagy at a late stage enhances imatinib-induced cytotoxicity in human malignant glioma cells. *International journal of cancer* 124: 1060-1071.
12. Oliver FJ, de la Rubia G, Rolli V, Ruiz-Ruiz MC, de Murcia G, et al. (1998) Importance of poly(ADP-ribose) polymerase and its cleavage in apoptosis. Lesson from an uncleavable mutant. *J Biol Chem* 273: 33533-33539.
13. Mizushima N, Yoshimori T (2007) How to interpret LC3 immunoblotting. *Autophagy* 3: 542-545.
14. Barth S, Glick D, Macleod KF (2010) Autophagy: assays and artifacts. *The Journal of pathology* 221: 117-124.
15. Bampton ET, Goemans CG, Niranjana D, Mizushima N, Tolkovsky AM (2005) The dynamics of autophagy visualized in live cells: from autophagosome formation to fusion with endo/lysosomes. *Autophagy* 1: 23-36.

16. Bowman EJ, Siebers A, Altendorf K (1988) Bafilomycins: a class of inhibitors of membrane ATPases from microorganisms, animal cells, and plant cells. *PNAS* 85: 7972-7976.
17. Yamamoto A, Tagawa Y, Yoshimori T, Moriyama Y, Masaki R, et al. (1998) Bafilomycin A1 prevents maturation of autophagic vacuoles by inhibiting fusion between autophagosomes and lysosomes in rat hepatoma cell line, H-4-II-E cells. *Cell structure and function* 23: 33-42.
18. Mizushima N, Sugita H, Yoshimori T, Ohsumi Y (1998) A new protein conjugation system in human. The counterpart of the yeast Apg12p conjugation system essential for autophagy. *J Biol Chem* 273: 33889-33892.
19. Mizushima N, Yamamoto A, Hatano M, Kobayashi Y, Kabeya Y, et al. (2001) Dissection of autophagosome formation using Apg5-deficient mouse embryonic stem cells. *The Journal of cell biology* 152: 657-668.
20. Chresta CM, Davies BR, Hickson I, Harding T, Cosulich S, et al. (2010) AZD8055 is a potent, selective, and orally bioavailable ATP-competitive mammalian target of rapamycin kinase inhibitor with in vitro and in vivo antitumor activity. *Cancer research* 70: 288-298.
21. Sini P, James D, Chresta C, Guichard S (2010) Simultaneous inhibition of mTORC1 and mTORC2 by mTOR kinase inhibitor AZD8055 induces autophagy and cell death in cancer cells. *Autophagy* 6.
22. Reubold TF, Eschenburg S (2012) A molecular view on signal transduction by the apoptosome. *Cellular signalling* 24: 1420-1425.
23. Kraft C, Peter M, Hofmann K (2010) Selective autophagy: ubiquitin-mediated recognition and beyond. *Nature cell biology* 12: 836-841.
24. Thoreen CC, Kang SA, Chang JW, Liu Q, Zhang J, et al. (2009) An ATP-competitive mammalian target of rapamycin inhibitor reveals rapamycin-resistant functions of mTORC1. *J Biol Chem* 284: 8023-8032.
25. Thoreen CC, Sabatini DM (2009) Rapamycin inhibits mTORC1, but not completely. *Autophagy* 5: 725-726.
26. Mihaylova MM, Shaw RJ (2011) The AMPK signalling pathway coordinates cell growth, autophagy and metabolism. *Nature cell biology* 13: 1016-1023.
27. Shen HM, Codogno P (2011) Autophagic cell death: Loch Ness monster or endangered species? *Autophagy* 7: 457-465.
28. Wong E, Cuervo AM (2010) Autophagy gone awry in neurodegenerative diseases. *Nature neuroscience* 13: 805-811.
29. Sheen JH, Zoncu R, Kim D, Sabatini DM (2011) Defective regulation of autophagy upon leucine deprivation reveals a targetable liability of human melanoma cells in vitro and in vivo. *Cancer cell* 19: 613-628.
30. Yang Z, Klionsky DJ (2010) Mammalian autophagy: core molecular machinery and signaling regulation. *Current opinion in cell biology* 22: 124-131.
31. Fan QW, Weiss WA (2011) Autophagy and Akt promote survival in glioma. *Autophagy* 7: 536-538.
32. Hosoi H, Dilling MB, Liu LN, Danks MK, Shikata T, et al. (1998) Studies on the mechanism of resistance to rapamycin in human cancer cells. *Molecular pharmacology* 54: 815-824.
33. Balgi AD, Fonseca BD, Donohue E, Tsang TCF, Lajoie P, et al. (2009) Screen for Chemical Modulators of Autophagy Reveals Novel Therapeutic Inhibitors of mTORC1 Signaling. *PLoS One* 4: e7124.

34. Kreuzaler P, Watson CJ (2012) Killing a cancer: what are the alternatives? *Nature reviews Cancer* 12: 411-424.
35. Shao Y, Gao Z, Marks PA, Jiang X (2004) Apoptotic and autophagic cell death induced by histone deacetylase inhibitors. *PNAS* 101: 18030-18035.
36. Gammoh N, Lam D, Puente C, Ganley I, Marks PA, et al. (2012) Role of autophagy in histone deacetylase inhibitor-induced apoptotic and nonapoptotic cell death. *PNAS* 109: 6561-6565.
37. Hammerova J, Uldrijan S, Taborska E, Vaculova AH, Slaninova I (2012) Necroptosis modulated by autophagy is a predominant form of melanoma cell death induced by sanguilutine. *Biological chemistry* 393: 647-658.
38. Korsnes MS (2012) Yessotoxin as a tool to study induction of multiple cell death pathways. *Toxins* 4: 568-579.
39. Molinski TF, Dalisay DS, Lievens SL, Saludes JP (2009) Drug development from marine natural products. *Nature reviews Drug discovery* 8: 69-85.
40. Gerwick WH, Tan LT, Sitachitta N (2001) Nitrogen-containing metabolites from marine cyanobacteria. *The Alkaloids Chemistry and biology* 57: 75-184.
41. Tan LT (2007) Bioactive natural products from marine cyanobacteria for drug discovery. *Phytochemistry* 68: 954-979.
42. Tripathi A, Puddick J, Prinsep MR, Rottmann M, Tan LT (2010) Lagunamides A and B: cytotoxic and antimalarial cyclodepsipeptides from the marine cyanobacterium *Lyngbya majuscula*. *J Nat Prod* 73: 1810-1814.
43. Simmons TL, Nogle LM, Media J, Valeriote FA, Mooberry SL, et al. (2009) Desmethoxymajusculamide C, a cyanobacteri depsipeptide with potent cytotoxicity in both cyclic and ring-opened forms. *J Nat Prod* 72: 101.

## Figures

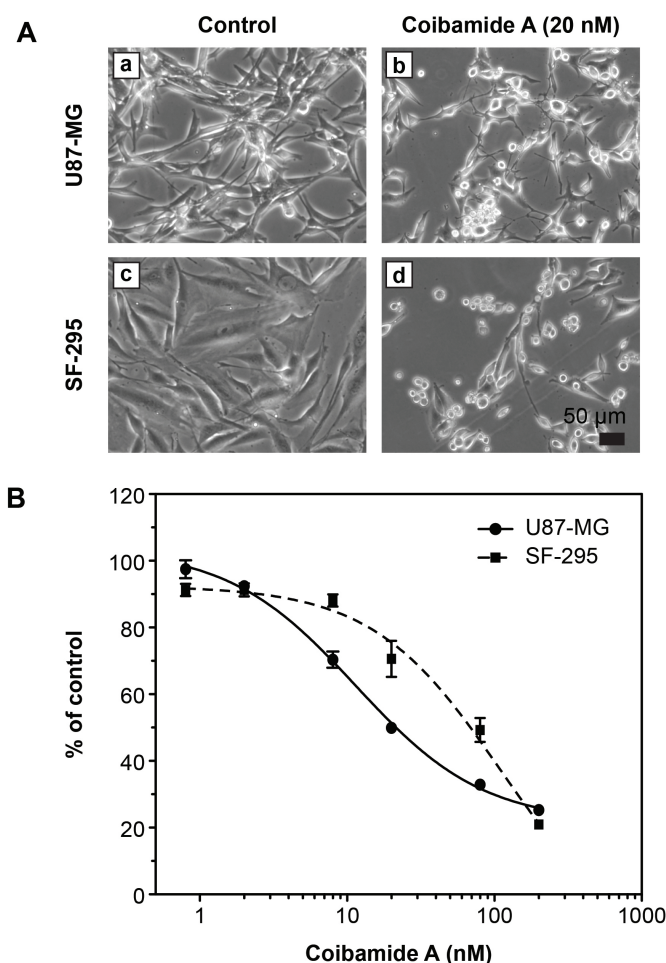


**Figure 2.1** Cytotoxic effect of coibamide A on human glioblastoma cells. **(A)** Cell death in U87-MG (upper panels) and SF-295 (lower panels) glioma cells after a 3-day exposure to coibamide A (20 nM). Cell death was documented by morphological evaluation of vehicle-(DMSO; panels a and c) or coibamide A-treated (panels b and d) cells using light microscopy. **(B)** Concentration-response profile for coibamide A-induced cytotoxicity in U87-MG and SF-295 cells. Glioma cells were treated with increasing concentrations of coibamide A (2.3 to 230 nM) for 3 days. Cytotoxicity was determined by MTT assay with the viability of control cells defined as 100%. Dose-response data represent mean viability  $\pm$  SE ( $n = 3$  wells per treatment) from a comparison that was repeated in at least four independent experiments.

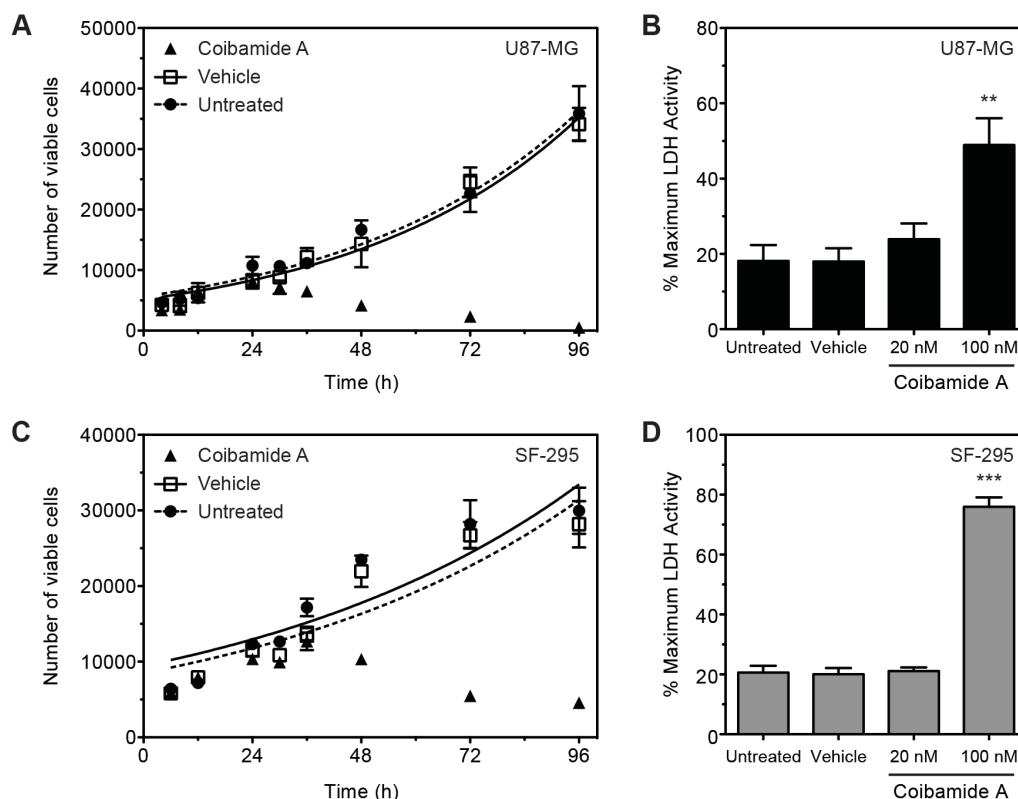


**Figure 2.2** Coibamide A induces a time- and concentration-dependent decrease in plasma membrane integrity. **(A)** Trypan blue exclusion test of cell viability in U87-MG cultures treated with or without coibamide A (20 nM) or vehicle (DMSO) over 4 days. **(B)** Concentration-response relationship of LDH efflux in U87-MG cells treated with or without coibamide A or vehicle for 4 days **(C)** Trypan blue exclusion test of cell viability and **(D)** concentration-response relationship of LDH efflux in SF-295 cells treated with or without coibamide A or vehicle (as above) for 4 days. Trypan blue exclusion profiles represent mean cell counts  $\pm$  SD of a representative time course performed in triplicate repeated at least three times in each cell line. Histograms represent mean LDH efflux  $\pm$  SE of at least three independent experiments performed in triplicate (\*\* $P < 0.01$  and \*\*\* $P < 0.001$ , coibamide A vs. untreated control).



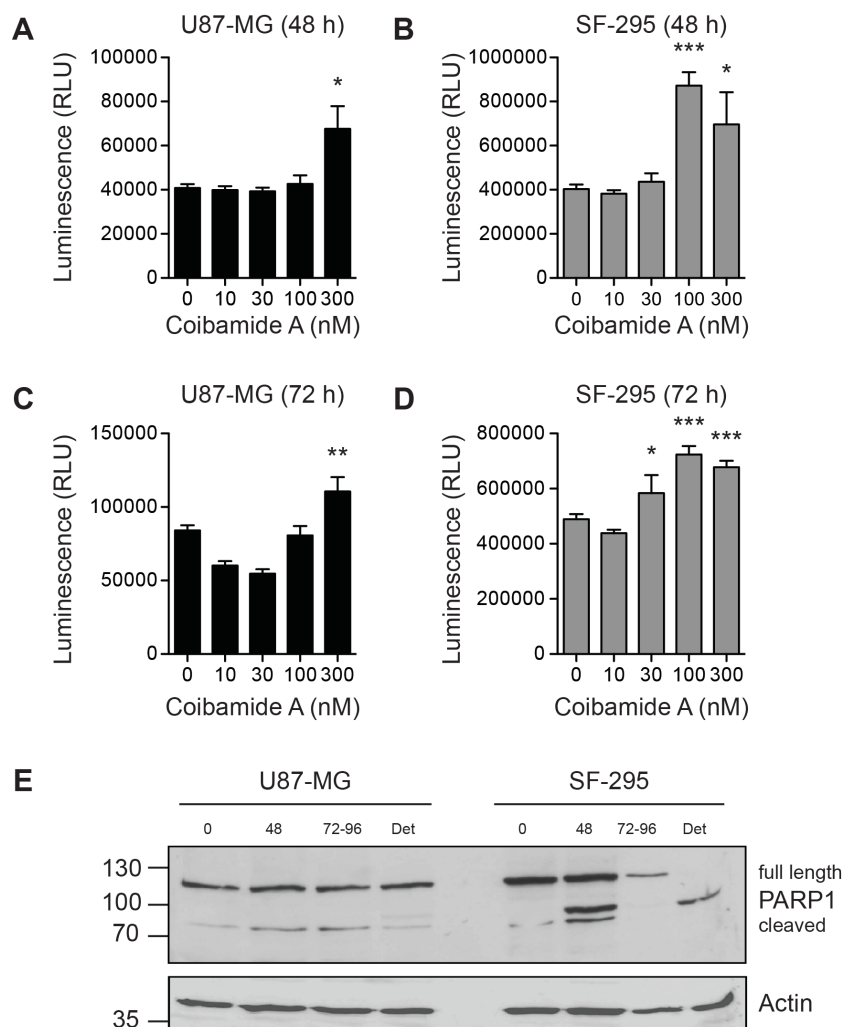


**Figure 2.3** Coibamide A induces activation of caspase-3,7 and apoptosis in a cell type-specific manner. Concentration-response relationship for coibamide A-induced caspase-3,7 activation in (A) U87-MG and (B) SF-295 cells exposed to coibamide A (10nM – 300 nM) or vehicle (DMSO) for 48h. Coibamide A-induced caspase-3,7 activation in (C) U87-MG and (D) SF-295 cells exposed to coibamide A (10nM – 300 nM) for 72h. Caspase-3,7 activity was measured at the end of each treatment using a luminescence-based assay coupled with automated luminescence detection. Histograms represent mean  $\pm$  SE of up to four independent determinations (\*\* $P < 0.01$  and \*\*\* $P < 0.001$ , coibamide A vs. vehicle control). (E) Immunoblot analysis of PARP1 in coibamide A-treated (100 nM) U87-MG and SF-295 cells lysates. Adherent and detached (Det) cells were harvested over 4 days and examined for expression of the large 89 kDa fragment of PARP1, a marker of apoptosis, plus actin as a loading control. Immunoblot is representative of an experiment repeated at least three times with similar results.

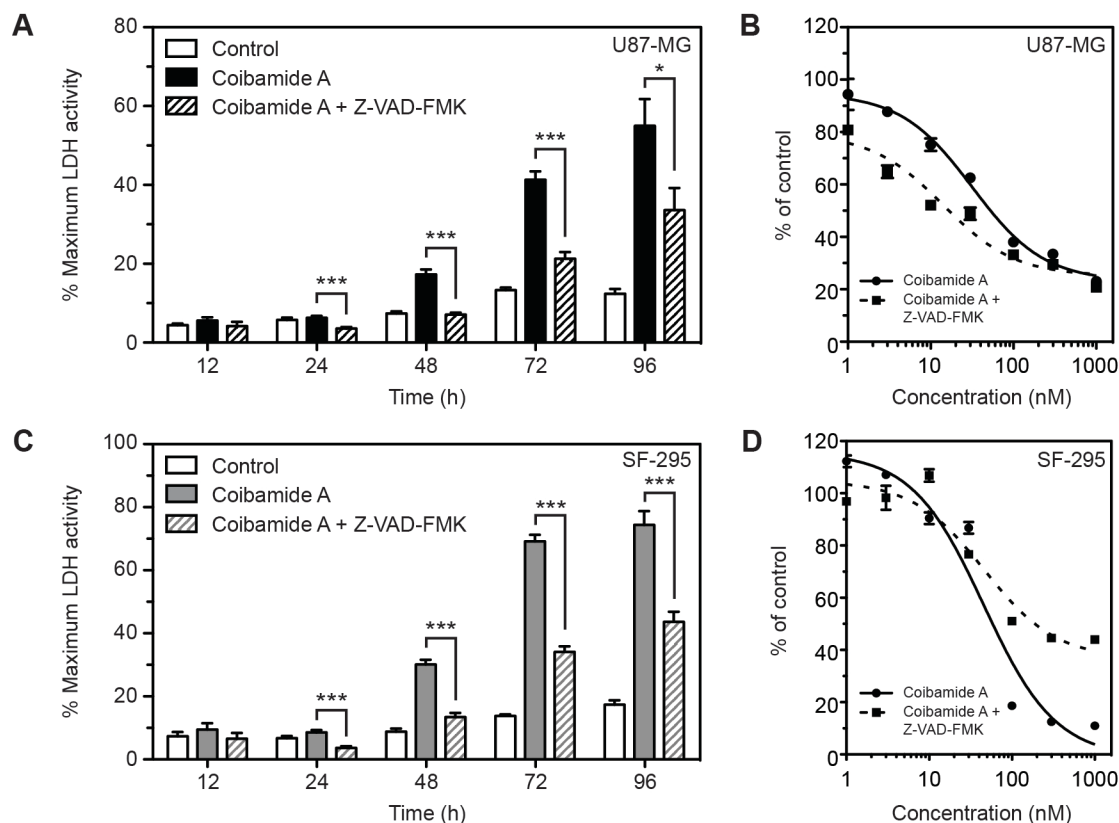


**Figure 2.4** The broad-spectrum caspase inhibitor Z-VAD-FMK inhibits LDH release but does not prevent coibamide A-induced cell death. **(A)** Time course of LDH efflux from U87-MG cells over a 4 day exposure to coibamide A (300 nM) in the presence or absence of Z-VAD-FMK (100  $\mu$ M). **(B)** Concentration-response relationship of coibamide A-induced cell death in the presence or absence of Z-VAD-FMK (100  $\mu$ M). **(C)** Time course of LDH efflux and, **(D)** concentration-response relationship of coibamide A-induced cell death in SF-295 cells measured in the presence or absence of Z-VAD-FMK (100  $\mu$ M). Histograms represent mean LDH efflux  $\pm$  SE of three independent experiments performed in triplicate (\*\* $P < 0.01$  and \*\*\* $P < 0.001$ , coibamide A vs. control). Cytotoxicity was determined by MTT assay after 3 days of exposure to coibamide A (300 nM) with the viability of control cells defined as 100%. Treatment with Z-VAD-FMK alone was not cytotoxic to either cell line (data not shown). Dose-response data represent mean viability  $\pm$  SE ( $n = 3$  wells per treatment) from a comparison that was repeated in three independent experiments.

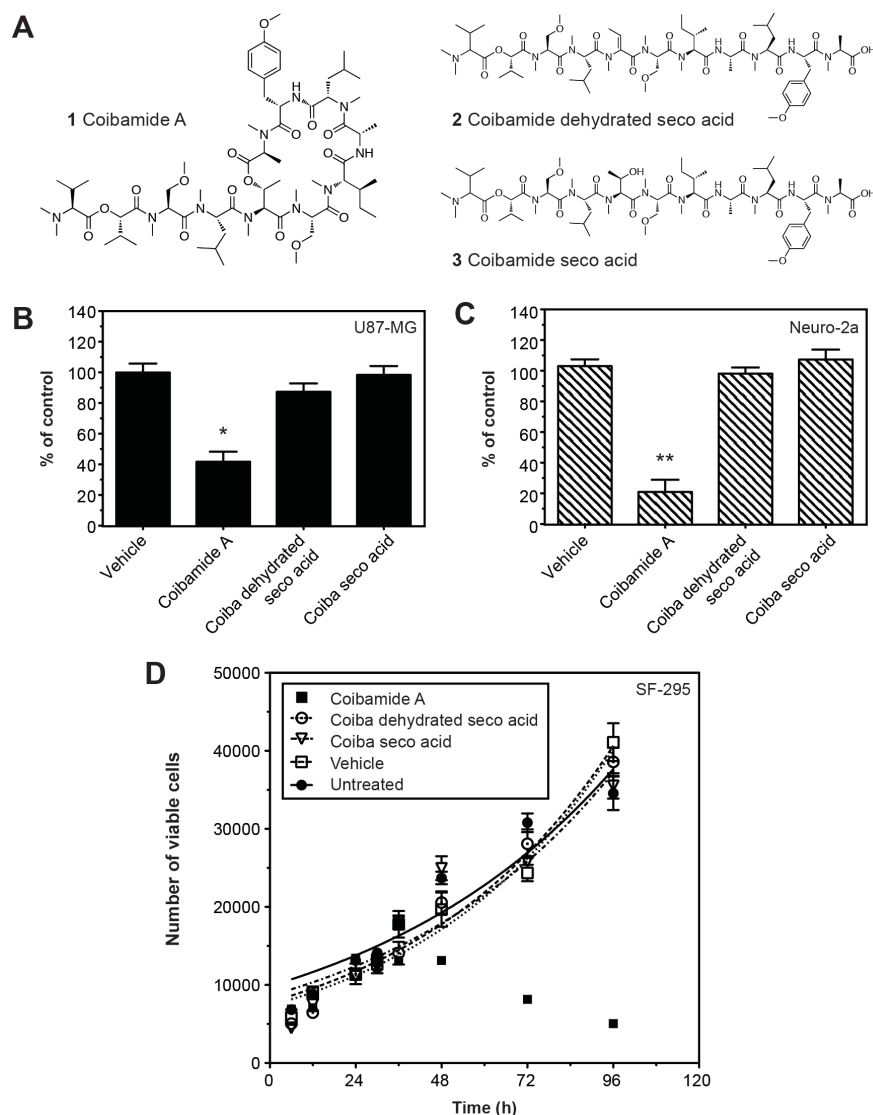


**Figure 2.5** Linearized analogs of coibamide A are not cytotoxic. **(A)** Structures of coibamide A (**1**), and two linearized derivatives: dehydrated seco acid (**2**), and seco acid (**3**). **(B and C)** Comparison of cell viability in human U87-MG glioblastoma and mouse Neuro-2A neuroblastoma cells, respectively, following exposure to the coibamide A (20 nM) parent structure, linear forms **2** and **3** (both 30  $\mu\text{g/mL}$ , ~230-260 nM), or vehicle (DMSO) for 4 days. **(D)** Trypan blue exclusion test of cell viability over 4 days in SF-295 cultures treated with or without the coibamide A (20 nM), linear forms **2** and **3** (both 30  $\mu\text{g/mL}$ , ~230-260 nM), or vehicle (DMSO). Histograms represent mean cell viability  $\pm$  SE of at least three independent MTT assays performed in triplicate (\* $P < 0.05$  and \*\*  $P < 0.01$ , coibamide A vs. control). Trypan blue exclusion profile represents mean cell counts  $\pm$  SD of a representative time course performed in triplicate that was repeated three times with similar results.

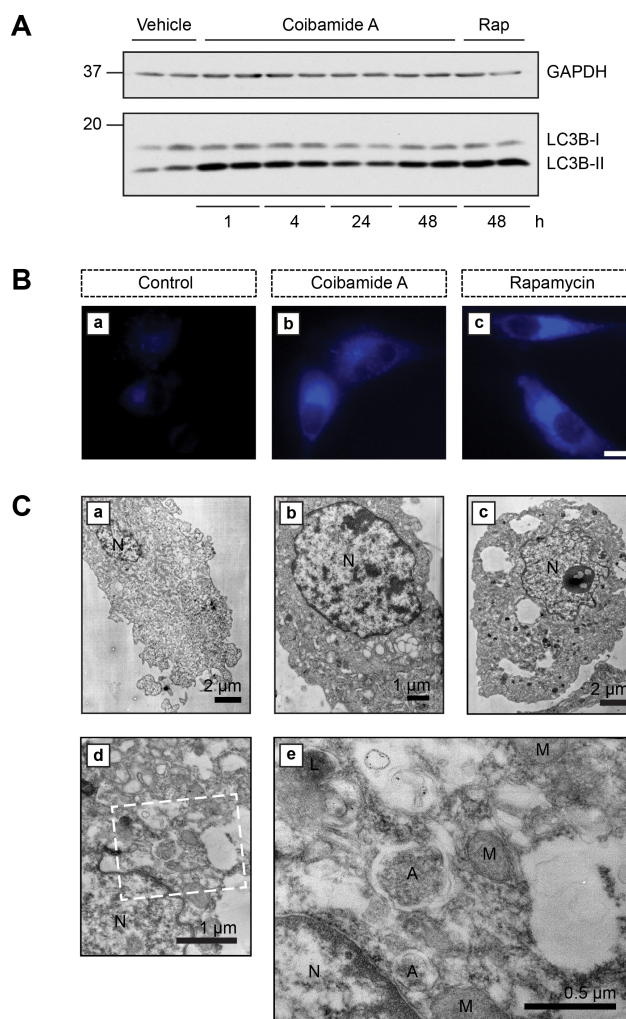


**Figure 2.6** Coibamide A induces biochemical and morphological features of autophagy. **(A)** Time course of endogenous LC3 expression in U87-MG cell lysates treated with coibamide A (20 nM) for up to 48 h, relative to vehicle (DMSO) or rapamycin- (100 nM)-treated control cells. Cell lysates were subjected to immunoblot analysis with an antibody recognizing both forms of LC3: cytosolic LC3-I and the autophagosome-associated LC3-II. Anti-GAPDH was used as a loading control. Data are representative of a time course repeated at least three times. **(B)** Monodansylcadaverine (MDC) staining of U87-MG cells treated with vehicle (DMSO; panel a), coibamide A (20 nM; panel b), or rapamycin (100 nM; panel c) for 48 h. After treatment cells were stained with MDC (50 mM) for 10 min. Images are representative of a pattern of staining observed in at least three independent experiments. Scale bar = 10  $\mu$ m. **(C)** Electron micrographs of adherent U87-MG cells treated with or without coibamide A (20 nM). Ultrastructure of representative control (panel a) and treated U87-MG cells at 16 (panel b) and 48h (panels c to e). By 48 h coibamide A-treated cells showed empty vacuoles that could be distinguished from autophagosomes (A) with a discernable double membrane. The nucleus (N), mitochondria (M), lysosome (L) and scale bars are indicated.

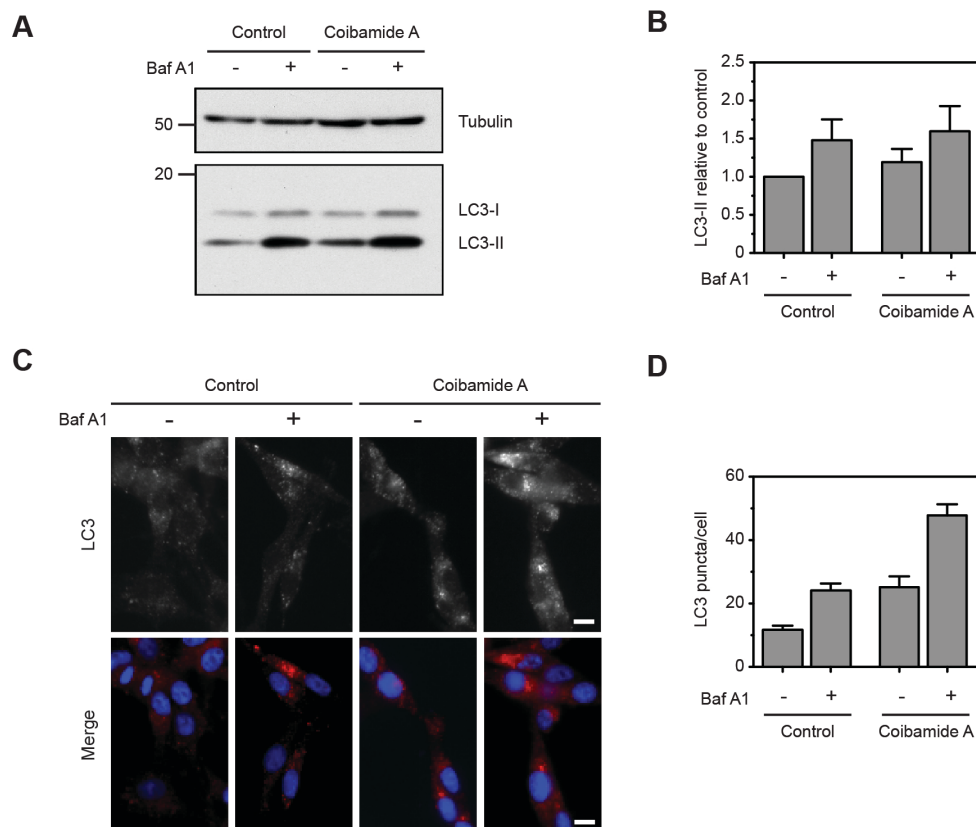


**Figure 2.7** Coibamide A induces autophagosome accumulation in U87-MG cells. **(A)** Immunoblot analysis of endogenous LC3 in U87-MG cell lysates treated with vehicle (control) or coibamide A (30 nM) for 4 h, each in the presence or absence of bafilomycin (10 nM) for the final 1 h of treatment. **(B)** Quantitation of LC3-II levels as shown in panel A. Histogram represents mean LC3-II intensity, normalized to tubulin, from immunoblots generated in three independent experiments. **(C)** Immunocytochemistry of U87-MG cells treated with vehicle (control) or coibamide A (30 nM) for 4 h, each in the presence or absence of bafilomycin (10 nM) for the final 1 h of treatment. Cells were stained for endogenous LC3 (red) and DAPI (blue). Scale bar, 10  $\mu$ m. **(D)** Quantitation of mean LC3 puncta per cell ( $n = 32$  cells) from three independent experiments.

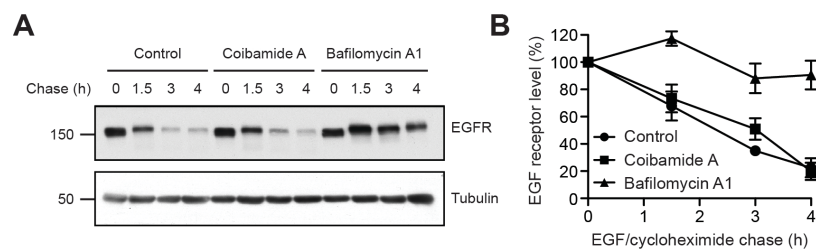


**Figure 2.8** Coibamide A does not block ligand-induced degradation of EGFR. **(A)** Immunoblot analysis of EGFR expression up to 4h after the addition of ligand (EGF) in the presence of vehicle (control), coibamide A (30 nM) or bafilomycin A1 (100 nM). On the day of the experiment U87-MG cells were starved of serum, to promote membrane localization of EGFR, and at t=0 were chased with EGF (100 ng/mL) and cycloheximide (25  $\mu$ g/mL), with or without coibamide A, or bafilomycin A1. Cells were lysed at the times indicated and processed for immunoblot analysis. **(B)** Quantitation of ligand-induced EGFR degradation from three independent experiments as described in A. Graph represents % EGFR expression, following the addition of EGF, as a function of incubation time in the presence of vehicle, coibamide A or bafilomycin A1. EGFR intensity was normalized to tubulin and determined relative to EGFR level at t = 0.

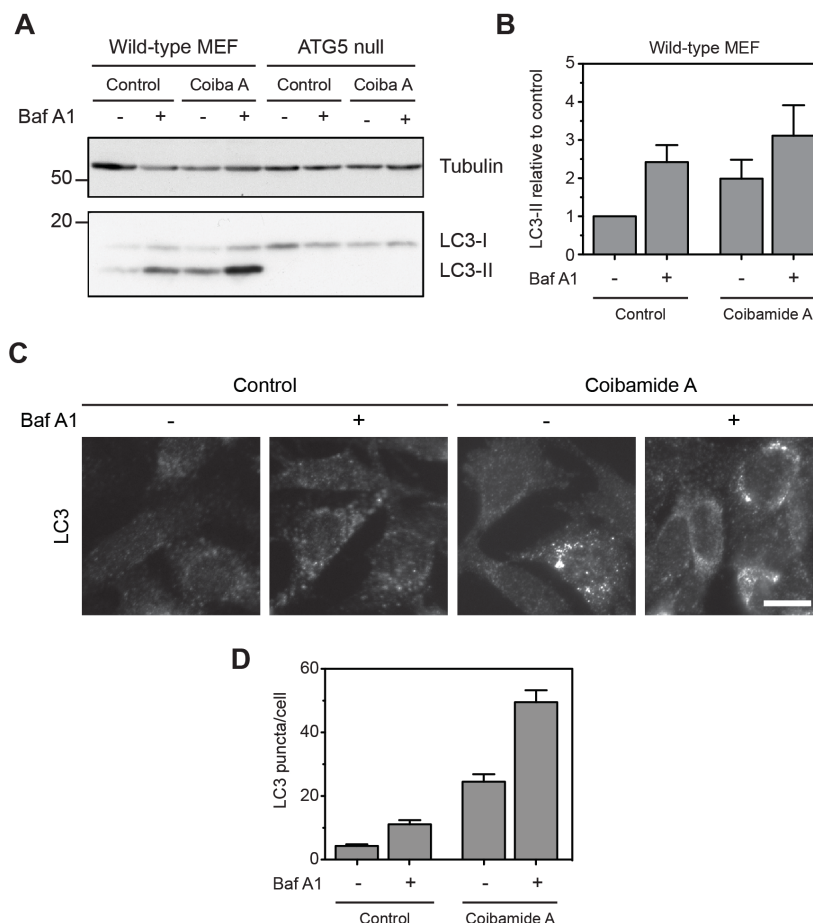


**Figure 2.9** Coibamide A induces autophagy in an ATG5-dependent manner. **(A)** Immunoblot analysis of endogenous LC3 in wild-type and ATG5 null MEF cell lysates treated with vehicle (control) or coibamide A (30 nM) for 4 h, each in the presence or absence of bafilomycin (10 nM) for the final 1 h of treatment. **(B)** Quantitation of LC3-II levels in wild-type MEF cells as shown in panel A. Histogram represents mean LC3-II intensity, normalized to tubulin, from immunoblots generated in three independent experiments. **(C)** Immunocytochemistry of wild-type MEF cells treated with vehicle (control) or coibamide A (30 nM) for 4 h, each in the presence or absence of bafilomycin (10 nM) for the final 1 h of treatment. Cells were stained for endogenous LC3 (red) and DAPI (blue). Scale bar, 10  $\mu$ m. **(D)** Quantitation of mean LC3 puncta per cell ( $n = 32$  cells) from three independent experiments.



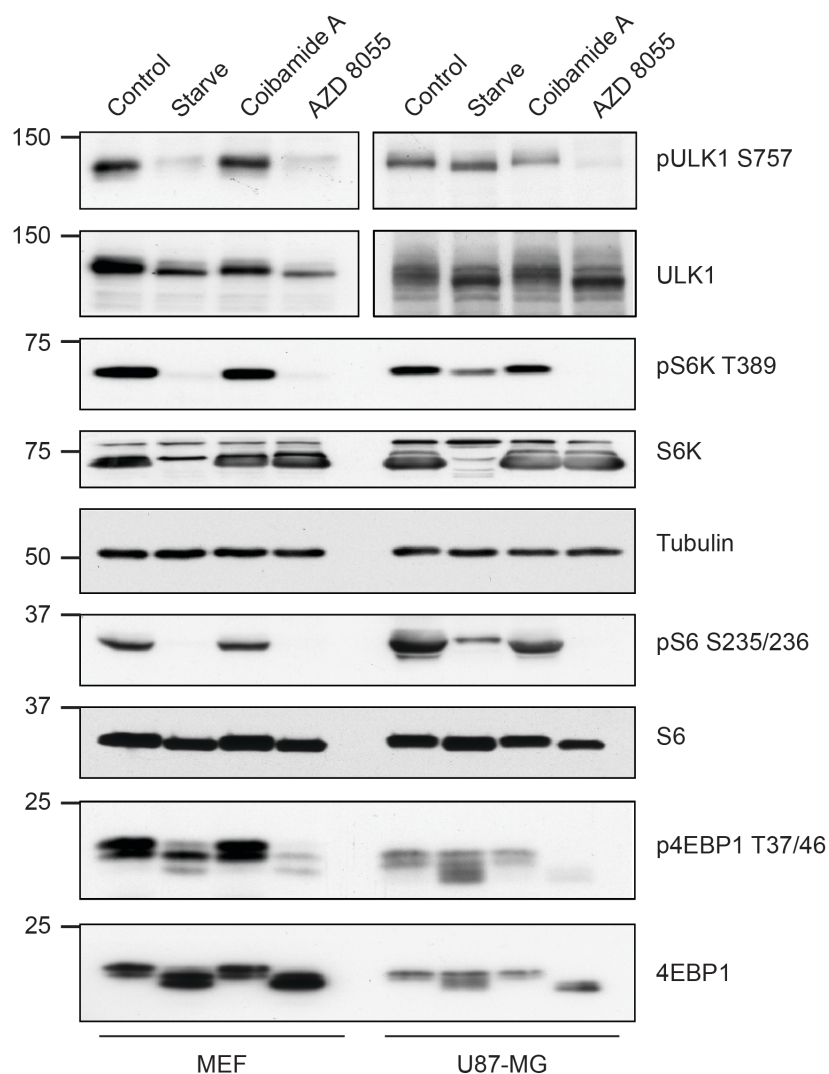


**Figure 2.10** Coibamide A induces mTOR-independent autophagy. Coibamide A-induced signaling is mTOR-independent and can be distinguished from starvation- and AZD 8055-induced autophagy in MEF and U87-MG cells. Cells were incubated in EBSS starvation medium, or treated with or without coibamide A (30 nM) or the dual mTOR inhibitor AZD 8055 (300 nM) in standard nutrient-rich medium for 4h. Following treatment cells were lysed and subjected to immunoblot analysis. The phosphorylation status of residues considered to be major targets of the mTOR pathway was assessed: phospho-ULK1 (Thr-757), phospho-p70 S6 Kinase (Thr-389), phospho-S6 ribosomal protein (Ser-235/236), and phospho-4E-BP1 (Thr-37/46) are shown relative to total ULK1, S6K1, S6 ribosomal protein and 4-E binding protein, respectively. Tubulin served as a loading control. Results are representative of at least three independent experiments.



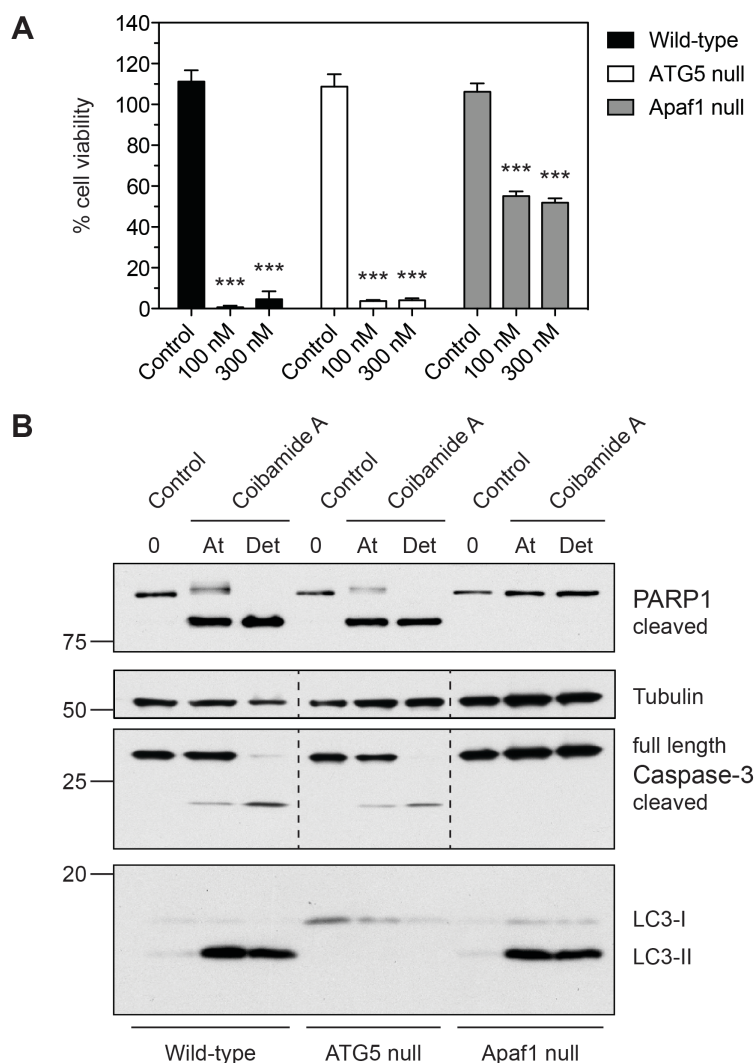


**Figure 2.11** Coibamide A induces cell death in the absence of ATG5 and intrinsic apoptotic activating factor 1 (Apaf-1). **(A)** Comparison of coibamide A-induced cytotoxicity in wild-type, ATG5 null and Apaf-1 null MEFs. MEFs cells were treated with increasing concentrations of coibamide A (0.1 to 300 nM) for 48 h. Cytotoxicity was determined by MTT assay with the viability of control cells defined as 100%. Dose-response data represent mean viability  $\pm$  SE ( $n = 3$  wells per treatment) from a comparison that was repeated in at least three independent experiments. **(B)** Immunoblot analysis of autophagy (LC3) and apoptotic (PARP1 and caspase-3) markers following treatment of wild-type, ATG5 null and Apaf-1 null MEFs with coibamide A (30 nM). Adherent and detached (Det) cells were harvested after 24 h and examined for expression of: the large 89 kDa fragment of PARP1, full length and cleaved caspase-3, LC3 isoforms I and II plus tubulin as a loading control. Immunoblot is representative of an experiment repeated at least three times with similar results.

### Supplementary Figures

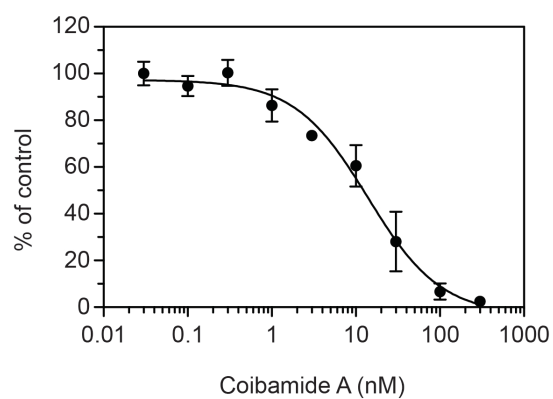


**Figure S2.1** Concentration-response profile for coibamide A-induced cytotoxicity in wild-type MEFs. Cells were treated with increasing concentrations of coibamide A (0.1 to 300 nM) for 48 h. Cytotoxicity was determined by MTT assay with the viability of control cells defined as 100%. Dose-response data represent mean viability  $\pm$  SE (n = 3 wells per treatment) from a comparison that was repeated in at least four independent experiments.

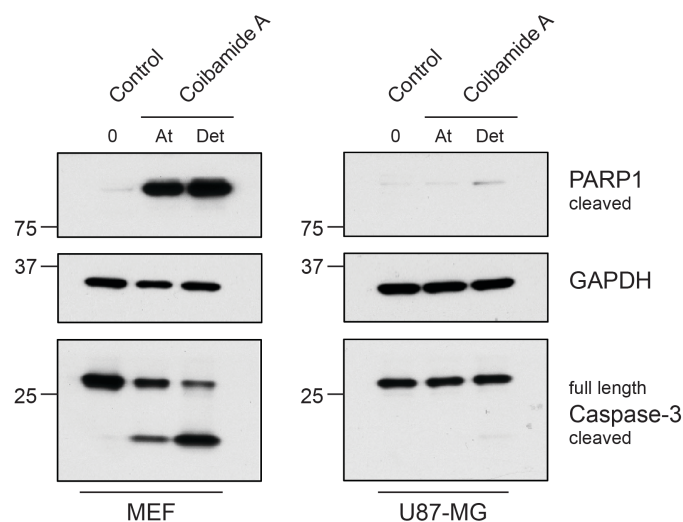


**Figure S2.2** Expression of apoptotic markers in wild-type MEFs and human U87-MG glioblastoma cells in response to coibamide A treatment. Immunoblot analysis of PARP1 and caspase-3 in wild-type MEFs and U87-MG cells after treatment with coibamide A (30 nM). Adherent and detached (Det) cells were harvested 24 h (MEFs) and 72 h (U87-MG) after treatment and examined for expression of the large 89 kDa fragment of PARP1, full length and cleaved caspase-3, and GAPDH as a loading control. Immunoblot is representative of an experiment repeated at least three times with similar results.

THE MARINE NATURAL PRODUCT COIBAMIDE A INDUCES A G1 PHASE  
SPECIFIC CELL CYCLE ARREST AND INHIBITS U87-MG GLIOBLASTOMA  
CELL INVASION

CHAPTER THREE

Andrew M. Hau, Daniel J. Coleman, Hyo Sang Jang, Arup K. Indra, Jeffrey A.  
Greenwood, Kerry L. McPhail, and Jane E. Ishmael

### Abstract

Glioblastoma multiforme is the most common type of primary brain tumor and is characterized by high vascularization with a tendency to infiltrate and invade into normal brain tissue. Therefore, new therapeutic agents that can suppress glioma tumor growth and inhibit cell motility are of particular interest. In this study, grade IV human U87-MG and SF-295 glioblastoma cell lines were used to investigate the anti-proliferative and cytostatic potential of a novel, highly-selective and potent anti-cancer compound, coibamide A, isolated from a new cyanobacterium that was collected from Coiba National Park, Panama. We report that coibamide A mediates a cytostatic effect by inhibiting cell invasion and not cell migration and also induces a G1 phase specific cell cycle arrest. The effects of coibamide A on cell invasion were substantially greater than ALLN and Marimastat, known inhibitors of the pro-invasion proteins, calpain and matrix metalloproteinases, respectively. Therefore, coibamide A may represent a new potent natural product with efficacy against invasive tumors.

## Introduction

The ability of cancer cells to metastasize and invade into surrounding tissues represents a defining stage in tumor growth [1]. Once a cancer becomes malignant treatment becomes a tremendous challenge and patient mortality is usually inevitable. Therefore, an understanding of the detailed mechanism(s) by which cancer cells acquire invasive capabilities would possibly reveal molecular targets that could be exploited for chemotherapy. Indeed, numerous proteins involved in cell migration and invasion, including actin, tubulin, calpains and matrix metalloproteinases (MMPs) have been identified and are the targets of a multitude of synthetic or natural products for the treatment of a wide range of human diseases or used as research tools. In addition to inhibiting cell motility, a number of these drugs also have efficacy as anti-mitotic agents. The cytoskeletal components actin and tubulin are both multi-functional proteins involved in maintaining cell structure and integrity, cell motility, cell division and cytokinesis and other dynamic processes and functional inhibition of either protein is detrimental to a cell [2]. The plant-derived diterpenoid paclitaxel from the bark of the Pacific yew tree *Taxus brevifolia*, for instance, is widely used in research as a tubulin stabilizer in *in vitro* motility assays while being clinically useful as the anti-proliferative drug Taxol® that induces a G2/M cell cycle arrest in several cancer cell lines [3,4]. Similar effects on cytoskeletal disruption and cell cycle progression are also observed from other inhibitors that belong to the tubulin stabilizing (e.g., epothilone, discodermolide) and destabilizing (e.g., dolastatins, halichondrin B) classes of compounds [5-8].

Along similar lines as the cytostatic and anti-mitotic compounds mentioned above, we recently reported the discovery of a novel marine cyclodepsipeptide named coibamide A that has shown potent anti-proliferative and cytotoxic effects across numerous cancers represented in the National Cancer Institute (NCI) 60 tumor cell line panel. Previous investigation also showed that coibamide A blocks G1 to S-phase cell cycle progression in NCI-MDA-MB-435 cancer cells and we confirm herein in two additional human glioblastoma cell lines that this G1 arrest is phase-specific [9]. Initial biological characterization has ruled out actin and tubulin as possible targets through which coibamide A mediates its cytostatic effects. Therefore, the

purpose of this investigation is to determine how coibamide A affects cell motility using a highly invasive human U87-MG glioblastoma cell line. While cell migration is not inhibited with concentrations of coibamide A below those found to be cytotoxic, the ability of U87-MG cells to invade appears to be hampered. We propose some possibilities to explain this finding.

## Materials and Methods

**Reagents.** The isolation of coibamide A has been described previously. Trypan Blue was purchased from MP Bio Science Ltd. (Hilton, Derby, UK). The myosin II inhibitor ML-7 was purchased from Sigma-Aldrich Corp. (St. Louis, MO). Blebbistatin and calpain inhibitor I (ALLN) were purchased from Calbiochem (San Diego, CA). Marimastat was purchased from Tocris Bioscience (Minneapolis, MN).

**Cell culture.** Human U87-MG and SF-295 glioblastoma cells were purchased from the American Type Culture Collection (ATCC, Manassas, VA) and the National Cancer Institute (NCI) cell line repository (Frederick, MD), respectively. U87-MG cells were routinely maintained in Dulbecco's Modification of Eagle's Medium (DMEM; MediaTech Inc., Manassas, VA) supplemented with 10% fetal bovine serum (FBS; HyClone, Logan, UT). SF-295 cells were cultured in RPMI-1640 medium supplemented with L-glutamine (2 mM), sodium pyruvate (1 mM), sodium bicarbonate (1.5 g/L), and 1% penicillin/streptomycin (MediaTech Inc.) and 10% FBS. Both cell lines were routinely maintained in a humidified chamber at 37°C with 5% CO<sub>2</sub>.

**Transwell Migration and Invasion Assays.** For migration assays, the underside of 24-well Corning Transwell permeable supports (pore size 8.0 µm; Corning Life Sciences, Lowell, MA) was coated with 50 µL human fibronectin (10 µg/mL in 0.05 N HCl; BD Biosciences, Franklin Lakes, NJ) for 1 h at room temperature. The membranes were then rinsed twice with DMEM medium plus 0.1% BSA and each insert transferred to 24-well plates already containing DMEM plus 10% FBS (650 µL per well). A suspension containing 100,000 U87-MG cells in serum-free DMEM (100 µL) was seeded into the upper compartment of each transwell insert and the test reagents (coibamide A, myosin inhibitor, or vehicle) added to both the upper and lower compartments of each transwell.

For invasion assays, the upper compartments of each transwell were coated with Matrigel (50 µL of 2.0 mg/mL; BD Biosciences) and allowed to solidify for 1 hr at 37°C. The transwells were then transferred to a 24-well plate with each well containing 10% FBS DMEM (650 µL). A suspension containing 500,000 U87-MG



cells in serum-free DMEM (200  $\mu$ L) was then pre-treated with test reagents (coibamide A, Marimastat, ALLN, or vehicle) for 30 min before seeding into the upper compartment of the transwell inserts. Drugs were also added to the lower compartments of the transwells. Plates for migration or invasion assays were allowed to incubate for 3 h or 20 h at 37°C, respectively, and then cells remaining on the upper side were gently removed with a cotton-tipped applicator. Cells on the bottom of the membrane were fixed in 100% methanol for 5 min, rinsed briefly in deionized water, air-dried, and mounted onto glass coverslips using ProLong Gold antifade reagent with DAPI counterstain (Molecular Probes, Invitrogen, Eugene, OR, USA). Images were obtained using a Zeiss Axiovert S100TV microscope using a Photometrics Cool SNAP HQ camera with a Hoechst DAPI filter (excitation/emission 360/460nm). Automated nuclei counts were made using Metamorph imaging software (MDS Analytical Technologies, Dowingtown, PA, USA).

**Cell Cycle Analysis.** U87-MG or SF-295 cells were cultured with and without coibamide A or vehicle for 36 h. Following treatment cells were washed in PBS, trypsinized and collected by centrifugation (240 $\times$ g for 5 min) in PBS. Cell pellets were gently resuspended, fixed in ice-cold 70% ethanol and stored overnight at -20°C. Prior to analysis, cells were again collected by centrifugation to remove the ethanol, gently resuspended in PBS and re-pelleted. Cells were then resuspended and permeabilized in 0.1% Triton-X 100 in PBS and incubated with RNase A (0.2  $\mu$ g/mL) and propidium iodide (20  $\mu$ g/mL) for 15 min 37°C. All cell samples were immediately analyzed for DNA content using a Beckman Coulter FC500 flow cytometer (Beckman Coulter, Brea, CA). Data were analyzed by WinCycle software (Phoenix Flow Systems, San Diego, CA).

**Immunocytochemistry of Ki-67.** U87-MG cells were cultured on 12 mm poly-L-lysine-coated glass coverslips with and without coibamide A or vehicle for 36 h. Cells were fixed in 4% paraformaldehyde in PBS for 20 min, rinsed three times with PBS, and permeabilized with 0.02% Triton-X 100 in PBS for 5 min followed by ice-cold 100% methanol for 1 min. Cells were blocked in 10% goat serum in PBS for 1 h at room temperature, then incubated with a rabbit anti-Ki-67 primary antibody (AbCam,

Cambridge, MA) rinsed three times in PBS and incubated with a Cy-3 labeled anti-rabbit secondary antibody for 1 h at room temperature. Coverslips were rinsed three times and mounted on glass coverslips using ProLong Gold antifade reagent with DAPI (Molecular Probes® Life Technologies, Grand Island, NY). Images were obtained using a Zeiss Axiovert S100TV and Photometrics Cool SNAP HQ camera with Hoechst DAPI (excitation/emission 360/460nm) and rhodamine (excitation/emission 545/610 nm) filters (Chroma Technology Corporation, Bellows Falls, VT).

## Results

### **The cytostatic action of coibamide A is not due to an effect on cell migration.**

Coibamide A is a potent inhibitor of cancer cell growth at concentrations below those found to be cytotoxic [9]. To understand the basis of this cytostatic action, U87-MG cells were treated with concentrations below the  $EC_{50}$  of coibamide A in these cells and growth characteristics monitored by Trypan Blue exclusion (response to 8 nM is shown in Figure 3.1A) [9]. Although coibamide A was much less toxic under these experimental conditions, untreated (Figure 3.1A) and vehicle-treated U87-MG cells (data not shown) showed normal logarithmic growth characteristics, whereas treated cells showed inhibited growth after 24 h and had failed to double by 96 h (Figure 3.1A). To determine if this response was due to an effect of coibamide A on cellular migration, transwell haptotactic migration assays were performed. For these studies, the porous membrane of each transwell chamber was coated on the underside with human fibronectin as a chemoattractant. Cells were added to the upper chamber and allowed to migrate for 3 h at 37°C in the presence of coibamide A (8 and 20 nM) or specific inhibitors of the molecular motor protein myosin II. There was no significant difference between the number of cells migrating in the presence of coibamide A and untreated or vehicle-treated U87-MG cells (Figure 3.1B). In contrast, two small molecule inhibitors of myosin II function, blebbistatin (50  $\mu$ M) and ML-7 (10  $\mu$ M), produced significant inhibition of cell migration (Figure 3.1B). Representative images of DAPI-stained nuclei on the underside of the membrane show no discernable difference in the number of cells that migrated in coibamide A and untreated cultures (Figure 3.1C-a and 3.1C-b), whereas control membranes without a fibronectin coating showed relatively few cells at the end of the assay (Figure 3.1C-a and 3.1C-c). Taken together, these findings suggest that coibamide A does not cause cytostasis by inhibiting the migratory capacity of U87-MG cells.

### **The anti-proliferative effect of coibamide A in U87-MG and SF-295 cells is mediated by a G1 cell cycle block.**

Given the time-sensitive nature of coibamide A-induced responses in unsynchronized U87-MG glioblastoma cells, and the absence of a change in migration, we performed cell cycle analysis of coibamide A-treated U87-MG and SF-295 cells by flow cytometry. By 48 h, the coibamide A-treated populations showed a significant increase in the percentage of cells in G1 phase, with a concomitant decrease in the percentage of cells in S phase relative to vehicle-treated controls (Figure 3.2A and B for U87-MG cells and Figure 3.2C and D for SF-295 cells). No significant change was observed in the population of cells in G2 phase (Figure 3.2). Figure 3.2A and 3.2C show representative cell cycle analyses at 48 h for vehicle and coibamide A-treated (20 nM) U87-MG and SF-295 cells, respectively, and Figures 3.2B and 3.2D, summaries of independent determinations.

We next analyzed the expression of Ki-67 in U87-MG cells by immunocytochemistry. Expression of the Ki-67 protein has been used extensively as a reliable diagnostic marker of cellular proliferation since it is absent in quiescent (phase G0) cells [10]. As shown in Figure 3.3A, the number of Ki-67-positive cells was significantly reduced in coibamide A-treated (20 nM) compared to vehicle-treated control cultures (Figure 3.3A). These findings were quantified by counting the fraction of immunoreactive Ki-67 cells relative to the total DAPI-stained population (Figure 3.3B). The data revealed a significant decrease in the fraction of Ki-67-positive U87-MG cells in response to coibamide A-treatment; the mean mitotic index was reduced from 0.31 in vehicle-treated to 0.19 in coibamide A-treated cells ( $P < 0.05$ ). These findings support our previous studies in MDA-MB-435 cancer cells and indicate that coibamide A exerts an anti-proliferative effect on U87-MG and SF-295 glioblastoma cells by blocking G1 to S phase progression.

### **Coibamide A inhibits cell motility by reducing the invasive capacity of U87-MG cells**

Despite evidence showing no effect on cell migration by coibamide A, we performed a pilot transwell invasion assays to determine if coibamide A could instead inhibit U87-MG cell invasion. After pre-treating cells with coibamide A (8 and 20 nM)

or positive controls (Marimastat, 10  $\mu$ M, or ALLN, 20  $\mu$ M) for 30 min, cells were seeding into the upper compartment of transwells and allowed to invade through a Matrigel protein matrix for 20 h at 37°C. Interestingly, the numbers of invading cells influenced by coibamide A exposure were drastically reduced compared to vehicle control even more so than the MMP inhibitor Marimastat (Figure 3.4A). Contrary to a known function of calpain as a regulator of cell migration and invasion, inhibition of calpain with ALLN did not affect the number of invading cells as dramatically as coibamide A or Marimastat. Images of DAPI stained nuclei of invading cells in Figure 4B show the pattern of invasion inhibition represented by the histogram in Figure 3.4A (Figure 3.4). Together, this result suggests that the capacity of U87-MG cells to migrate is not dependent on mechanisms that allow them to invade when exposed to coibamide A.

## Discussion

Coibamide A is a natural cyclic depsipeptide that has been identified by the NCI as potentially having a unique mechanism of action [9]. Consistent with the studies in U87-MG and SF-295 glioblastoma cells reported previously, we have shown that coibamide A induces time-dependent changes in growth rate and a pattern of decreasing viability upon a G1 phase cell cycle arrest [11]. The phase-specific cytostatic action of coibamide A in U87-MG and SF-295 cells is also in agreement with the results of our previous cell cycle analysis of treated MDA-MB-435 cells [9]. This finding is significant because there are many examples of chemotherapeutic drugs that are considered non-phase specific, such as the bacterial-derived anthracyclines, the antitumor antibiotic bleomycin and the platinum-based drugs. It is therefore possible that a specific arrest of cell cycle progression at the G1 phase underlies the antiproliferative mechanism of action of coibamide A in other sensitive human cancer cells.

We found no evidence for a change in the migratory capacity of U87-MG cells at concentrations of coibamide A (20 nM) that induce both a block in G1 to S phase progression and a decrease in the expression of the nuclear proliferation marker Ki-67. Interestingly, however, a pilot transwell invasion assay revealed that coibamide A drastically reduces the ability of U87-MG cells to invade and this effect was more pronounced than known inhibitors of cell invasion. Although this result is in need of replication, it is possible that the cytostatic effects of coibamide A operate through pathways that regulate cell invasion and not cell migration.

The ubiquitous calpain-1 and -2 belong to a family of calcium-activated cysteine proteases that regulate the proteolytic activation of numerous substrates that control cell processes such as focal adhesion, cell cycle and apoptosis, migration and invasion, and angiogenesis [12,13]. Interestingly, calpains are also known regulators of autophagy through substrate proteolysis of the indispensable autophagy regulator ATG5. Cleavage of ATG5 by calpain not only inhibits autophagy but also enhances cell susceptibility to intrinsic apoptosis in a time-dependent manner [14]. Therefore, it is possible that cell stress induced by coibamide A modulates intracellular calcium

levels following autophagy induction. Sufficient calcium concentrations would then time-dependently trigger the activation of calpain, mediate autophagy inhibition, and induce cell death. Depending on cell type and sensitivity to apoptosis, cell death mediated by calpain proteolysis of ATG5 could either occur via caspase-dependent apoptotic or through caspase-independent non-apoptotic pathways as in the cases observed with SF-295 and U87-MG cells, respectively, from our previous studies [11].

Studies documenting the substrates of calpain have revealed direct and indirect evidence of the involvement of matrix metalloproteinases (MMPs), which are a group of secreted proteases that have functions similar to calpains [15]. MMPs have predominately been thought of as endopeptidases essential for the degradation of the extracellular matrix (ECM) to facilitate cell migration though it is now understood that MMPs also regulate cell growth, apoptosis and angiogenesis. Thus, it is without surprise that aberrant expression and/or uncontrolled regulation of calpain or MMPs are implicated in tumorigenesis. Subsequently, calpain and MMPs have been attractive targets for inhibition in anti-cancer therapy but to date this strategy has been met with limited clinical usefulness [12,15]. Part of the problem with the unsuccessful development of calpain and MMP inhibitors is due to the vast number of calpains (14) and MMPs (>21) that share some degree of functional redundancy. Despite the lack of clinical success of these drugs as anti-cancer agents, the capability of compounds such as the isoform-specific inhibitors of calpain, ALLN and ALLM, to inhibit cell migration and suppress cell cycle progression and proliferation continues to be a promising mechanism that can be exploited [16]. Similarly, the broad-spectrum MMP inhibitors marimastat and batimastat have been clinically evaluated in the United States for effects against angiogenesis and metastasis of gastrointestinal tumors [17].

MMPs are structurally divided into eight classes—five are secreted and three are membrane-associated—and are synthesized as inactive zymogens regulated by endogenous proteinases [15]. Initiation of cell invasion first requires migration through the activation of MMP-2 and -14 that localize to the basement membrane of cells where they cleave the ECM protein laminin-5 [18,19]. As cells begin to migrate, the extracellular domain of the cell surface hyaluronan receptor CD44 is cleaved by MMP-14 and released into the ECM [20]. MMP-9 is then recruited to cell surface

where it forms a complex with CD44 that promotes cell invasion via detachment from neighboring cells and the surrounding matrix. Considering that coibamide A does not inhibit cell migration it is therefore unlikely that it directly affects the activities of MMP-2 or -14. However, it is conceivable that MMP-9 activation and/or localization to the cell surface could be inhibited by coibamide A as the CD44-MMP-9 complex is dispensable for cell migration but required for invasion. Recently, Jang et al. reported the requirement of calpain-2 for U87-MG cell invasion and also demonstrated that MMP-2 but not MMP-9 activity is indirectly modulated by calpain-2 in 72 h transwell invasion assays [21]. Using calpain-2 shRNA knockdown U87-MG cells the authors found that pro-MMP-2 and MMP-2 levels were only moderately (24% and 39%, respectively) reduced compared to control. Considering that MMP-2 functions in cell migration and the effect on MMP-2 activity due to calpain-2 knockdown was limited even after an extended 72 h assay, the absence of an inhibitory effect on migration due to coibamide A treatment is consistent with the much shorter 3 h studies presented herein.

Aside from direct inhibition of MMPs, it is alternatively possible that coibamide A can alter pro-survival signaling pathways that are activated upon cell detachment from the ECM. Anoikis, for example, is an unconventional caspase-dependent cell death program that is induced following ECM detachment and it has been proposed that metastasizing tumors are able to overcome anoikis by activation of autophagy. In the context of our studies, the capacity of U87-MG cells to invade while undergoing constitutive autophagy induced by coibamide A may therefore be too overwhelming for a cell. These events may then lead to cytostasis and time-dependent cell death. Consequently, the molecular mechanism(s) by which coibamide A induces cytostasis, potentially through alterations of pathways involving calpain and/or MMP activity, will be pursued in future studies.



### Bibliography

1. Fidler IJ (2003) The pathogenesis of cancer metastasis: the 'seed and soil' hypothesis revisited. *Nat Rev Cancer* 3: 453-458.
2. Hall A (2009) The cytoskeleton and cancer. *Cancer Metastasis Rev* 28: 5-14.
3. Jordan MA, Wilson L (2004) Microtubules as a target for anticancer drugs. *Nat Rev Cancer* 4: 253-265.
4. Altmann KH, Gertsch J (2007) Anticancer drugs from nature--natural products as a unique source of new microtubule-stabilizing agents. *Nat Prod Rep* 24: 327-357.
5. Bollag DM, McQueney PA, Zhu J, Hensens O, Koupal L, et al. (1995) Epothilones, a new class of microtubule-stabilizing agents with a taxol-like mechanism of action. *Cancer Res* 55: 2325-2333.
6. ter Haar E, Kowalski RJ, Hamel E, Lin CM, Longley RE, et al. (1996) Discodermolide, a cytotoxic marine agent that stabilizes microtubules more potently than taxol. *Biochemistry* 35: 243-250.
7. Bai R, Pettit GR, Hamel E (1990) Dolastatin 10, a powerful cytostatic peptide derived from a marine animal. Inhibition of tubulin polymerization mediated through the vinca alkaloid binding domain. *Biochem Pharmacol* 39: 1941-1949.
8. Bai RL, Paull KD, Herald CL, Malspeis L, Pettit GR, et al. (1991) Halichondrin B and homohalichondrin B, marine natural products binding in the vinca domain of tubulin. Discovery of tubulin-based mechanism of action by analysis of differential cytotoxicity data. *J Biol Chem* 266: 15882-15889.
9. Medina RA, Goeger DE, Hills P, Mooberry SL, Huang N, et al. (2008) Coibamide A, a potent antiproliferative cyclic depsipeptide from the Panamanian marine cyanobacterium *Leptolyngbya* sp. *J Am Chem Soc* 130: 6324-6325.
10. Scholzen T, Gerdes J (2000) The Ki-67 protein: from the known and the unknown. *J Cell Physiol* 182: 311-322.
11. Hau AM, Greenwood JA, Löhr CV, Serrill JD, Proteau PJ, et al. (201X) Coibamide A induces mTOR-independent autophagy and cell death in glioblastoma cells. *PLOS ONE (submitted)*.
12. Leloup L, Wells A (2011) Calpains as potential anti-cancer targets. *Expert Opin Ther Targets* 15: 309-323.
13. Storr SJ, Carragher NO, Frame MC, Parr T, Martin SG (2011) The calpain system and cancer. *Nat Rev Cancer* 11: 364-374.
14. Yousefi S, Perozzo R, Schmid I, Ziemiecki A, Schaffner T, et al. (2006) Calpain-mediated cleavage of Atg5 switches autophagy to apoptosis. *Nat Cell Biol* 8: 1124-1132.
15. Egeblad M, Werb Z (2002) New functions for the matrix metalloproteinases in cancer progression. *Nat Rev Cancer* 2: 161-174.
16. Carragher NO, Westhoff MA, Riley D, Potter DA, Dutt P, et al. (2002) v-Src-induced modulation of the calpain-calpastatin proteolytic system regulates transformation. *Mol Cell Biol* 22: 257-269.
17. Coussens LM, Fingleton B, Matrisian LM (2002) Matrix metalloproteinase inhibitors and cancer: trials and tribulations. *Science* 295: 2387-2392.

18. Giannelli G, Falk-Marzillier J, Schiraldi O, Stetler-Stevenson WG, Quaranta V (1997) Induction of cell migration by matrix metalloprotease-2 cleavage of laminin-5. *Science* 277: 225-228.
19. Koshikawa N, Giannelli G, Cirulli V, Miyazaki K, Quaranta V (2000) Role of cell surface metalloprotease MT1-MMP in epithelial cell migration over laminin-5. *J Cell Biol* 148: 615-624.
20. Yang W, Aii S, Gorrin-Rivas MJ, Mori A, Onodera H, et al. (2001) Human macrophage metalloelastase gene expression in colorectal carcinoma and its clinicopathologic significance. *Cancer* 91: 1277-1283.
21. Jang HS, Lal S, Greenwood JA (2010) Calpain 2 is required for glioblastoma cell invasion: regulation of matrix metalloproteinase 2. *Neurochem Res* 35: 1796-1804.

## Figures

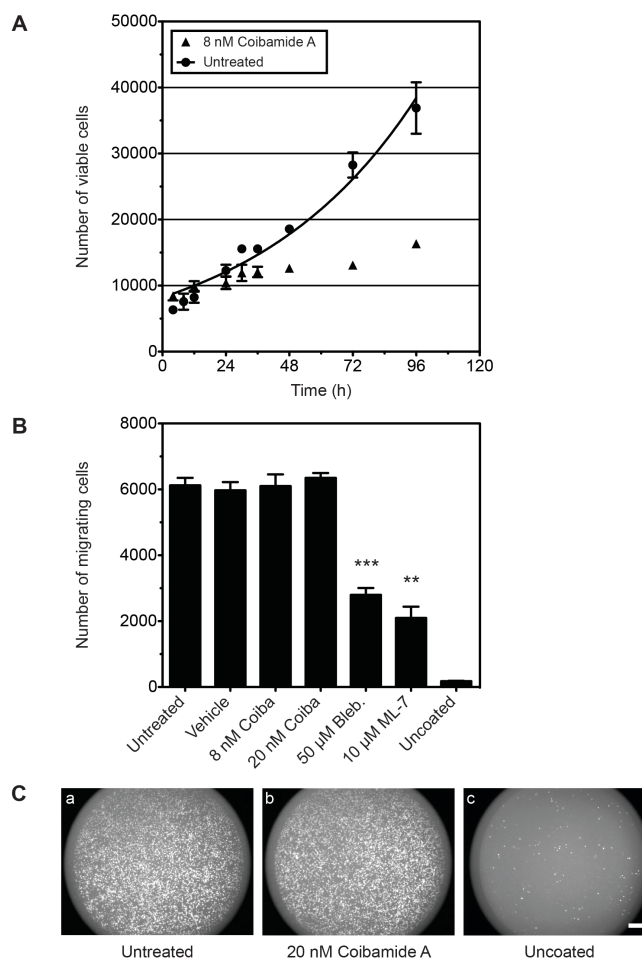


**Figure 3.1** Reduced proliferation of U87-MG cells in response to coibamide A treatment is not due to a change in migratory capacity. **(A)** U87-MG cells were treated with a single concentration of coibamide A (8 nM) for up to 96 h. Cell viability was determined in treated and untreated cells by Trypan Blue dye exclusion ( $n = 6$  wells pre treatment). Data points represent mean  $\pm$  SD of a representative time course that was repeated three times with similar results. **(B)** Histogram of haptotactic migration of U87-MG cells in response to human fibronectin in the presence of coibamide A or myosin II inhibitors. U87-MG cells were seeded into the upper chamber of transwell inserts coated underneath with human fibronectin, and migration was measured after 3 h. Upper and lower chambers of each insert contained: vehicle (0.0025% DMSO), coibamide A (Coiba; 8 nM and 20 nM), blebbistatin (Bleb.; 50  $\mu$ M) or ML-7 (10  $\mu$ M). Untreated cells in the presence (Untreated) and absence of fibronectin (Uncoated) were also included in each experiment. Histogram represents mean nuclei counts  $\pm$  SE of five independent migration experiments. Significant at  $P < 0.01$  (\*\*) and  $P < 0.001$  (\*\*\*) compared to untreated control. **(C)** Representative images of DAPI-stained cells on the underside membrane of transwell inserts from: untreated, coibamide A-treated (20 nM Coiba) and Uncoated supports.

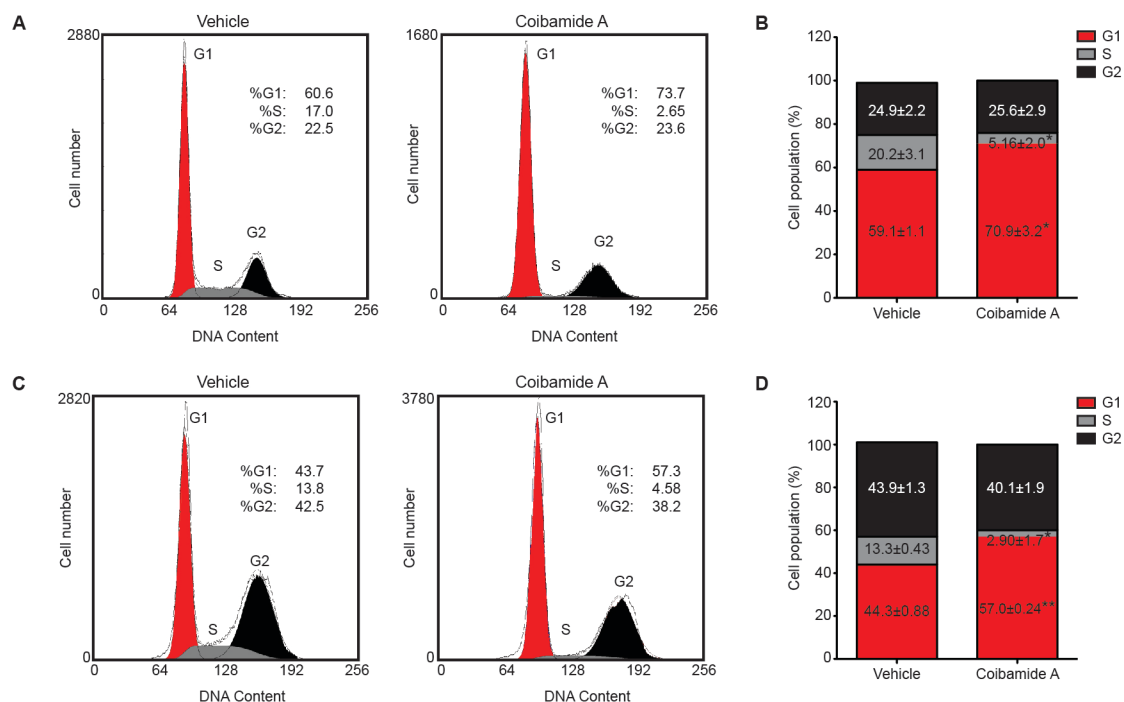


**Figure 3.2** The anti-proliferative action of coibamide A is induced by a block in G1 cell cycle progression. Cell cycle analysis of **(A)** U87-MG or **(C)** SF-295 cells ( $1 \times 10^6$ ) treated with coibamide A (20 nM) or vehicle (0.001% DMSO) for 36 h. Cells were stained with propidium iodide and analyzed by flow cytometry to determine the percentage of cells in each stage of the cell cycle. Profiles are shown from a representative experiment repeated at least two times with similar results. Quantitation of the percentage of **(B)** U87-MG or **(D)** SF-295 cells  $\pm$  SE in G1, S, and G2 phase after independent cell cycle analyses. (\*) and (\*\*) denote  $P < 0.05$  or  $P < 0.01$ , respectively, when compared to vehicle control.

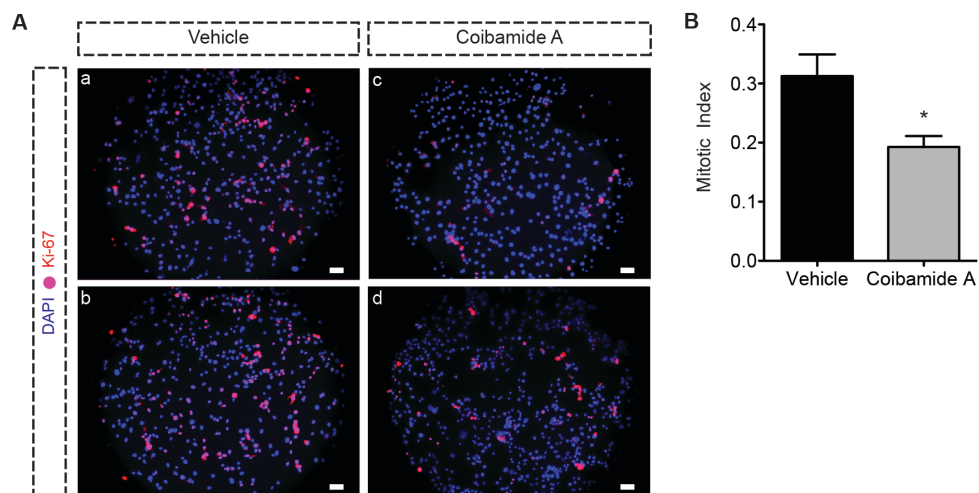


**Figure 3.3** Expression of the nuclear proliferation marker Ki-67 is decreased in coibamide A-treated cells. **(A)** U87-MG cells were treated with vehicle (0.001% DMSO; sub-panels a and b) or coibamide A (20 nM; sub-panels c and d) for 36 h. Cells were fixed and labeled with anti-Ki67 and a secondary antibody conjugated to Cy-3 (red). Nuclei were visualized with DAPI stain (blue); the overlay of Ki-67 immunoreactivity and DAPI stain appears magenta. Scale bar = 50  $\mu$ m. **(B)** Histogram quantifying the mean mitotic index of vehicle and coibamide-treated cells  $\pm$  SE, as determined by immunocytochemistry of Ki-67 expression in three independent cultures. Significant at  $P < 0.05$  (\*) when compared to vehicle control.

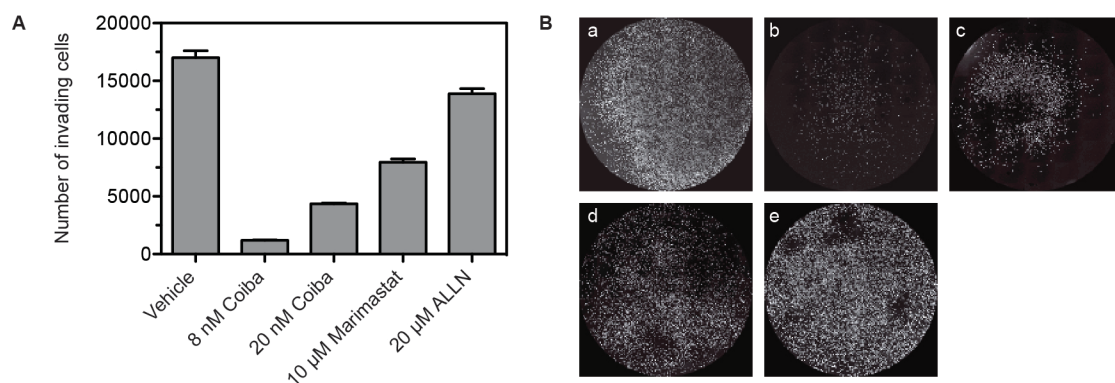


**Figure 3.4** The invasive capacity of U87-MG cells is reduced upon coibamide A exposure. **(A)** Histogram of transwell invasion assay of U87-MG cells in the presence of coibamide A or cell invasion inhibitors. U87-MG cells pre-treated with drug for 30 min prior to seeding into the upper chamber of transwell inserts coated with Matrigel, and invasion was measured after 20 h. The lower chambers of each insert also contained vehicle (0.45% DMSO), coibamide A (Coiba; 8 nM and 20 nM), Marimastat (10  $\mu$ M) or ALLN (20  $\mu$ M). Histogram represents mean nuclei counts  $\pm$  SE of one pilot experiment. **(B)** Representative images of DAPI-stained nuclei of invading cells on the underside membrane of transwell inserts from: (a) vehicle, (b and c) coibamide A (8 and 20 nM, respectively), (d) Marimastat (10  $\mu$ M), and (e) ALLN (20  $\mu$ M) treatment.

CYTOTOXICITIES AND STRUCTURE ACTIVITY RELATIONSHIPS OF PUTATIVE  
COIBAMIDE A AND RELATED STRUCTURES

CHAPTER FOUR

Andrew M. Hau, Dong Li, Takashi L. Suyama, Philip J. Proteau, Kerry L. McPhail,  
and Jane E. Ishmael

### Abstract

Marine organisms continue to be a valuable source for the discovery of new natural products with promising anti-cancer activity. Coibamide A, an anti-proliferative and highly potent cytotoxin isolated from a Panamanian cyanobacterium, represents a novel structure characterized by a depsipeptide lariat macrocycle with a high degree of *N*-methylation. Because of limited accessibility to the natural supply from the producing organism that has hindered extensive biological characterization, the total synthesis of putative coibamide A and related structures is in progress. Presented herein are eleven synthetic products that have been tested for cytotoxicity against human U87-MG glioblastoma and MDA-MB-231 breast cancer cells. Collectively, our results suggest that the presence of D instead of L isomers of the *N,O*-diMeSer and *O*-MeTyr residues within coibamide A is not well-tolerated for retention of activity. Furthermore, the presence of the lariat side chain and *N*-methylation are important structural features that likely impart specificity and structural rigidity for drug-target binding, and *N,O*-methylation increases lipophilicity for diffusion across cell membranes without active transport.



## Introduction

Cancer is one of the most deadly diseases in the world accounting for an estimated 580,000 deaths in the United States for 2012 (Source: Cancer Facts & Figures 2012, American Cancer Society, [www.cancer.org](http://www.cancer.org)). However, the remarkable progress in early cancer diagnoses and preventative measures in combination with the development of novel cures to supplement and improve existing therapies has helped steadily reduce cancer mortality rates in the US since the early 1990s. New medicines have in part been developed as a result of pharmaceutical research efforts focusing on the discovery of unique biologically active compounds of marine origin in contrast to those derived from plants and terrestrial microorganisms.

Over the past few decades, marine organisms have been an attractive source for structurally diverse bioactive natural products that show promise over a wide range of therapeutic indications. In 2009 and 2010 combined, 2014 new compounds (out of ~22,000 known) of marine origin were reported and these numbers continue to grow annually with improvements in deep-sea sample collection, automated screening, and large-scale drug production technologies [1-3]. Natural products that have potential therapeutic utility are often candidates for large-scale chemical synthesis because harvesting such compounds from their natural sources can be tedious, time-consuming and expensive, as well as environmentally unsustainable. However, not all natural products can be synthesized, due to their structural complexity. Additionally, isolation and purification of compounds from their natural sources often leads to very low yields that are barely enough for initial structure elucidation and/or basic biological characterization. Regardless of these challenges, the discovery and chemical synthesis of new natural products is an important approach for introducing structural diversity to the repertoire of bioactive compounds that can be used in medicine or as research tools in molecular biology and pharmacology.

As part of our ongoing marine natural products research, we reported the discovery of a cyanobacterial macrocyclic depsipeptide named coibamide A that serves as a hopeful lead in anti-cancer drug discovery [4]. Coibamide A was

evaluated against the National Cancer Institute (NCI) 60 cancer in vitro cell line panel and was found to have potent cytostatic and cytotoxic selectivity at nanomolar concentrations over a wide range of cancers including CNS, breast, colon, and ovarian. Notably, coibamide A was designated “COMPARE-negative” indicating that it likely inhibits tumor cell proliferation through a unique mechanism. Given the potential utility of coibamide A as an anti-cancer agent, this study documents the biological testing of putative coibamide A synthetic products, analogs and synthetic intermediates generated in our laboratory. In the context of the selectivity of coibamide A towards CNS and breast cancers, the compounds described herein were tested for activity in a grade IV human U87-MG malignant glioblastoma cell line and in highly invasive human NCI-MDA-MB-231 breast cancer cells. Glioblastoma represents one of the deadliest types of cancer with a poor prognosis, while breast cancer is the most common cancer among women of all races (Source: Cancer Among Women, Center for Disease Control and Prevention, [www.cdc.gov](http://www.cdc.gov)). Although the total synthesis of the naturally occurring stereoisomer of coibamide A is still ongoing, our data suggest that the overall stereostructure of the compound is important to impart cytotoxicity and perhaps specificity to its currently unknown molecular target.

## Materials and Methods

**Reagents.** The isolation of coibamide A has been previously described [4]. The syntheses of putative coibamide A, analogs and related structures tested in this study are the subject of a Ph.D. thesis project (Mr. Dong Li) and several publications in preparation (Suyama, Li, Proteau, McPhail, et al.). D-*N*-MeAla coibamide was kindly provided by Dr. Shinya Oishi (Kyoto University, Kyoto, Japan). Thiazolyl blue tetrazolium bromide (MTT) was purchased from Sigma-Aldrich Corp. (St. Louis, MO, USA).

**Cell culture.** Human U87-MG malignant glioblastoma, human PC-3 prostate cancer and human H292 lung cancer cell lines were purchased from the American Type Culture Collection (ATCC; Manassas, VA, USA). Human SF-295 malignant glioblastoma and human MDA-MB-231 breast cancer cell lines were obtained from the NCI cell line repository (Frederick, MD, USA). U87-MG and PC-3 cells were routinely maintained in Dulbecco's Modified Eagle's Medium (DMEM; MediaTech Inc., Manassas, VA, USA) containing 10% fetal bovine serum (FBS; Hyclone, Logan, UT, USA). SF-295, MDA-MB-23, H292, and Neuro-2A cells were cultured in RPMI-1640 medium supplemented with L-glutamine (2 mM), sodium pyruvate (1 mM), sodium bicarbonate (1.5 g/L) and 10% FBS. All cell lines except U87-MG also contained 1% penicillin/streptomycin (MediaTech Inc.). Cells were maintained in a humidified chamber containing 5% CO<sub>2</sub>.

**Cell viability assays.** For MTT assays, cells ( $3 \times 10^3$  per well in 90  $\mu$ L) were seeded into 96-well flat-bottom plates (BD Biosciences, Franklin Lakes, NJ, USA) and maintained overnight before the addition of the appropriate test compound or vehicle (DMSO). Each 96-well plate also contained untreated control wells. In all experiments, final DMSO concentration was  $\leq 0.6\%$ , which was not associated with any cytotoxicity compared to untreated control. Treated and untreated cells were maintained under standard cell culture conditions for 72 h. To determine cell viability, MTT reagent in PBS was added to each well at a final concentration of 0.5 mg/mL

and the plates allowed to incubate for 2 h at 37°C. The medium was then gently aspirated from all wells and the purple formazan product was solubilized with DMSO (50  $\mu$ L). The optical density of each well was determined at 550 nm using a BioTek Synergy HT microplate reader with Gen5 software (Bio-Tek, Winooski, VT). Cytotoxicity was determined in at least two independent experiments, with viability of untreated control cells defined as 100%.

**Data Analysis.** Concentration-response relationships were analyzed using Graphpad Prism Software (Ver. 5.0c, Graphpad Software Inc., San Diego, CA, USA), and EC<sub>50</sub> values derived using nonlinear regression analysis fit to a logistic equation.

## Results

Coibamide A is a depsipeptide that features a highly methylated 22-membered macrocycle and tetrameric side chain [4]. Considering that coibamide A is composed of two prominent structural features, synthesis of the natural product was approached by independently creating the lariat side chain and macrocycle prior to tethering the components in a final coupling reaction. Of several synthetic intermediates generated towards this goal, two tetrameric side chains and two unique macrocycles were selected for biological characterization. Structural confirmation of the terminally *N,N*-desmethylated tetrameric side chain (**1a**) and benzyl (Bn)-*N,N*-desmethyl tetrameric side chain (**1b**), containing *N*-MeLeu, *N,O*-diMeSer, HIV and Val (Figure 4.1), revealed a 70% *R/S* or *S/R* diastereomic mixture for each product. These side chain tetramers were characterized in human U87-MG glioblastoma and MDA-MB-231 breast cancer cells using MTT cell viability assays, with the hypothesis that the side chain of coibamide A alone could impart partial activity relative to the natural product. It is also interesting to note that the side chain of coibamide A shares structural similarity to the potent anti-proliferative depsipeptides dolastatin 10 and 15 originally isolated from the sea hare, *Dolabella auricularia*, in the 1970s by Pettit et al. (reviewed in [5]). Therefore, we anticipated some level of activity exhibited by **1a-b** and indeed, both side chains had micromolar activity while **1a** (EC<sub>50</sub> 56.8 and 86.7  $\mu$ M in U87-MG and MDA-MB-231 cells, respectively) exhibited dose-dependent cytotoxicity over the concentration range tested (Figure 4.1 and Supplementary Figure S4.1). Considering that the only structural disparity between **1a** and **1b** is the presence of a Bn protecting group on the carboxyl terminus of **1a**, it may be that the increased potency observed is due to better cell permeability of this more lipophilic product.

Ring size is an important factor for successful cyclization of linear peptides [6]. Although cyclization of heptapeptides usually proceeds well, the activated peptide must adopt an energetically unfavorable conformation(s) before formation of the final product. Heptapeptide TLS-I-80A2 (**2**) represents one of three Cbz-protected macrocycles generated by a common synthetic route under three different reaction conditions (Figure 4.2). In addition, a second macrocycle structure, desmethyl

nonapeptide LD4-75a (**3**), that contains a pendant Leu-O-MeSer unit was synthesized. Configurational analysis of these products revealed a persistent racemization issue for the O-MeTyr and O-MeSer residues in **2** and **3**, as was the case for the *N,O*-diMeSer residue in tetramer **1**. Testing of the macrocycles showed that both **2** and **3** had little activity ( $EC_{50} > 10.5 \mu\text{M}$  for **2** and  $EC_{50} > 30 \mu\text{M}$  for **3**) against U87-MG and MDA-MB-231 cells (Figure 4.2 and Supplementary Figure S4.2). All three Cbz-protected macrocycles represented by **2** had comparable activity (data not shown). At the highest concentrations tested, **2** and **3** reduced cell viabilities to 83.9% and 88.6% in U87-MG cells, respectively, and 68.8% and 91.5% in MDA-MB-231 cells, respectively. These results suggest that the nanomolar cancer cell toxicity of coibamide A requires the presence of both the macrocycle and side chain features of the compound and in a specific absolute configuration.

The feasibility of cyclization of a linear heptapeptide was demonstrated by the synthesis of macrocycles **2** and **3**. Therefore, progression to the synthesis of putative coibamide A or its desmethyl analog involved successful coupling of a tetrapeptide or depsipeptide side chain to macrocycles **2** and **3**, respectively. Under varying reaction conditions a series of three undecameric putative coibamide products (**4a-c**; Figure 4.3) were generated, although the problems involving racemization of the *N,O*-diMeSer residues in the syntheses of **1a-b**, **2** and **3** were also apparent in these compounds. Based on assessment of the analytical data, TLS-III-20 (**4a**) and TLS-III-115B4 (**4b**) contain a mixture of D/L-O-MeTyr and D/L for both *N,O*-diMeSer residues. Similarly, TLS-IV-17 (**4c**) is a racemic mixture of D/L for both *N,O*-diMeSer residues but with good enantiomeric purity of L-O-MeTyr, although the permutation L-*N,O*-diMeSer, L-*N,O*-diMeSer and L-O-MeTyr appears not to be represented in detectable quantities. As a result, up to eight diastereomers (four for **4c**) in varying ratios may be represented in the final products. Although these compounds failed to show nanomolar activity comparable to natural coibamide A, testing in U87-MG cells revealed a successive rank-order decrease in potency ( $EC_{50}$  48.3  $\mu\text{M}$  for **4a**,  $EC_{50}$  121  $\mu\text{M}$  for **4b**, and  $EC_{50} > 100 \mu\text{M}$  **4c**) starting from **4a** through **4c** (Figure 4.3 and Supplementary Figure S4.3). A similar pattern was also observed in the more-sensitive MDA-MB-231 cell line ( $EC_{50}$  14.2  $\mu\text{M}$  for **4a**,  $EC_{50}$  19.8  $\mu\text{M}$  for **4b** and  $EC_{50}$

>100  $\mu\text{M}$  for **4c**) although the activities of **4a** and **4b** are comparable (Figure 4.3 and Supplementary Figure S4.3).

Independent of synthetic efforts at OSU, we became aware that Dr. Shinya Oishi in Professor Nobutaka Fujii's group at Kyoto University was actively pursuing the total synthesis of coibamide A (personal communication). A collaboration was initiated with Dr. Oishi that resulted in receipt of the Kyoto synthetic product (~1.1 mg) for comparative biological testing with natural product coibamide A, as well as assignment of absolute configuration. LC-MS, NMR and degradative Marfey's analysis of the Kyoto putative coibamide A product [herein referred to as D-*N*-MeAla coibamide (**5**)] revealed that **5** comprised a single diastereomer in which the only difference to the natural product was the presence of a D-*N*-MeAla residue as shown in Figure 4.3. Extensive testing in four NCI human cancer cell lines (PC-3, MDA-MB-231, H292 and SF-295) showed that **5** had nanomolar activity ( $\text{EC}_{50}$  420-820 nM) but was ~4-8 times less potent than the natural compound ( $\text{EC}_{50}$  66-220 nM) (Table 4.1 and Supplementary Figure S4.4). This result suggests again that the cytotoxicity of coibamide A likely depends on the specific three dimensional shape of the molecule.

A unique structural feature of coibamide A is its high degree of *N*-methylation, which likely lends conformational rigidity to the molecule. To determine if the *N*-methylation of coibamide A contributes to its cytotoxicity, a series of four desmethylcoibamide analogs were generated and tested for activity. Whereas per-*N*-desmethylcoibamide (**6a**) and Boc-per-*N*-desmethylcoibamide (**6b**) possess none of the *N*-methyls present in the natural product, *N*-desmethyl analogs LD4-143 (**6c**) and LD4-198 (**6d**), with a terminal *N,N*-dimethyl Val residue, were synthesized (Figure 4.4). In addition, the side chain O-MeSer residue in **6d** was also selected to retain its *N*-methylation. In agreement with our expectation that *N*-demethylation would reduce the potency of coibamide A, we saw no dose-dependent cytotoxicity for desmethylcoibamide analogs **6a**, **6c** and **6d** ( $\text{EC}_{50}$  >30  $\mu\text{M}$  in both cell lines). However, similar to the trend seen for the side chain tetramers, Boc protection of per-*N*-desmethylcoibamide (**6b**) produced slight activity ( $\text{EC}_{50}$  38.2  $\mu\text{M}$  and 40.7  $\mu\text{M}$  in U87-MG and MDA-MB-231 cells, respectively; Figure 4.4 and Supplementary Figure S4.5). Based on these results, it would appear that the *N*-methylation of the Val and/or O-MeSer residues in the side chains of **6c** and **6d** does not impart significant

bioactivity. Presumably, the introduction of a larger lipophilic protecting group significantly improves cell permeability, as suggested by the shift in potency observed between tetramers **1a** and **1b**, as well as coibamide analogs **6a** and **6b** (Supplementary Figure S4.5).



## Discussion

Following the discovery and structure elucidation of the novel depsipeptide cytotoxin coibamide A, efforts to synthesize the compound were initiated at OSU due to scarcity of the natural supply from an ephemeral cyanobacterium, and the potential for discovery of a new mechanism of anticancer action and/or development of a pharmaceutical drug lead from coibamide A. Towards this goal, eleven coibamide A-related synthetic products were tested for activity in human U87-MG glioblastoma and MDA-MB-231 breast cancer cells. One of the major challenges faced in the synthetic approach, however, is the lack of enantioselectivity of the *O*-MeTyr and both *N,O*-diMeSer residues, all of which are L-amino acids in the natural product. Consequently, the final synthetic products are mixtures of up to eight diastereomers in different ratios depending on how entropically favored certain reactions are for one diastereomer over the other throughout the synthetic schemes. The observation that all of the tested synthetic products have only micromolar potencies can therefore be misleading since all but one diastereomer, potentially in very low titer in the mixture, may completely lack activity. Under this assumption, a single active diastereomer would account for 100% activity from the mixture but at fractionally lower corresponding concentrations than being reported depending on its titer in the final product. In spite of this issue, it is encouraging that nearly all of the synthetic products presented in this study exhibited varying degrees of activity and some at fairly biologically relevant concentrations. Furthermore, consistent with the NCI data previously reported, we observed an increased sensitivity of MDA-MB-231 breast cancer compared to U87-MG glioma cells to the synthetic compounds tested herein [4].

Biological investigations of other natural product depsipeptide cytotoxins such as kulokekahilide-2 from the Cephalaspidean mollusk *Phillinopsis* sp., aurilide from the sea hare *Dolabella auricularia*, and grassypeptolides A and C from the marine cyanobacterium *Lyngnya confervoides* have also demonstrated the importance of correct absolute configuration for activity [7-9]. In the case of kulokekahilide-2, inversion of one amino acid from D to L reduced cytotoxicity by 10 to 20 times in HeLa

and P388 cells, respectively. Similarly for synthetic analogs of aurilide, substitution of an L instead of D amino acid completely abolished activity in HeLa cells [8]. Interestingly, and in contrast to the above examples, enantiomeric inversion from *R* to *S* of one residue between grassypeptolides A and C drastically increased potency by 16-23 times in HT29 and HeLa cells [7].

Two of the more interesting features of coibamide A are its lariat tetrameric side chain, which closely resembles the structures of dolastatins 10 and 15, and its high degree of *N*-methylation. Considering that dolastatins were established as tubulin inhibitors with nanomolar potency we hypothesized that the side chain of coibamide A alone would impart partial activity relative to the entire structure. Importantly, however, it was previously ruled out that coibamide A interferes with tubulin or actin in cytoskeletal assays, suggesting that coibamide A operates through a different mechanism [4]. While both tetrameric side chains presented herein showed micromolar potency in two human cancer cell lines, their activities were not comparable to the natural product. Peculiarly, both macrocycle structures were only modestly active. These results hint that a combination of: (1) the removal of the side chain, (2) demethylation of the lariat terminal valine residue, and/or (3) racemization of the *N,O*-diMeSer residues are not well-tolerated structural modifications of coibamide A for retention of biological activity. Both structural components of coibamide A are therefore essential to achieve a significant cytotoxic effect.

*N*-methylation has been recognized for many years as a way to alter the pharmacological properties of peptides because it can confer improved oral bioavailability and may increase specificity of a drug for its receptor by introducing conformational rigidity [10]. Chatterjee et al. recently demonstrated that multiple strategic *N*-methylations of a cyclic hexapeptide  $\alpha\text{IIb}\beta\text{3}$  integrin receptor antagonist dramatically enhances its specificity and/or activity to certain integrin receptor subtypes by 'locking' it into a conformation that is more easily accepted by its receptor [11]. Based on this study, it is reasonable to assume that the lack of activity observed for the desmethylcoibamide analogs tested here can be attributed to the loss of structural rigidity that may be necessary for recognition by its cognate target. Along these lines, it is interesting to comment on the differences in activity observed within the pairs of per-*N*-desmethylcoibamide analogs **6a** and **6b** and the tetrameric

side chains **1a** and **1b**. For each pair, the structures differ from each other only in the presence or absence of a lipophilic protecting group (Bn in **1b** and Boc in **6b**), and the protected products were more active than their non-protected counterparts. These results therefore suggest that coibamide A may passively diffuse into cells, as opposed to being actively transported, before acting on its biological target.

Further insight into the structure activity relationships (SAR) of coibamide A was also revealed by the putative coibamide A product synthesized by Dr. Oishi. The compound contained only one inverted chiral center (D instead of L) in the *N*-MeAla residue coupled to the ring junction *N*-MeThr in the macrocycle, and resulted in an approximately 4- to 8-fold decrease in potency compared to natural coibamide A when tested across four different cancer cell lines. Considering that **5** still exhibited nanomolar potency, this result suggests that chiral inversion of the *N*-MeAla residue is somewhat dispensable for activity. It is generally recognized that Ala residues within a peptide are chemically inert and do not play direct roles in target binding. It will be interesting to determine if amino acid substitution at this position will have any effect on the cytotoxicity of coibamide A in future SAR studies. Collectively, our results suggest that the activity of coibamide A may minimally depend on the specific configuration of the *O*-MeTyr and *N,O*-diMeSer residues in the macrocycle. Successful synthesis of coibamide A will therefore require reaction conditions that favor the formation of the L enantiomer so that the final product is not a mixture of diastereomers. The extensive *N*-methylation of coibamide A also appears to be an important structural feature that may serve to impart target specificity by inducing coibamide A to adopt the specific conformation required for drug-target binding, as well as making the molecule sufficiently lipophilic to penetrate cell membranes without active transport. Together with the total synthesis of the natural product coibamide A structure itself, the disruption of interaction(s) that may be occurring with the desmethylcoibamide analogs presented in this study will be the subjects of future investigations.

### Bibliography

1. Blunt JW, Copp BR, Munro MH, Northcote PT, Prinsep MR (2011) Marine natural products. *Nat Prod Rep* 28: 196-268.
2. Blunt JW, Copp BR, Keyzers RA, Munro MH, Prinsep MR (2012) Marine natural products. *Nat Prod Rep* 29: 144-222.
3. Houssen WE, Jaspars M (2012) Isolation of marine natural products. *Methods Mol Biol* 864: 367-392.
4. Medina RA, Goeger DE, Hills P, Mooberry SL, Huang N, et al. (2008) Coibamide A, a potent antiproliferative cyclic depsipeptide from the Panamanian marine cyanobacterium *Leptolyngbya* sp. *J Am Chem Soc* 130: 6324-6325.
5. Simmons TL, Andrianasolo E, McPhail K, Flatt P, Gerwick WH (2005) Marine natural products as anticancer drugs. *Mol Cancer Ther* 4: 333-342.
6. White CJ, Yudin AK (2011) Contemporary strategies for peptide macrocyclization. *Nat Chem* 3: 509-524.
7. Kwan JC, Ratnayake R, Abboud KA, Paul VJ, Luesch H (2010) Grassypeptolides A-C, cytotoxic bis-thiazoline containing marine cyclodepsipeptides. *J Org Chem* 75: 8012-8023.
8. Suenaga K, Kajiwarra S, Kuribayashi S, Handa T, Kigoshi H (2008) Synthesis and cytotoxicity of aurilide analogs. *Bioorg Med Chem Lett* 18: 3902-3905.
9. Takada Y, Umehara M, Katsumata R, Nakao Y, Kimura J (2012) The total synthesis and structure–activity relationships of a highly cytotoxic depsipeptide kulokekahlide-2 and its analogs. *Tetrahedron* 68: 659-669.
10. Chatterjee J, Laufer B, Kessler H (2012) Synthesis of N-methylated cyclic peptides. *Nat Protoc* 7: 432-444.
11. Chatterjee J, Gilon C, Hoffman A, Kessler H (2008) N-methylation of peptides: a new perspective in medicinal chemistry. *Acc Chem Res* 41: 1331-1342.

## Figures

1

	R	EC <sub>50</sub> (μM)	
		U87-MG	MDA-MB-231
<b>1a</b> <i>N,N</i> -desmethyl tetrameric side chain	H	>300	100-300
<b>1b</b> Bn- <i>N,N</i> -desmethyl tetrameric side chain	Bn	56.8	86.7

**Figure 4.1** Structures of *N,N*-desmethyl tetrameric side chains and corresponding EC<sub>50</sub> values in U87-MG and MDA-MB-231 cells. The red bond line indicates racemization of the amino acid residue leading to a mixture of products possessing D or L configurations at this chiral site. HIV, hydroxyisovaleric acid.

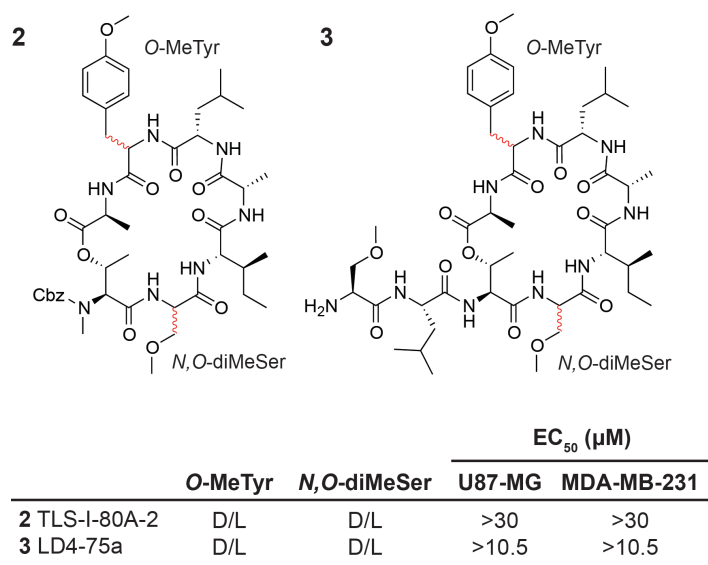
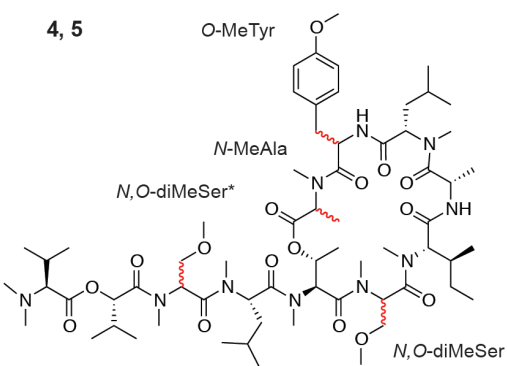


**Figure 4.2** Structures of hepta- and nonapeptide macrocycles and corresponding EC<sub>50</sub> values in U87-MG and MDA-MB-231 cells. Red bond lines indicate racemization of the amino acid residues leading to a mixture of products possessing D or L configurations at these chiral sites.

**4, 5**



	O-MeTyr	N,O-diMeSer	N-MeAla	N,O-diMeSer*	EC <sub>50</sub> (μM)	
					U87-MG	MDA-MB-231
<b>4a</b> TLS-III-20	D/L	D/L	L	D/L	48.3	14.2
<b>4b</b> TLS-III-115B4	D/L	D/L	L	D/L	121	19.8
<b>4c</b> TLS-IV-017	L	D/L	L	D/L	>30	>30
<b>5</b> D-N-MeAla coibamide	L	L	D	L	NT	0.55

**Figure 4.3** Structures of putative coibamide A compounds and corresponding EC<sub>50</sub> values in U87-MG and MDA-MB-231 cells. Red bond lines indicate racemization of the amino acid residues leading to a mixture of products possessing D or L configurations at these chiral sites. *NT*, not tested.

**Table 4.1** Potency comparison of D-*N*-MeAla coibamide and coibamide A in four NCI human cancer cell lines.

Cell line	EC <sub>50</sub> (nM)		Fold difference
	D- <i>N</i> -MeAla coibamide	Coibamide A	
H292	610	124	4.9
MDA-MB-231	550	66	8.3
PC-3	420	80	5.3
SF-295	820	220	3.7



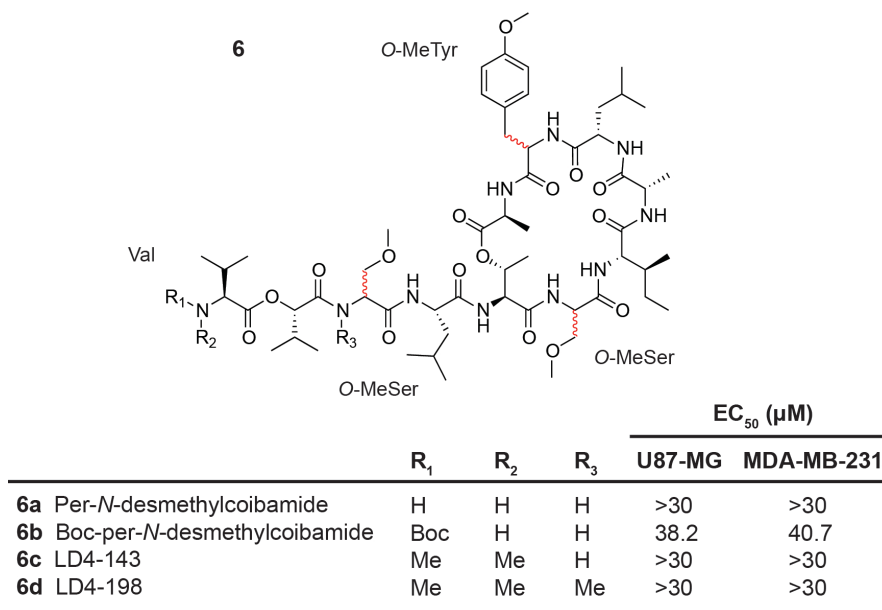
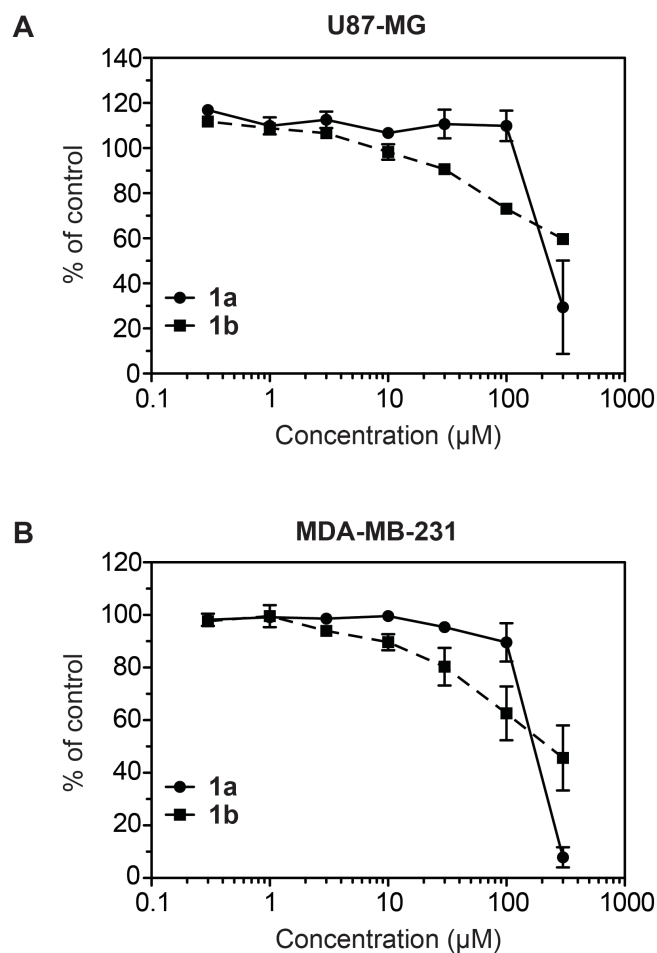
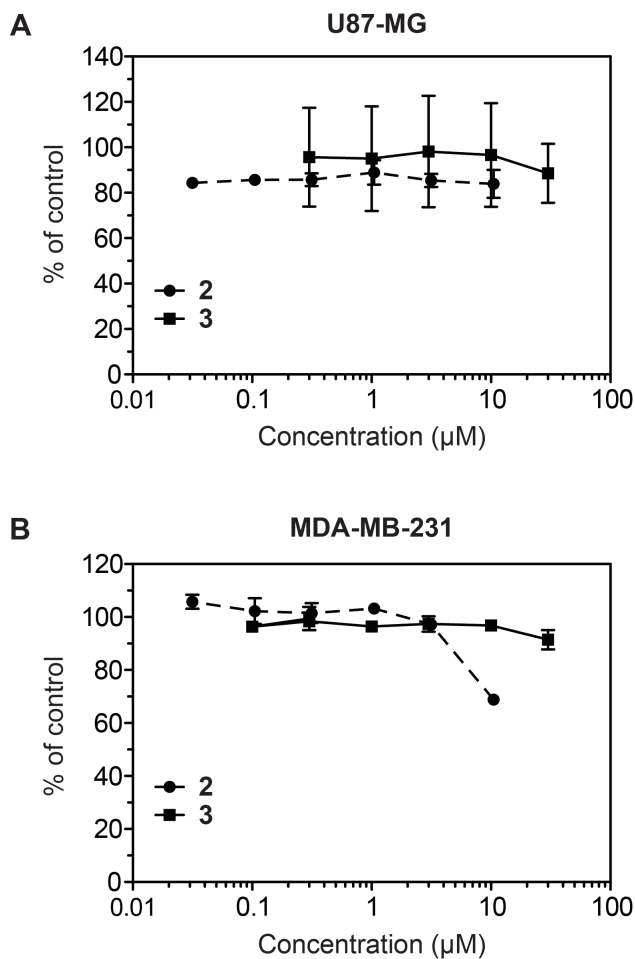


**Figure 4.4** Structures of desmethylcoibamide analogs and corresponding  $EC_{50}$  vales in U87-MG and MDA-MB-231 cells. Red bond lines indicate racemization of the amino acid residues.

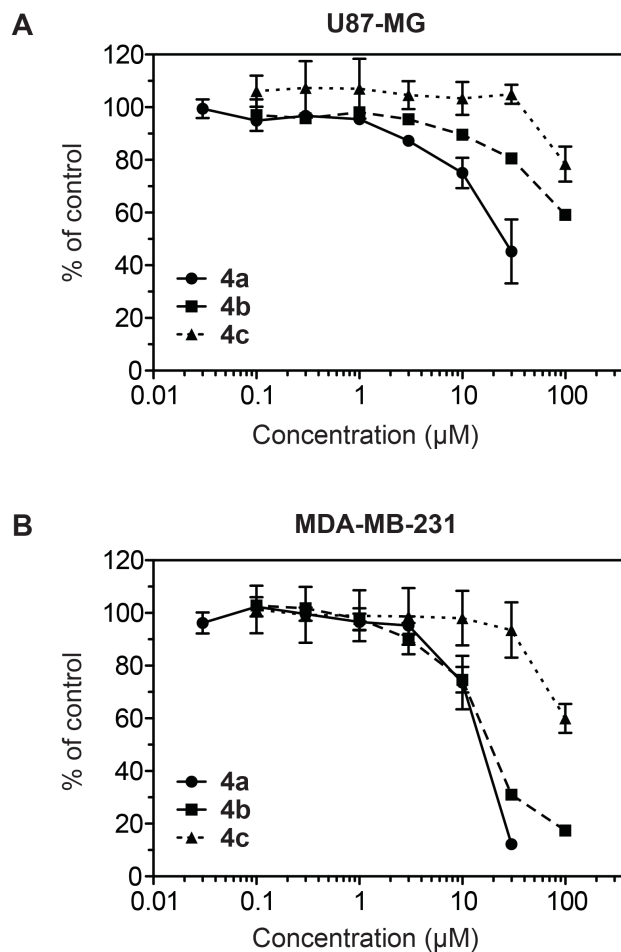
## Supplementary Figures



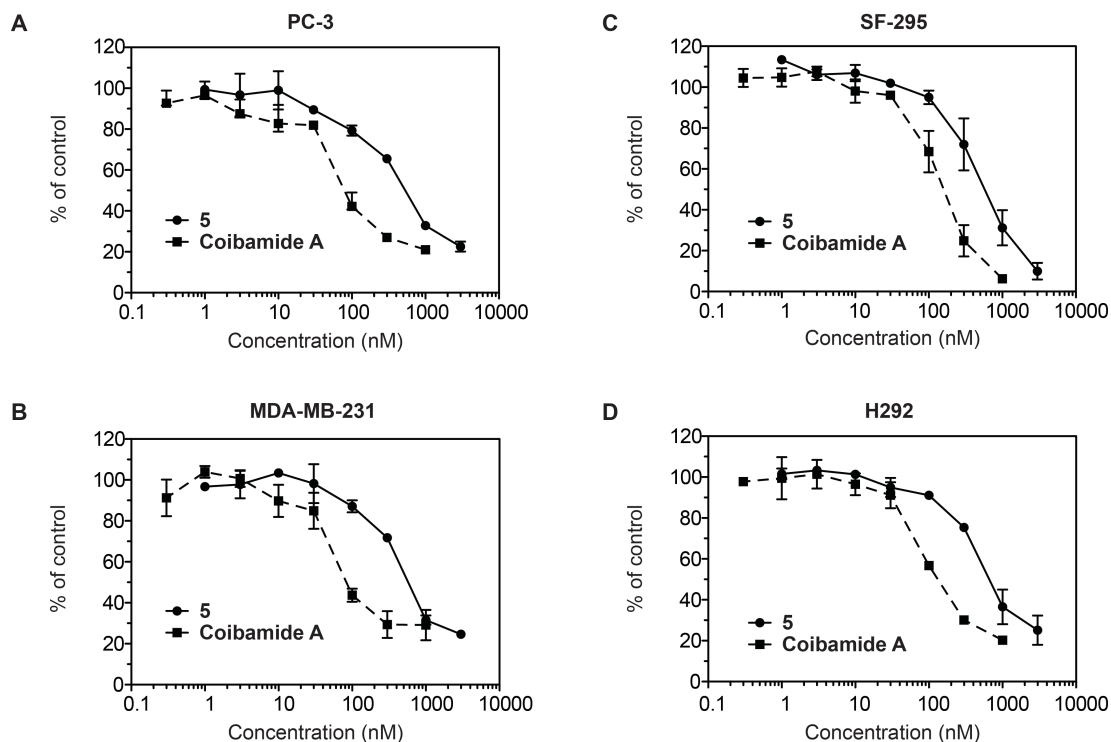
**Supplementary Figure S4.1** Dose-response plots for *N,N*-desmethyl tetrameric side chains (**1a** and **1b**). (**A**) U87-MG or (**B**) MDA-MB-231 cells were treated (n=3 wells per treatment) with increasing concentrations of test compound (up to 300 μM) for 72 h and cytotoxicity was determined by MTT assay. The viability of untreated control cells was defined as 100%. Each data point represents average cell viability ± SE of at least two independent experiments.



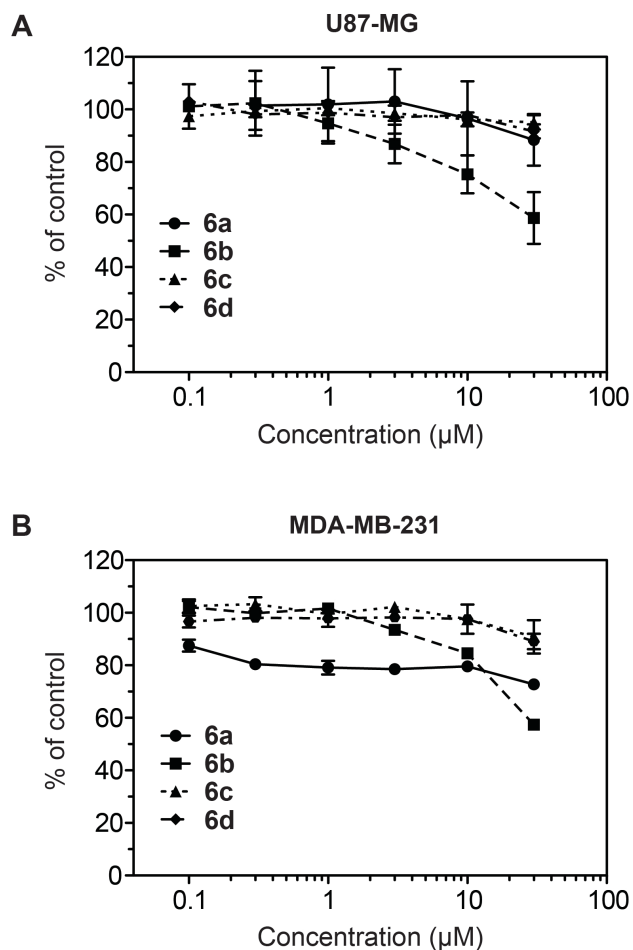
**Supplementary Figure S4.2** Dose-response plots for hepta- and nanopeptide macrocycles (**2** and **3**). (**A**) U87-MG or (**B**) MDA-MB-231 cells were treated ( $n=3$  wells per treatment) with increasing concentrations of test compound (up to 30  $\mu$ M) for 72 h and cytotoxicity was determined by MTT assay. The viability of untreated control cells was defined as 100%. Each data point represents average cell viability  $\pm$  SE of at least two independent experiments.



**Supplementary Figure S4.3** Dose-response plots for putative coibamide A structures (**4a-c**). (**A**) U87-MG or (**B**) MDA-MB-231 cells were treated ( $n=3$  wells per treatment) with increasing concentrations of test compound (up to 100  $\mu\text{M}$ ) for 72 h and cytotoxicity was determined by MTT assay. The viability of untreated control cells was defined as 100%. Each data point represents average cell viability  $\pm$  SE of at least two independent experiments.



**Supplementary Figure S4.4** Dose-response plots for D-*N*-MeAla coibamide (**5**) and coibamide A. (**A**) PC-3, (**B**) MDA-MB-231, (**C**) SF-295 and (**D**) H292 cells were treated (n=3 wells per treatment) with increasing concentrations of test compound (up to 3  $\mu$ M) for 72 h and cytotoxicity was determined by MTT assay. The viability of untreated control cells was defined as 100%. Each data point represents average cell viability  $\pm$  SE of at least two independent experiments.



**Supplementary Figure S4.5** Dose-response plots for desmethylcoibamide analogs (**6a-d**). (**A**) U87-MG or (**B**) MDA-MB-231 cells were treated ( $n=3$  wells per treatment) with increasing concentrations of test compound (up to 30  $\mu\text{M}$ ) for 72 h and cytotoxicity was determined by MTT assay. The viability of untreated control cells was defined as 100%. Each data point represents average cell viability  $\pm$  SE of at least two independent experiments.

## GENERAL CONCLUSIONS

## CHAPTER FIVE

Andrew M. Hau

The marine world has increasingly become a rich source of natural products with unique chemistry and interesting pharmacological activities against a spectrum of human diseases including cancer. It has been common for decades to elapse from the time of drug isolation to its development and use. Currently, only three marine-derived drugs have been approved by the US Food and Drug Administration and/or European Agency for the Evaluation of Medicinal Products, which include cytarabine (Cytosar-U®, Depocyt®), vidarabine (Vira-A®), trabectedin (Yondelis®) and ziconotide (Prialt®) (reviewed in [1]). Other marine natural products that have been pipelined include dolastatin-10 and analogs, and dehydrodidemnin B (Aplidin®). These drugs have been developed through various phases of clinical trials as DNA or tubulin interfering agents with anti-mitotic activity or as pro-apoptotic drugs 10-20 years after their discovery [2-4]. This lengthy timeline therefore underscores the need for greater efforts in drug discovery to identify new agents with therapeutic potential.

The recent discovery of the potent and selective cytotoxin coibamide A reaffirms the wealth of structural diversity of the marine environment. Biological investigation of coibamide A in a human U87-MG glioblastoma cell line has revealed that it induces autophagy and causes non-apoptotic cell death. Comparison of coibamide A to the mTOR inhibitor and inducer of autophagy, rapamycin, as well as other small molecule pro-autophagic drugs (valproate, imatinib, Torin1, butyrate and SAHA) reported in the literature show that coibamide A is unlike any of these compounds [5-8]. This finding is retrospectively supported by the COMPARE-negative designation of coibamide A when it was screened against the NCI-60 tumor cell line panel in 2006 and indeed, we have found that activation of autophagy by coibamide A occurs independently of mTOR inhibition [9]. Future work will therefore focus on the cyclical  $\text{Ca}^{2+}$ /calpain/ $\text{G}\alpha_s$  and cyclic AMP/exchange protein directly activated by cAMP/phospholipase C $\epsilon$ /inositol triphosphate (cAMP/Epac/PLC $\epsilon$ /IP $_3$ ) mTOR-independent autophagy pathways.

Programmed cell death (PCD) independent of caspase activation is well documented, especially in transformed cells. Autophagy, for instance, had been long thought of as a mechanism of non-apoptotic cell death but an abundance of studies now support that this process is a pro-survival response for cells under stress conditions. Even more extreme interpretations of autophagy function suggest that



autophagy can actually promote tumorigenesis by rescuing cells undergoing PCD. Regardless of these possibilities, while constitutive autophagy can perhaps overwhelm a cell, it is likely that atypical cell death pathways (discussed in Chapter 1) are activated independently of autophagy in cell specific contexts where caspase-dependent death mechanisms are dysfunctional. Coibamide A would appear to operate under this principle as: (1) cell death occurs independently of functional autophagy in MEFs lacking ATG5, (2) Apaf1 null MEFs are not rescued following coibamide A treatment, and (3) different patterns of caspase-3 activation are observed between U87-MG and SF-295 cells. Furthermore, caspase inhibition with Z-VAD-FMK rescues SF-295 cells but attenuates U87-MG cell viability in the presence of coibamide A. Careful deduction of PCD pathways will therefore be the next step in elucidating the cytotoxic action of coibamide A where it may serve as a valuable tool for studying caspase-independent cell death.

The pro-survival function of autophagy in tumor cells makes this process an interesting target for inhibition. Indeed, many studies in cell and animal models have shown that autophagy inhibition enhances chemosensitivity to apoptotic drugs. However, only a limited number of compounds have been identified that block autophagy and many of these (wortmannin, 3-methyladenine, LY294002) are phosphoinositide-3 kinase (PI3K) inhibitors that prevent autophagy at the pre-initiation stage (reviewed in [10]). Because PI3Ks are involved in a wide range of cellular functions including cell growth, proliferation, differentiation, motility, survival and trafficking, prolonged chemical inhibition of PI3K signaling is often toxic to healthy tissues and therefore not a desirable therapeutic approach for cancer therapy. Therefore, a more attractive strategy to prevent autophagy is by the use of late-stage inhibitors. Among this small class of inhibitors are bafilomycin A1, a vacuolar H<sup>+</sup> ATPase (V-ATPase) inhibitor that prevents autophagosomal-lysosomal fusion, and chloroquine analogs and monensin, which are lysosomotropic drugs that prevent acidification of lysosomes. The discovery of bafilomycin A1 from *Streptomyces griseus* in 1984 as an antibiotic compound initially underscored the utility of microorganisms as producers of various metabolites with anti-microbial activity and sparked efforts to develop more specific and potent analogs through structure activity relationship (SAR) studies [11,12]. When the molecular target of bafilomycin A1 was

identified several years later, a new field of research involving the function of V-ATPases in human diseases was opened and has culminated to the evolution of bafilomycin A1 from an antibiotic to a research tool for studying autophagy. More recently, the benzoporphyrin derivative, verteporfin, which is used as a photosensitizer in the treatment of macular degeneration has been proposed as an early-stage inhibitor of autophagy by blocking phagophore elongation and maturation into an autophagosome [13]. Using natural product library screens, similar to that described by Donohue et al. in the discovery of verteporfin, may therefore lead to the identification of new autophagy-inhibiting agents with utility as research tools or anti-cancer drugs [13].

The cytostatic potential of coibamide A appears to be mediated by inhibiting the invasive capacity of cancer cells and is followed by a G1 phase specific cell cycle arrest. Consistent with these results, previous investigation on potential targets or pathways affected by coibamide A have ruled out actin and tubulin, which are dynamic cytoskeletal components critical for mitosis and cell migration [9]. In contrast to a G2/M anti-mitotic effect, the inhibition of a G1 to S phase transition induced by coibamide A may therefore involve proteins that function in cell growth and cell invasion. Two families of proteases that have functions in regulating these processes are calpains and matrix metalloproteinases (MMPs), which interestingly have also been implicated as 'suicidal' proteases in caspase-independent, cell death pathways that lead to the proteolysis of the DNA repair protein PARP. As reviewed by Chaitanya et al., calpain-1 and MMP-2 proteolysis of PARP results in signature ~70-40 kD N-terminal and <48 kD and 66 kD fragments, respectively [14]. In contrast, caspase-3 or -7 cleavage of PARP produces 89 kD C-terminal and 24 kD N-terminal fragments which are consistently observed in SF-295 and MEF but not U87-MG cells exposed to coibamide A (Chapter 2). These findings suggest that the cytotoxic action of coibamide A involves caspase-dependent or -independent cell death pathways in cell line specific contexts. Future investigations will consequently focus on the activities of calpains and MMPs as they relate to cell growth, invasion and cell death.

The high degree of *N*-methylation of coibamide A potentially makes it a suitable candidate for drug development as this structural feature has been documented to improve the pharmacological properties of peptide drugs. This effect

on increased druggability has been observed among the undecameric putative coibamide A structures and desmethylcoibamide analogs. Although the structures representing each compound are mixtures of diastereomers making direct comparison between putative coibamide A and desmethylcoibamide analogs and derivation of SAR difficult, the cytotoxicity trends show that *N*-demethylation decreases the potency of coibamide A. Considering all the challenges discussed in Chapter 4 regarding the synthesis of the naturally occurring stereoisomer of coibamide A, one must develop a deeper appreciation for Nature's ability to produce such a structurally diverse compound with anti-cancer therapeutic potential in a marine environment where (the role of) cancer is largely unknown.

Collectively, the research presented herein has highlighted the role of natural products in drug discovery, with coibamide A serving as an example of a novel anti-proliferative compound with a unique mechanism of action. Despite the wealth of knowledge about PCD, the cytotoxic effect of coibamide A can occur independently of autophagy and does not appear to be mediated through a single death pathway as observed by the differences in caspase-3 and PARP cleavage we reported in two human glioblastoma cell lines. This finding may be advantageous from a clinical standpoint as drugs with multiple mechanisms of action could be used against apoptosis-sensitive and resistant tumors. Furthermore, cell death observed without functional autophagy upon coibamide A exposure in MEF cells hints at the existence of atypical or uncharacterized PCD pathways. The development of coibamide A into drug status will likely take years as its total synthesis for large scale production has not been achieved even after half a decade since its discovery and structure elucidation. Furthermore, aquaculture of the coibamide A-producing cyanobacterium has resulted in inadequate quantities given the time, cost and labor involved in sustaining this approach. Potentially better alternatives such as biosynthesis should be explored more heavily since the organism and thus the gene cluster involved in coibamide A biosynthesis is already accessible, albeit yet to be identified. Although we are confounded by challenges in synthesis, a small pilot glioma xenograft model study to determine the *in vivo* efficacy of coibamide A has yielded promising results and represents a critical next step in drug development. In spite of current challenges,

coibamide A continues to be a promising lead structure for the treatment of drug-resistant glioblastoma and potentially other cancers.

### Bibliography

1. Mayer AM, Glaser KB, Cuevas C, Jacobs RS, Kem W, et al. (2010) The odyssey of marine pharmaceuticals: a current pipeline perspective. *Trends Pharmacol Sci* 31: 255-265.
2. Bai R, Pettit GR, Hamel E (1990) Dolastatin 10, a powerful cytostatic peptide derived from a marine animal. Inhibition of tubulin polymerization mediated through the vinca alkaloid binding domain. *Biochem Pharmacol* 39: 1941-1949.
3. Garcia-Rocha M, Garcia-Gravalos MD, Avila J (1996) Characterisation of antimitotic products from marine organisms that disorganise the microtubule network: ecteinascidin 743, isohomohalichondrin-B and LL-15. *Br J Cancer* 73: 875-883.
4. Urdiales JL, Morata P, Nunez De Castro I, Sanchez-Jimenez F (1996) Antiproliferative effect of dehydrodidemnin B (DDB), a depsipeptide isolated from Mediterranean tunicates. *Cancer Lett* 102: 31-37.
5. Fu J, Shao CJ, Chen FR, Ng HK, Chen ZP (2010) Autophagy induced by valproic acid is associated with oxidative stress in glioma cell lines. *Neuro Oncol* 12: 328-340.
6. Shingu T, Fujiwara K, Bogler O, Akiyama Y, Moritake K, et al. (2009) Inhibition of autophagy at a late stage enhances imatinib-induced cytotoxicity in human malignant glioma cells. *Int J Cancer* 124: 1060-1071.
7. Thoreen CC, Kang SA, Chang JW, Liu Q, Zhang J, et al. (2009) An ATP-competitive mammalian target of rapamycin inhibitor reveals rapamycin-resistant functions of mTORC1. *J Biol Chem* 284: 8023-8032.
8. Shao Y, Gao Z, Marks PA, Jiang X (2004) Apoptotic and autophagic cell death induced by histone deacetylase inhibitors. *Proc Natl Acad Sci U S A* 101: 18030-18035.
9. Medina RA, Goeger DE, Hills P, Mooberry SL, Huang N, et al. (2008) Coibamide A, a potent antiproliferative cyclic depsipeptide from the Panamanian marine cyanobacterium *Leptolyngbya* sp. *J Am Chem Soc* 130: 6324-6325.
10. Yang ZJ, Chee CE, Huang S, Sinicrope FA (2011) The role of autophagy in cancer: therapeutic implications. *Mol Cancer Ther* 10: 1533-1541.
11. Werner G, Hagenmaier H, Drautz H, Baumgartner A, Zahner H (1984) Metabolic products of microorganisms. 224. Bafilomycins, a new group of macrolide antibiotics. Production, isolation, chemical structure and biological activity. *J Antibiot (Tokyo)* 37: 110-117.
12. Deeg M, Hagenmaier H, Kretschmer A (1987) Chemical modifications of bafilomycin-type 16-membered dienlactone macrolides. *J Antibiot (Tokyo)* 40: 320-328.
13. Donohue E, Tovey A, Vogl AW, Arns S, Sternberg E, et al. (2011) Inhibition of autophagosome formation by the benzoporphyrin derivative verteporfin. *J Biol Chem* 286: 7290-7300.
14. Chaitanya GV, Steven AJ, Babu PP (2010) PARP-1 cleavage fragments: signatures of cell-death proteases in neurodegeneration. *Cell Commun Signal* 8: 31.

